Centro de Investigación y de Estudios Avanzados del I.P.N.
Unidad Guadalajara

# Modelos Avanzados de Dispositivos de Sistemas de Potencia en el Dominio Armónico Dinámico

Tesis que presenta:

**José de Jesús Chávez Muro**

para obtener el grado de:

**Doctor en Ciencias**

en la especialidad de:

**Ingeniería Eléctrica**

Director de Tesis

**Dr. Amner Israel Ramírez Vázquez**



Guadalajara, Jalisco, Agosto de 2009.

ID 163423-1001

# Modelos Avanzados de Dispositivos de Sistemas de Potencia en el Dominio Armónico Dinámico

**Tesis de Doctorado en Ciencias**
**Ingeniería Eléctrica**


Por:

**José de Jesús Chávez Muro**

Maestro en Ciencias en Ingeniería Eléctrica
CINVESTAV - Guadalajara 2004-2006



Becario de CONACYT, expediente no. 203408


Director de Tesis

**Dr. Amner Israel Ramírez Vázquez**


CINVESTAV del IPN Unidad Guadalajara, Agosto de 2009.

Ccntro de Investigación y de Estudios Avanzados

del I.P.N.

Unidad Guadalajara

# Advanced Models of Power System Devices in the Dynamic Harmonic Domain

A thesis presented by:

**José de Jesús Chávez Muro**

to obtain the degree of:

**Doctor of Sciences**

in the subject of:

**Electrical Engineering**

Thesis Advisors:

**Dr. Amner Israel Ramírez Vázquez**

Guadalajara, Jalisco, August 2009.

# Advanced Models of Power System Devices in the Dynamic Harmonic Domain

**Doctor of Science Thesis**
**In Electrical Engineering**

By·
**José de Jesús Chávez Muro**
Master in Science in Electrical Engineering
CINVESTAV Guadalajara 2004-2006

Scholarship granted by CONACYT, No. 203408

Thesis Advisors:
**Dr. Amner Israel Ramírez Vázquez**

CINVESTAV del IPN Unidad Guadalajara, August, 2009.

# Acknowledgements

*I would like to thank to:*

*God.*

*My father and mother, who have supported me without hesitate, for their love and patience.*

*My brothers and sister: Ruben, Javier, Mary, and their children to make me feel always happy. And how forget my siblings-in-law; Paulo, Lupita, and Lupita.*

*All the professors who have helped me in this career, for the knowledge, feedback and suggestions provided by them. Specially thanks a lot to Dr. Abner and Dr. Venkata.*

*My friends, for their true friendship.*

*CONACYT, for the scholarship.*

# Contents

# List of Figures

# List of Tables

# Abstract

THIS thesis presents an advanced modeling of power system elements such as transmission line and synchronous machine for analysis of harmonics under transient conditions. Additionally, it analyzes harmonic resonance conditions in steady-state when electronic devices are involved in a transmission network. The proposed models take aim on the dynamic harmonic domain (DHD) technique. The advantages of this methodology over traditional techniques are: its natural capability to accurately follow the harmonic content during transient conditions, its ability to include nonlinear loads in a straightforward manner, and its ability to serve as a visual active indicator of the steady-state in a signal.

The thesis is divided in three main parts as follows:

First, the basic power system elements (resistor, inductor, capacitor, and nonlinear reactor) are modeled in the DHD. A major contribution of this part is the DHD modeling of the transmission line, based on the traveling waves approach, and the DHD modeling of the synchronous generator. The interconnection of these two network elements is also presented.

Second, the harmonic domain is taken as a basis to analyze resonance conditions using an eigenanalysis-based technique. The technique is applied to power system networks that include transmission lines, underground cables, linear loads and switching devices (TCR, SVC).

Third, the interconnection (in the DHD) of the transmission line and linear loads is implemented in real-time using a custom C/C++ program in Matlab/SIMULINK environment and a PC-cluster based real-time simulator from OPAL-RT Technologies Inc.

# Resumen

ESTA tesis presenta el modelo avanzado de los elementos de sistemas eléctricos de potencia: línea de transmisión y máquina síncrona, para el análisis del comportamiento de los armónicos en condiciones transitorias. Además, se analizan las condiciones de resonancia armónica en el estado estable cuando la red eléctrica incluye dispositivos electrónicos. Los modelos propuestos se basan en la técnica del dominio armónico dinámico. Las ventajas de ésta metodología sobre las técnicas tradicionales son: a) su capacidad natural de seguir con precisión el contenido armónico en condiciones transitorias, b) facilidad para incluir en forma directa elementos no lineales, y c) su capacidad para indicar visualmente el estado, transitorio o estable de una señal.

La tesis se divide en tres partes principales:

En primer lugar, los elementos básicos del sistema eléctrico de potencia (resistor, inductor, capacitor y reactor no lineal) se modelan en el dominio armónico dinámico (DHD por sus siglas en Inglés). Una contribución importante en esta parte es el modelo en el DHD de la línea de transmisión, basado en ondas viajeras, y el modelo de la máquina síncrona. También se presenta la interconexión de estos dos elementos en la red.

En segundo lugar, el dominio armónico se toma como base para analizar posibles condiciones de resonancia mediante la técnica de eigenvalores/eigenvectores. Esta técnica se aplica en sistemas eléctricos de potencia que incluyen líneas de transmisión, cables subterráneos, cargas lineales y dispositivos de conmutación (TCR, SVC).

En tercer lugar, la interconexión de la línea de transmisión con cargas lineales (modelados en el DHD), se implementan en tiempo real utilizando el código de programación C/C++ en el programa Matlab / Simulink para ser procesado en el **R**eal-**T**ime e**X**perimental Laboratory de OPAL-RT Technologies Inc.

Chapter 1

# Introduction

*We operating men, I think, all agree that we have harmonics. I think we all agree that, like the poor, the harmonics will always be with us. If we could get rid of them, we would be very glad to do so.*

*J.B. Fisken (September 8, 1916)*

## 1.1 History of Harmonics in Power Systems

SINCE the beginning of the electrical power industry, problems associated with harmonic components of voltage and/or current waveforms have tormented power systems engineers.

One of the first harmonic analysis was carried out by Steinmetz when a motor heating problem was studied in 1893 [1]. He suspected the possibility of harmonic resonance due to the motor-transmission line coupling and made supporting calculations and tested his theory against measured quantities obtained with a primitive instrument known as the "wave meter" (a type of galvanometer).

According to the specialized literature, problems associated to harmonic disturbance have appeared in the following order:

- 1893 - At Hartford Conn., USA, a motor heating problem; probably the first problem studied by a pioneer harmonic analysis technique.
- 1895 - G.E. and Westinghouse introduced a new generator design using distributed armature windings to substantially improve the voltage waveform and overcome the problems of limited transmission line length and resonance effects.
- 1895 - Excessive neutral currents was reported when generators were solid grounded and operated in parallel (today a familiar problem involving zero-sequence third harmonic).
- 1910 - Communications interference factor. Power and telephone services where placed often in common rights-of-way. Harmonic currents produced by transformer magnetizing currents caused inductive interference with open-wire telephone systems.
- 1960 - Shunt capacitors are used as filters to improve power factor.

- 1980 Power electronic devices. Nowadays, the most common sources of harmonics are power electronic loads such as switch-mode power supplies.

Harmonic analysis is the name given by Thomson and Tai [1] to a method based on Fourier series, first used in mathematical physics and latter used by Bernoulli and Euler in the middle of the 18th century [1]. Maxwell applied it to physical (electromagnetic) problems.

One of the first documents where the word "harmonic" appeared and used in the context of Fourier series applied to electrical systems is a paper written in 1894 by Houston and Kenelly, entitled "The harmonics of alternating current"

The harmonic domain (HD) methodology, based on constant Fourier coefficients, was pioneered by Xia and Heydt, using a decoupled positive sequence circuit for a full wave bridge rectifier [33], [34]. Later on, Densem *et. al.* reported that the network must be modeled in the abc frame due to the characteristic harmonics not being properly evaluated by a positive sequence frequency [35]. The HD methodology was extended tot he dynamic case *i.e.* with variable Fourier coefficients, for transients studies by Acha, *et. al.* [8], and it is hereafter referred to as the dynamic harmonic domain methodology.

## 1.2 General Terms and Definitions

### 1.2.1 Harmonic

According to the IEEE Standard Dictionary we have the following definitions [54]:

*Harmonic*: A sinusoidal component of a periodic wave or quantity having a frequency that is an integral multiple of the fundamental frequency. *Note:* For example, a component, the frequency of which is twice the fundamental frequency, is called a second harmonic.

*Harmonic content*: (1) Distortion of a sinusoidal waveform characterized by indication of the magnitude and order of the Fourier series terms describing the wave. (2) A measure of the presence of harmonics in a voltage or current wave form expressed as a percentage of the amplitude of the fundamental frequency at each harmonic frequency.

### 1.2.2 Harmonic Sources

Any device with nonlinear characteristics may be responsible for injecting harmonic currents and voltages into the electrical system [3].

There are two general categories of harmonic sources:

- Saturable devices produce harmonics due to iron saturation, as in the case of transformers, machines, and fluorescent lamps.

- Power electronic devices function as switching devices, thus producing high frequency components when passing from the "on" state to the "off" state and vice-versa.

### 1.2.3 Effects of Harmonics

Power system problems such as communication interference, heating and solid-state device malfunctioning can be the direct results of harmonics [4]. These problems are categorized and listed below.

- *Communication interference.* Magnetic or electrostatic coupling between electrical power circuits and communication circuits:
  - Induce line noise.
  - Produce interference with power line carrier systems.
  - Provoke relay malfunctions.
- *Heating losses.* The relation $I^2R$ involves:
  - Excessive losses and heating in motors, capacitors and transformers.
  - Blow capacitor fuses.
- *Solid-state device malfunctions.* A resonance condition can cause a current waveform to have zero crossing more than once every half cycle, thus producing:
  - Errors in measurement equipment.
  - Nuisance tripping of relays and breakers.
  - Unstable operation of zero voltage crossing firing circuits.
  - Interference with motor controllers.
- *Harmonics resonance conditions.* Produce excessive amount of harmonic currents and/or harmonic over voltages.

## 1.3 Justification

In the past, measurements were the only harmonics identification procedure. Nowadays, models of electrical devices have been modified to include harmonics in such a way that prediction/analysis of harmonics in the network becomes fairly easy. That analysis has been generally focused on steady-state. Nevertheless, the fact that disturbances, change of loads, disconnection of network elements, and implementation of electronic devices are continuous along the time, it brings the necessity of modeling network elements as function of time-varying harmonics.

In order to account for time-varying harmonics, advanced models of generation and transmission elements are needed. Among those elements one can consider the generators, the transmission lines, and nonlinear loads (reactors, electronic devices, etc.) as the most important elements of a power network.

Additionally, a power network model is needed for analyzing possible resonance conditions due to harmonic interactions between its elements. A few works have proposed analytical methods; however, they become impractical to apply for large networks. Thus, the need of numerical techniques for solving the resonance conditions assessment, especially when electronic devices are present.

## 1.4 Objectives

The objectives of this thesis are:

- To propose advanced models of power system devices, such as: transmission lines, synchronous machines, and linear/nonlinear loads for harmonics analysis.

- To interface the proposed models to each other.
- To perform resonance analysis of systems including electronic devices tied to transmission networks.
- To perform real-time simulation of transmission lines and linear loads modeled in the DHD for harmonics analysis.

Chapter 2

# Fundamentals of the Dynamic Harmonic Domain

THIS chapter outlines the basic theory of the dynamic harmonic domain (DHD), primarily involving the transformation of a variable from time domain (TD) to DHD and vice-versa. The described theory is based on Fourier series; nevertheless, the DHD can be conducted in other orthogonal series such as Hartley [5], [6]. Additionally, the DHD models for the basic linear and nonlinear power system elements are described in this chapter.

## 2.1 Transformation from TD to DHD

In general, we can consider that electrical power networks can be represented by a linear time periodic (LTP) system of ordinary differential equations (ODEs). This set of equations can be converted into a linear time invariant (LTI) system via the DHD technique [7], [8]. The use of the DHD permits to represent in a natural way the harmonic dynamics of the variables involved in the system modeling. Furthermore, the time periodic coefficients in the TD become constant Toeplitz-type matrices in the DHD, as shown in the following.

Consider the LTP system for the scalar case

$$\dot{x} = a_p x + b_p u, \tag{2.1a}$$

$$y = c_p x + d_p u, \tag{2.1b}$$

where the subscript $p$ stands for time periodic. Consider also that any variable (or coefficient) in (2.1) can be expressed by its Fourier series with corresponding coefficients assumed to be time-varying. For example, $x_p$ and its derivative (with respect to time) can be defined as:

$$x_p(t) = x_{-h}(t)e^{-jh\omega_o t} + \cdots + x_{-1}(t)e^{-j\omega_o t} + x_o(t) + x_1(t)e^{j\omega_o t} + \cdots + x_h(t)e^{jh\omega_o t}, \tag{2.2a}$$

$$\dot{x}_p(t) = (\dot{x}_{-h}(t) - jh\omega_o x_{-h}(t))e^{-jh\omega_o t} + \cdots + \dot{x}_o(t) + \cdots + (\dot{x}_h(t) + jh\omega_o x_h(t))e^{jh\omega_o t}, \tag{2.2b}$$

where $h$ represents the highest harmonic considered in the analysis and $\omega_o$ corresponds to the fundamental power frequency. Expressing all the variables from (2.1) by their Fourier

series, as in (2.2), and by dropping out all the exponential terms, the state representation of (2.1) in the DHD becomes:

$$\dot{\mathbf{x}} = (\mathbf{A} - \mathbf{S})\mathbf{x} + \mathbf{B}\mathbf{u}, \tag{2.3a}$$

$$\mathbf{y} = \mathbf{C}\mathbf{x} + \mathbf{D}\mathbf{u}. \tag{2.3b}$$

The variables in (2.3), represented by bold-type letters in this work, have been arranged as harmonic vectors (generally complex) with time-varying elements, for instance $\mathbf{x}$ is defined as:

$$\mathbf{x} = [x_{-h}(t), \cdots, x_{-1}(t), x_o(t), x_1(t), \cdots, x_h(t)]^T, \tag{2.4}$$

where superscript $T$ denotes the transpose. The diagonal matrix $\mathbf{S}$ is called the operational matrix of differentiation and it is defined (using a Matlab representation) by [7], [9]:

$$\mathbf{S} = diag\{-jh\omega_o, \cdots, -j\omega_o, 0, j\omega, \cdots, jh\omega_o\} \tag{2.5}$$

Note that the derivative in TD involves the transformation to DHD as:

$$(TD) \qquad \dot{x} \Longleftrightarrow \dot{\mathbf{x}} + \mathbf{S}\mathbf{x} \qquad (DHD). \tag{2.6}$$

In addition, matrix $\mathbf{A}$ (as well as $\mathbf{B}$, $\mathbf{C}$ and $\mathbf{D}$) contains the harmonic coefficients of $a_p$ in a Toeplitz-type arrangement as follows:

$$\mathbf{A} = \begin{bmatrix} a_o & a_{-1} & \cdots & a_{-h} & \\ a_1 & a_o & & & a_{-h} \\ \vdots & & & & \vdots \\ a_h & & & a_o & a_{-1} \\ & a_h & \cdots & a_1 & a_o \end{bmatrix} \tag{2.7}$$

Note that since (2.1) has been considered as LTP, the coefficient matrices in the DHD system given by (2.3) now become constant matrices, as in (2.7), thus (2.3) represents an LTI system [10].

The system of coupled ODEs in (2.3) has dimensions of $2h+1$ and it becomes decoupled (diagonal) when dealing with an LTI system (*i.e.*, $a_p$, $b_p$, $c_p$, and $d_p$ being constants). Furthermore, the dimensions can be reduced to $h+1$ when considering half-wave symmetry; that is, when only odd harmonics are considered due to sinusoidal sources.

## 2.2 From Dynamic-State to Steady-State

For steady-state analysis the Fourier coefficients of a time-periodic variable are constants. Additionally, the derivative of a harmonic vector becomes zero. Thus, the steady-state of the system (2.3) can be easily obtained by setting to zero its derivatives, yielding [11]:

$$\mathbf{x} = (\mathbf{S} - \mathbf{A})^{-1}\mathbf{B}\mathbf{u}, \tag{2.8a}$$

$$\mathbf{y} = \mathbf{C}\mathbf{x} + \mathbf{D}\mathbf{u}, \tag{2.8b}$$

where now the harmonic vectors contain time-invariant coefficients, for instance:

$$\mathbf{x} = [x_{-h}, \cdots, x_{-1}, x_o, x_1, \cdots, x_h]^T \tag{2.9}$$

The evolution of the harmonic content with respect to time can be obtained by substituting for instance (2.4) for transient-state or (2.9) for steady-state into its corresponding Fourier series, similar to (2.2a).

## 2.3 Modeling of Basic Elements

For simplicity of presentation, in this work the basic elements of an electrical power system are cataloged by linear (resistor, inductor, and capacitor) and nonlinear (reactor) elements. Their DHD modeling is presented in the following.

### 2.3.1 Linear Elements

The voltage/current relations for resistive, inductive, and capacitive elements in TD are represented by:

$$i_R = \frac{1}{R} v, \tag{2.10a}$$

$$i_C = C\frac{dv}{dt}, \tag{2.10b}$$

$$v_L = L\frac{di_L}{dt}. \tag{2.10c}$$

In the DHD, (2.10) can be respectively expressed as [7]:

$$\mathbf{I}_R = \mathbf{Y}_R \mathbf{V}, \tag{2.11a}$$

$$\mathbf{I}_C = C\mathbf{S}\mathbf{V} = \mathbf{Y}_C \mathbf{V} \tag{2.11b}$$

$$\mathbf{I}_L = \frac{1}{L}\mathbf{S}^{-1}\mathbf{V} = \mathbf{Y}_L \mathbf{V}. \tag{2.11c}$$

where $\mathbf{Y}_R$, $\mathbf{Y}_L$, and $\mathbf{Y}_C$ are diagonal admittance matrices with their $h$-th diagonal element being equal to $1/R$, $jh\omega_o C$, and $1/(jh\omega_o L)$, respectively.

From (2.11) one can notice that, for linear elements, there exists a perfect decoupling between the various harmonic frequencies. In other words, no interaction takes place between pre-existing harmonics and no new harmonics are generated.

### 2.3.2 Validation of the DHD with Linear Elements

To ascertain the accuracy of the DHD methodology, a case study including linear elements is now presented. The results provided here were compared against those obtained by a TD solution. Fig. 2.1 shows the test case where a source $v(t) = \sin(\omega_o t) + \frac{1}{2}\sin(5\omega_o t)$, with $\omega_o = 377\text{rad/s}$, is connected to the network. In the TD, the set of ODEs for the circuit is:

$$\frac{d}{dt}\begin{bmatrix} i_x(t) \\ v_x(t) \end{bmatrix} = \begin{bmatrix} R/L & 0 \\ -1/C & 0 \end{bmatrix}\begin{bmatrix} i_x(t) \\ v_x(t) \end{bmatrix} + \begin{bmatrix} Y_f/L \\ Y_f \end{bmatrix} v(t). \tag{2.12}$$

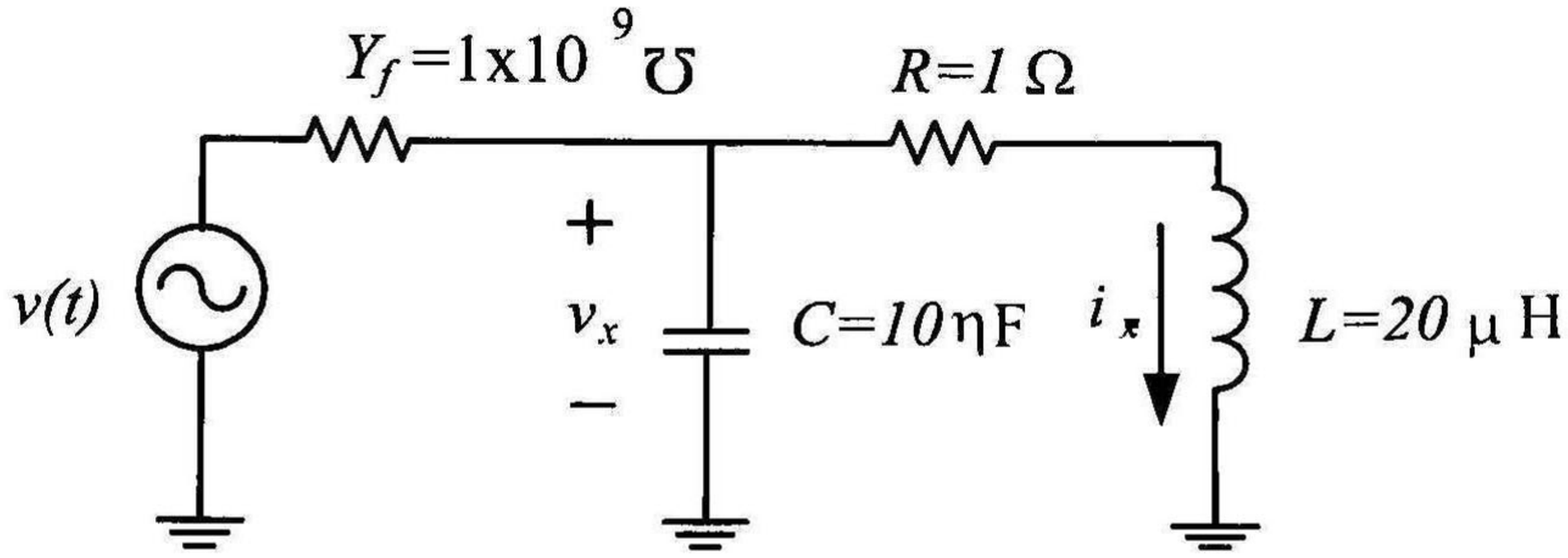


Figure 2.1: Electrical network with linear elements.

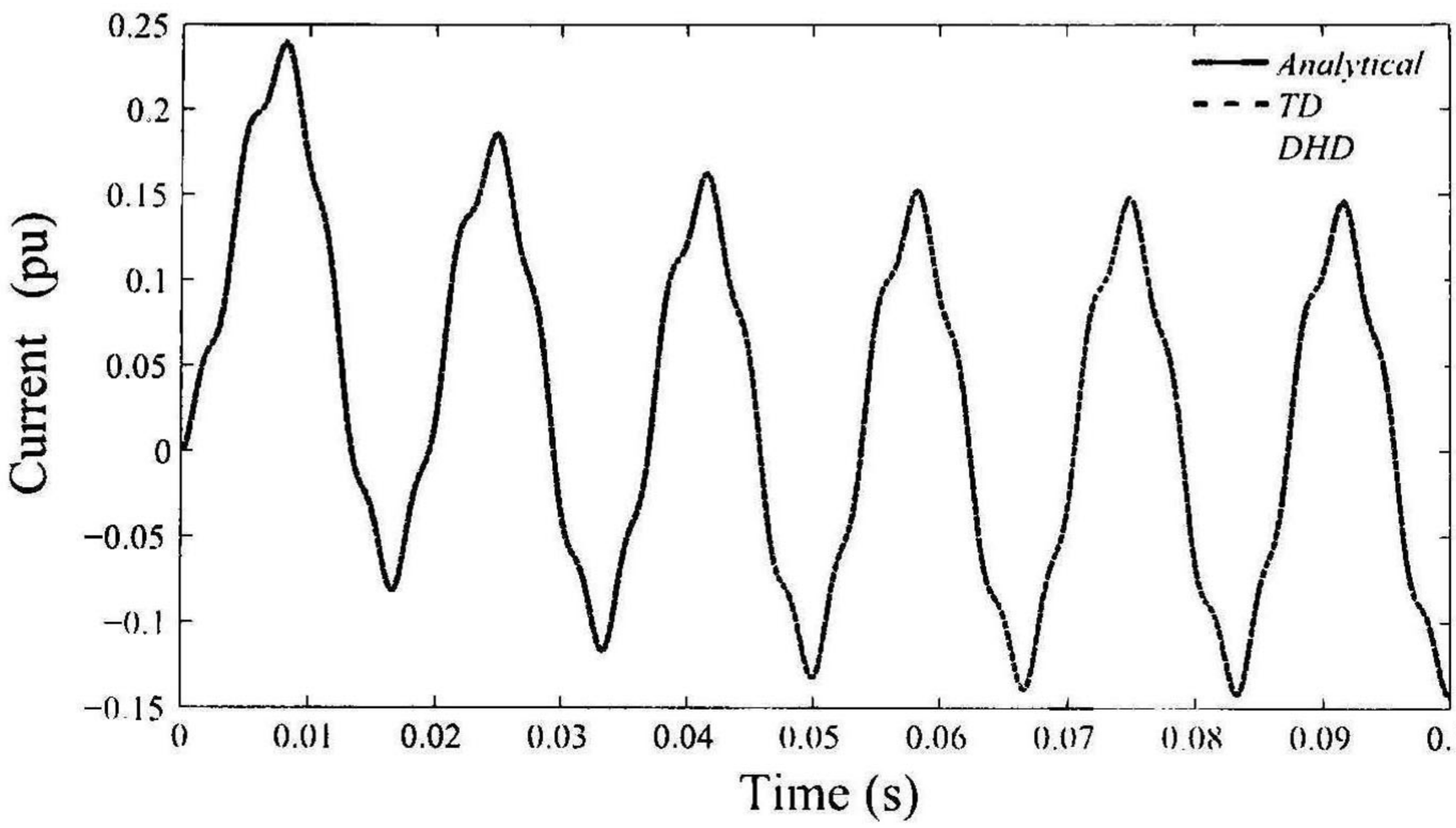


Figure 2.2: Current $i_x$.

Table 2.1: Time/Error Comparison

| **Technique** | **CPU-time** | **RMS-error** |
|---|---|---|
| TD | 0.016s | $5.3712 \times 10^{-4}$ |
| DHD | 0.061s | $4.5623 \times 10^{-4}$ |

By following the procedure outlined in Section 2.1, (2.12) is expressed in the DHD as:

$$\frac{d}{dt}\begin{bmatrix} \mathbf{i}_x \\ \mathbf{v}_x \end{bmatrix} = \begin{bmatrix} \frac{R}{L}\mathbf{I}_d - \mathbf{S} & 0 \\ \mathbf{I}_d/C & -\mathbf{S} \end{bmatrix}\begin{bmatrix} \mathbf{i}_x \\ \mathbf{v}_x \end{bmatrix} + \begin{bmatrix} \mathbf{Y}_f/L \\ \mathbf{Y}_f \end{bmatrix}\mathbf{v} \tag{2.13}$$

where $\mathbf{I}_d$ is the identity matrix with corresponding dimensions.

The numerical solution of (2.12) and (2.13) consists on applying the Trapezoidal Rule with a time step $\Delta t$ equal to $10\mu s$ for both TD and DHD. In the latter, five harmonics are

used. Fig. 2.2 presents the results with TD, DHD, and the analytical solution. Taking the analytical solution as the basis, Table 2.1 shows the absolute error and the computational time for TD and DHD, using a computer with 3GHz processor, 500MB RAM and Matlab 7.0.

From Table 2.1, one can notice that both TD and DHD give results with an error around $10^{-4}$ Additionally, from Table 2.1 it can be noticed that DHD takes almost four times the CPU time required by TD. This is due to the increased size of the ODEs system in the DHD.

### 2.3.3 Nonlinear Elements

Among the different nonlinear elements within a power network, in this work the nonlinear flux/current relation $i(t) = f(\psi)$ has been chosen to represent a nonlinear reactor. Specifically, it is represented by the polynomial approximation:

$$i = \alpha\psi + \beta\psi^n \tag{2.14}$$

In the DHD (2.14) becomes [11]:

$$\mathbf{i} = \alpha\mathbf{\Psi} + \beta\mathbf{\Psi}^n \tag{2.15}$$

The harmonic vector $\mathbf{\Psi}^n$ in (2.15) is calculated by harmonic convolution, denoted here with the symbol $\otimes$ and given by:

$$\mathbf{\Psi}^2 = \mathbf{\Psi} \otimes \mathbf{\Psi} = \mathbf{T}_o\mathbf{\Psi}, \tag{2.16}$$

where

$$\mathbf{T}_o = \begin{bmatrix} \psi_o & \psi_{-1} & \cdots & \psi_{-h} & \\ \psi_1 & \psi_o & & & \psi_{-h} \\ \vdots & & & & \vdots \\ \psi_h & & & \psi_o & \psi_{-1} \\ & \psi_h & \cdots & \psi_1 & \psi_o \end{bmatrix}$$

For the general case, it can be easily shown that

$$\mathbf{\Psi}^n = \mathbf{\Psi} \otimes \cdots \otimes \mathbf{\Psi} = \mathbf{T}_o^{n-1}\mathbf{\Psi}. \tag{2.17}$$

The complete representation of the nonlinear load requires the voltage/flux relation

$$v(t) = \dot{\psi}, \tag{2.18}$$

which in the DHD becomes [11]

$$\mathbf{v} = \dot{\mathbf{\Psi}} + \mathbf{S}\mathbf{\Psi}. \tag{2.19}$$

### 2.3.4 Validation of the DHD with a Nonlinear Load

As a more elaborated example, consider the circuit shown in Fig. 2.3. It consists of a source $u_o = \sin(\omega_o t) + 0.1\sin(3\omega_o t) + 0.05\sin(5\omega_o t)$, with $\omega_o = 1$, $R_o = 0.1$, $L_o = 0.3$, a lumped parameters transmission line with $R = 0.2$, $L = 0.2$, $C = 0.2$, and a nonlinear reactor as a load having a current/flux relation given by $i = 1.2\psi + 0.5\psi^3$ (all parameters in pu). The set of nonlinear ODEs in the TD for the circuit is

$$\dot{\mathbf{x}} = \begin{bmatrix} \dot{x}_1 \\ \dot{x}_2 \\ \dot{x}_3 \\ \dot{x}_4 \\ \dot{x}_5 \end{bmatrix} = \mathbf{ax} + \mathbf{bu}, \tag{2.20}$$

where

$$\mathbf{a} = \begin{bmatrix} -R_o/L_o & -1/L_o & 0 & 0 & 0 \\ 1/C & 0 & -1/C & 0 & 0 \\ 0 & 1/L & -R/L & -1/L & 0 \\ 0 & 0 & 1/C & 0 & -(\alpha + \beta x_5^2)/C \\ 0 & 0 & 0 & 1 & 0 \end{bmatrix}, \mathbf{b} = \begin{bmatrix} -1/L_o \\ 0 \\ 0 \\ 0 \\ 0 \end{bmatrix}$$

The DHD counterpart of (2.20) is

$$\dot{\mathbf{X}} = (\mathbf{A} - \mathbf{S})\mathbf{X} + \mathbf{BU}, \tag{2.21}$$

where:

$$\mathbf{A}-\mathbf{S} = \begin{bmatrix} -(\frac{R_o}{L_o}\mathbf{I}_d + \mathbf{S}) & -\mathbf{I}_d/L_o & 0 & 0 & 0 \\ \mathbf{I}_d/C & -\mathbf{S} & -\mathbf{I}_d/C & 0 & 0 \\ 0 & \mathbf{I}_d/L & -(\frac{R}{L}\mathbf{I}_h + \mathbf{S}) & -\mathbf{I}_d/L & 0 \\ 0 & 0 & \mathbf{I}_d/C & 0 & -(\alpha + \beta\Psi^2)/C \\ 0 & 0 & 0 & \mathbf{I}_d & -\mathbf{S} \end{bmatrix}, \mathbf{B} = \begin{bmatrix} -\mathbf{I}_d/L_o \\ 0 \\ 0 \\ 0 \\ 0 \end{bmatrix}$$

The source in the network (see Fig. 2.3) is connected at $t = 0$ and the current through the nonlinear load is calculated by solving both the TD set of nonlinear ODEs (2.20) and the corresponding set of DHD nonlinear ODEs (2.21) with $h = 15$ and a time step $\Delta t = 0.0017(rad/s)$. The voltage is shown in Fig. 2.4a where it can be observed that the two resultant waveforms (labeled TD and DHD) are superimposed. It is mentioned at this point that the accuracy of the DHD results depends on the number of harmonics included in the modeling. In this specific case we have taken up to 15 harmonics, being the most representative in magnitude for the transient. Additionally, Fig. 2.4b presents the harmonics behavior along the time.

## 2.4 DHD versus WFFT

The DHD technique has been further compared in this work with alternate techniques. One of the frequently used methods for harmonic estimation is the windowed fast Fourier transform (WFFT) [12], [32]. The WFFT consists on using a sliding window through the TD signal for obtaining its harmonic variation via FFT operations each time the window

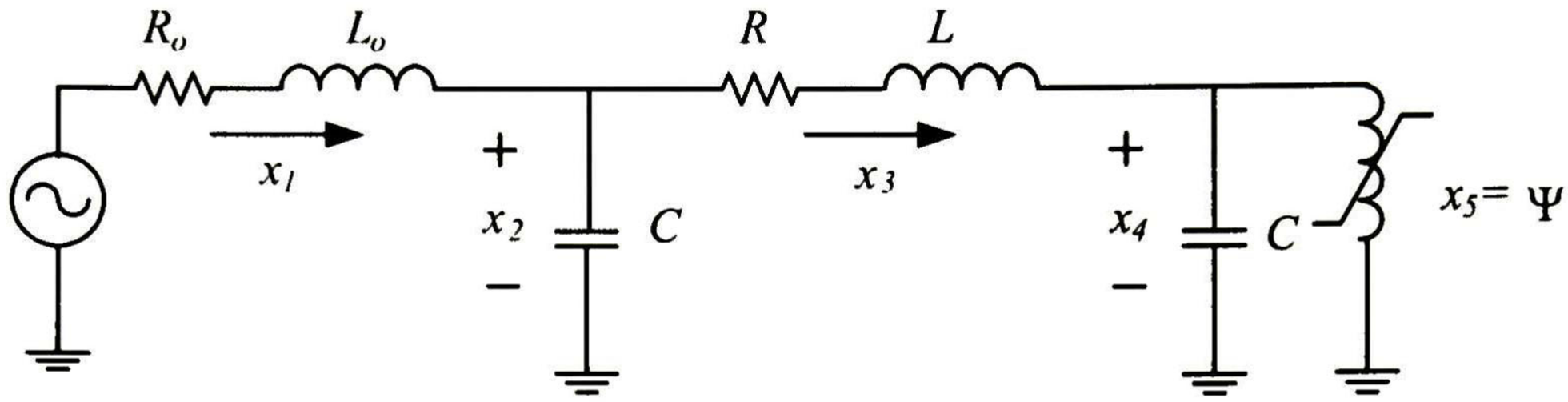


Figure 2.3: Electrical network with nonlinear load, testing the DHD.

slides. However, WFFT suffers of several numerical errors, such as picket-fence, leakage, etc. as described in [4]. For the example described in Section 2.3.4, the continuous signal shown in Fig. 2.1a is discretized with 1280 points and the WFFT is applied by using a sliding window with 128 points wide (sampling rate of 7.68 kHz). In order to diminish the leakage error, each time the FFT is applied, it is multiplied by the data window by Von Hann (also known as Hanning). The corresponding results are presented in Fig. 2.4b. From this figure, one can notice that the harmonics dynamics resulting from the WFFT are unacceptable during the transient period. It is also noticed from Fig. 2.4b. that the error of the WFFT becomes smaller as the waveform settles to steady state, as expected.

It is important to mention that, although FFT-based methods are accurate and efficient in stationary conditions, they lose accuracy under time-varying conditions, especially for fast disturbances. See [13] and [14] for a detailed analysis of the WFFT technique and its companion errors.

For this example, the computational times by the DHD and the WFFT are 11.5s and 2.5s, respectively, using a Pentium IV, 3-GHz, 512-MB RAM.

## 2.5 Conclusions

In this Chapter, the DHD technique was described and applied to circuit networks that include linear and nonlinear elements yielding results similar in precision to those obtained by the TD. A major disadvantage of the DHD is the increased size of the ODEs system, thus making the computational time larger than the one by using TD. Nevertheless, the DHD permits to follow step-by-step the harmonics behavior along the transient with accuracy dictated by a predefined number of harmonics and without the need of a postprocessing procedure, such as the WFFT. Additionally, the instantaneous voltage/current waveform can be constructed (step-by-step) from its corresponding harmonic (Fourier) coefficients which are arranged as DHD vectors.

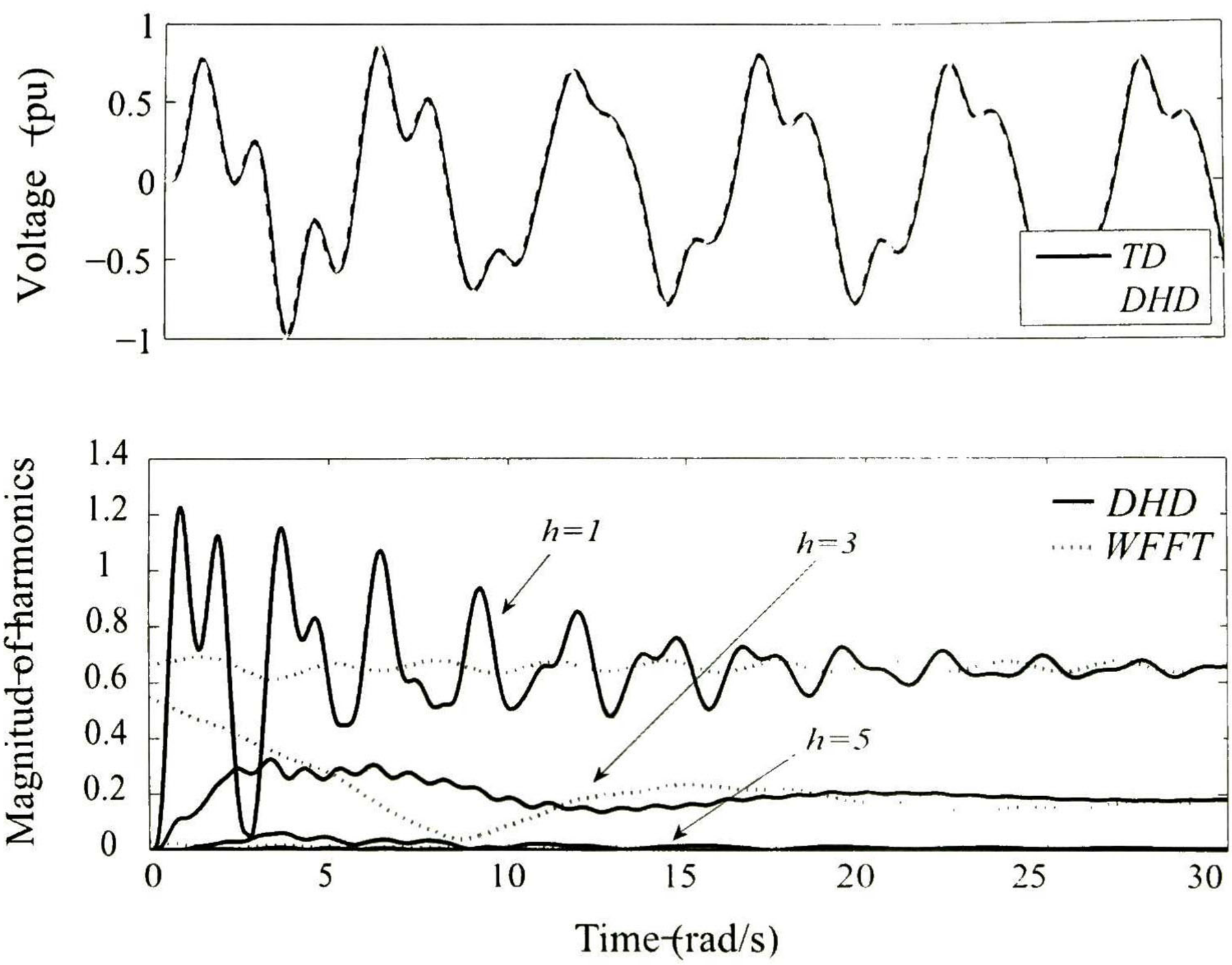


Figure 2.4: a) Voltage $x_4$, and b) harmonic content, nonlinear load.

Chapter 3

# Transmission Line DHD Modeling

TRANSMISSION lines are usually modeled for transient studies either in the frequency domain (FD) or in the time domain (TD). A partial list of important developments in the line modeling area is [15]- [22]. In general, the line and its termination are considered as linear elements. However, the increasing use of electronic devices and nonlinear loads in power systems has produced the necessity of considering also nonlinear terminations in the line modeling.

In this Chapter the model of the transmission line, based on the traveling wave approach and combined with the dynamic harmonic domain (DHD) technique [14], is presented. Additionally, the interfacing between the transmission line and nonlinear/linear loads is outlined.

## 3.1 Traveling Waves Method in the TD

Considering the reference directions for a three phase transmission line as depicted in Fig. 3.1, the FD relations between incident currents ($i'$) and reflected currents ($i''$) for both ends of the line (and for a given mode) are:

$$i'_m = H_{mode} i''_n, \tag{3.1a}$$
$$i'_n = H_{mode} i''_m, \tag{3.1b}$$

where $H_{mode}$ represents the modal propagation function [23], [24]. Approximating $H_{mode}$ by rational functions [21], we can express (3.1) as:

$$i'_m = [\mathbf{c}_1(s\mathbf{I} - \mathbf{A}_1)^{-1}\mathbf{b}_1] i''_n, \tag{3.2a}$$
$$i'_n = [\mathbf{c}_1(s\mathbf{I} - \mathbf{A}_1)^{-1}\mathbf{b}_1] i''_m. \tag{3.2b}$$

In (3.2), the set of poles ($k$ poles), obtained from the rational fitting, are contained in the diagonal matrix $\mathbf{A}_1$ of dimensions $k \times k$; the column vector $\mathbf{b}_1(k \times 1)$ has all entries equal to 1, and the residues of the realization are contained in the row vector $\mathbf{c}_1(1 \times k)$.

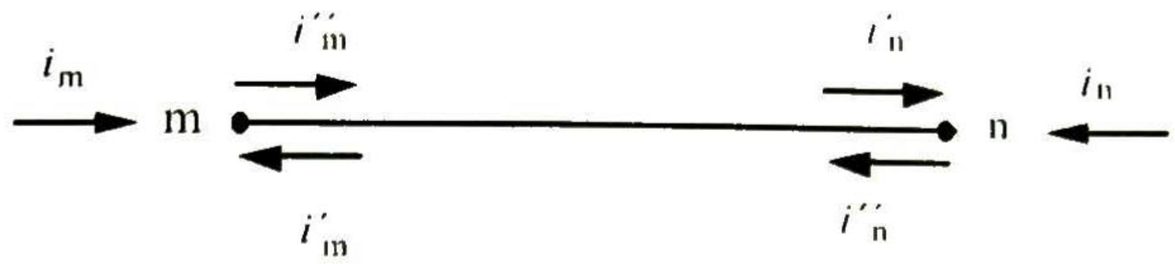


Figure 3.1: Transmission line reference directions

Additionally, $s$ represents the complex frequency given by $s = \alpha + j\omega$. From (3.2) we define:

$$\mathbf{x}_1 = (s\mathbf{I} - \mathbf{A}_1)^{-1}\mathbf{b}_1 i''_n, \tag{3.3a}$$
$$\mathbf{x}_2 = (s\mathbf{I} - \mathbf{A}_1)^{-1}\mathbf{b}_1 i''_m. \tag{3.3b}$$

Now, the TD image of (3.3) becomes

$$\dot{\mathbf{x}}_1 = \mathbf{A}_1 x_1 + \mathbf{b}_1 i''_n, \tag{3.4a}$$
$$\dot{\mathbf{x}}_2 = \mathbf{A}_1 x_2 + \mathbf{b}_1 i''_m. \tag{3.4b}$$

Thus, the state-space realization for the two line nodes $(m, n)$ is:

$$\begin{bmatrix} \dot{\mathbf{x}}_1 \\ \dot{\mathbf{x}}_2 \end{bmatrix} = \begin{bmatrix} \mathbf{A}_1 & \\ & \mathbf{A}_1 \end{bmatrix} \begin{bmatrix} \mathbf{x}_1 \\ \mathbf{x}_2 \end{bmatrix} + \begin{bmatrix} \mathbf{b}_1 & \\ & \mathbf{b}_1 \end{bmatrix} \begin{bmatrix} i''_n \\ i''_m \end{bmatrix}, \tag{3.5a}$$
$$\begin{bmatrix} i'_n \\ i'_m \end{bmatrix} = \begin{bmatrix} \mathbf{c}_1 & \\ & \mathbf{c}_1 \end{bmatrix} \begin{bmatrix} \mathbf{x}_1 \\ \mathbf{x}_2 \end{bmatrix} \tag{3.5b}$$

It is mentioned here that the reflected currents $i''_n$ and $i''_m$ are calculated at time $t - \tau$, with $\tau$ being the travel time. Additionally, the terminal relations in phase domain between currents and voltages are described by:

$$\mathbf{Y}_c v_m - \mathbf{i}_m = 2i'_m, \tag{3.6a}$$
$$\mathbf{Y}_c v_n - \mathbf{i}_n = 2i'_n, \tag{3.6b}$$

where $\mathbf{Y}_c$ corresponds to the characteristic admittance of the line, being also approximated by rational functions. Following a similar procedure, the state-space representation of (3.6a) is given as:

$$\dot{\mathbf{x}}_3 = \mathbf{A}_2\mathbf{x}_3 + \mathbf{B}_2\mathbf{v}_m, \tag{3.7a}$$
$$\mathbf{i}_m = \mathbf{C}_2\mathbf{x}_3 + \mathbf{D}_2\mathbf{v}_m - 2\mathbf{i}'_m, \tag{3.7b}$$

and of (3.6b) is given as:

$$\dot{\mathbf{x}}_4 = \mathbf{A}_2\mathbf{x}_4 + \mathbf{B}_2\mathbf{v}_n, \tag{3.8a}$$
$$\mathbf{i}_n = \mathbf{C}_2\mathbf{x}_4 + \mathbf{D}_2\mathbf{v}_n - 2\mathbf{i}'_n. \tag{3.8b}$$

## 3.2 Traveling Waves Method in the DHD

Since (3.5a) corresponds to a set of linear ODEs, its DHD counterpart is easily found as:

$$\begin{bmatrix} \dot{\mathbf{x}}_1 \\ \dot{\mathbf{x}}_2 \end{bmatrix} = \begin{bmatrix} \mathbf{A}_1 - \mathbf{S}' & \\ & \mathbf{A}_1 - \mathbf{S}' \end{bmatrix} \begin{bmatrix} \mathbf{x}_1 \\ \mathbf{x}_2 \end{bmatrix} + \begin{bmatrix} \mathbf{B}_1\boldsymbol{\Gamma} & \\ & \mathbf{B}_1\boldsymbol{\Gamma} \end{bmatrix} \begin{bmatrix} \mathbf{i}'_{m} \\ \mathbf{i}'_{n} \end{bmatrix}. \tag{3.9}$$

and the output relation (3.5b) becomes

$$\begin{bmatrix} \mathbf{i}'_{m} \\ \mathbf{i}'_{n} \end{bmatrix} = \begin{bmatrix} \mathbf{C}_1 & \\ & \mathbf{C}_1 \end{bmatrix} \begin{bmatrix} \mathbf{x}_1 \\ \mathbf{x}_2 \end{bmatrix}. \tag{3.10}$$

The size and the arrangement of the state-realization in the DHD differ from the TD formulation. Based on (3.9) and (3.10), in the DHD we have the following definitions with corresponding dimensions shown in round parentheses:

$$\mathbf{A}_1 = diag\{\mathbf{a}_1\mathbf{I}_d, \mathbf{a}_2\mathbf{I}_d, \ldots \mathbf{a}_k\mathbf{I}_d\}, (kh \times kh), \tag{3.11a}$$

$$\mathbf{S}' = diag\{\mathbf{S}, \mathbf{S} \ldots \mathbf{S}\}, (kh \times kh), \tag{3.11b}$$

$$\mathbf{B}_1 = [\mathbf{I}_d, \mathbf{I}_d, \ldots \mathbf{I}_d]^T, (kh \times h), \tag{3.11c}$$

$$\mathbf{C}_1 = [c_1\mathbf{I}_d, c_2\mathbf{I}_d, \ldots c_k\mathbf{I}_d], (h \times kh). \tag{3.11d}$$

The time delay for all harmonics is taking into account by:

$$\boldsymbol{\Gamma} = diag\{e^{j\beta_{\omega_0}\tau} \ldots e^{j\beta_{\omega_0}\tau}, 1, e^{-j\beta_{\omega_0}\tau}, \ldots, e^{-j\beta_{\omega_0}\tau}\}. \tag{3.12}$$

Following a similar procedure, the DHD state-space representation of (3.7) and (3.8) are:

$$\dot{\mathbf{x}}_3 = (\mathbf{A}_2 - \mathbf{S}')\mathbf{x}_3 + \mathbf{B}_2\mathbf{v}_m, \tag{3.13a}$$

$$\mathbf{i}_m = \mathbf{C}_2\mathbf{x}_3 + \mathbf{D}_2\mathbf{v}_m - 2\mathbf{i}'_m, \tag{3.13b}$$

and

$$\dot{\mathbf{x}}_4 = (\mathbf{A}_2 - \mathbf{S}')\mathbf{x}_4 + \mathbf{B}_2\mathbf{v}_n, \tag{3.14a}$$

$$\mathbf{i}_n = \mathbf{C}_2\mathbf{x}_4 + \mathbf{D}_2\mathbf{v}_n - 2\mathbf{i}'_n, \tag{3.14b}$$

respectively: where $\mathbf{A}_2$, $\mathbf{B}_2$, $\mathbf{C}_2$ are defined in accordance with (3.11a)-(3.11d) and $\mathbf{D}_1 = d_1\mathbf{I}_h$. In addition to the propagation equations (3.9) and the terminal relations (3.13) and (3.14), we have to consider the terminations of the line. This is explained in the next Section.

## 3.3 Transmission Line-Nonlinear Load Interfacing

In this section the interfacing of the transmission line DHD model to a nonlinear load is presented. More advanced terminations such as synchronous machine and power electronic devices are outlined in Chapters 4 and 5.

Consider that a nonlinear load (the reactor described in Section 2.3.3) is connected in parallel to a linear resistive load (identical loads at each phase), both at the receiving end

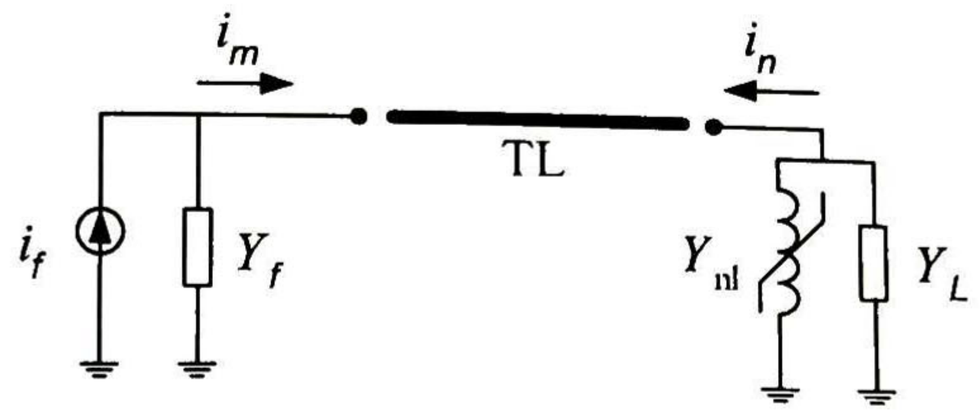


Figure 3.2: Transmission line end, nonlinear load

of the line (see Fig. 3.2). Hence, the expression for the entering current at node **n** is given by:

$$\mathbf{i}_n = -\left(\alpha\boldsymbol{\Psi} + \beta\boldsymbol{\Psi}^n + \mathbf{R}^{-1}\mathbf{v}_n\right). \tag{3.15}$$

First, substituting (3.15) into (3.14b) gives

$$\mathbf{v}_n = \mathbf{K}\left\{-(\alpha + \beta\Psi^{(n-1)})\Psi - \mathbf{C}_2\mathbf{x}_4 + 2\mathbf{i}'_n\right\}. \tag{3.16}$$

where $\mathbf{K} = (\mathbf{D}_2 + \mathbf{R}^{-1})^{-1}$ Next, substituting (3.16) into (3.14a) and taking the following voltage/flux relation into account:

$$\dot{\boldsymbol{\Psi}} + \mathbf{S}\boldsymbol{\Psi} = \mathbf{v}_n, \tag{3.17}$$

one obtains the final relations for node **n**

$$\begin{bmatrix} \dot{\mathbf{x}}_4 \\ \dot{\boldsymbol{\Psi}} \end{bmatrix} = \begin{bmatrix} \mathbf{A}_2 - \mathbf{S}' - \mathbf{B}_2\mathbf{K}\mathbf{C}_2 & -\mathbf{B}_2\mathbf{K}\left(\alpha + \beta\Psi^{(n-1)}\right) \\ -\mathbf{K}\mathbf{C}_2 & -\mathbf{K}\left(\alpha + \beta\Psi^{(n-1)}\right) - \mathbf{S} \end{bmatrix} \begin{bmatrix} \mathbf{x}_4 \\ \Psi \end{bmatrix} + 2\begin{bmatrix} \mathbf{B}_2\mathbf{K} \\ \mathbf{I}_h \end{bmatrix} \mathbf{i}'_n, \tag{3.18a}$$

$$\mathbf{i}_n = \begin{bmatrix} -\mathbf{R}^{-1}\mathbf{K}\mathbf{C}_2 & -(\mathbf{I}_h + \mathbf{R}^{-1}\mathbf{K})(\alpha + \beta\Psi^{(n-1)}) \end{bmatrix} \begin{bmatrix} \mathbf{x}_4 \\ \boldsymbol{\Psi} \end{bmatrix} - 2\mathbf{R}^{-1}\mathbf{K}\mathbf{i}'_n. \tag{3.18b}$$

Finally, after calculating $\mathbf{i}_n$ from (3.18b), the reflected current is updated with

$$\mathbf{i}_n = \mathbf{i}''_n - \mathbf{i}'_n. \tag{3.19}$$

Similarly for the node **m**

$$\mathbf{i}_m = \mathbf{i}''_m - \mathbf{i}'_m, \tag{3.20}$$

In the case of a network with several transmission lines, the procedure described above can be used. First, the incident currents are calculated for each line using expressions similar to (3.9) and (3.10). Then the solution for each load node can be calculated by using the nodal elimination as in (3.18). Finally, the reflected currents are updated with (3.19) and (3.20).

## 3.4 Case Example

### 3.4.1 Harmonic Dynamics

As an example of the proposed model and the interfacing methodology, the sequential closure of a three-phase transmission line with the geometrical configuration as shown in

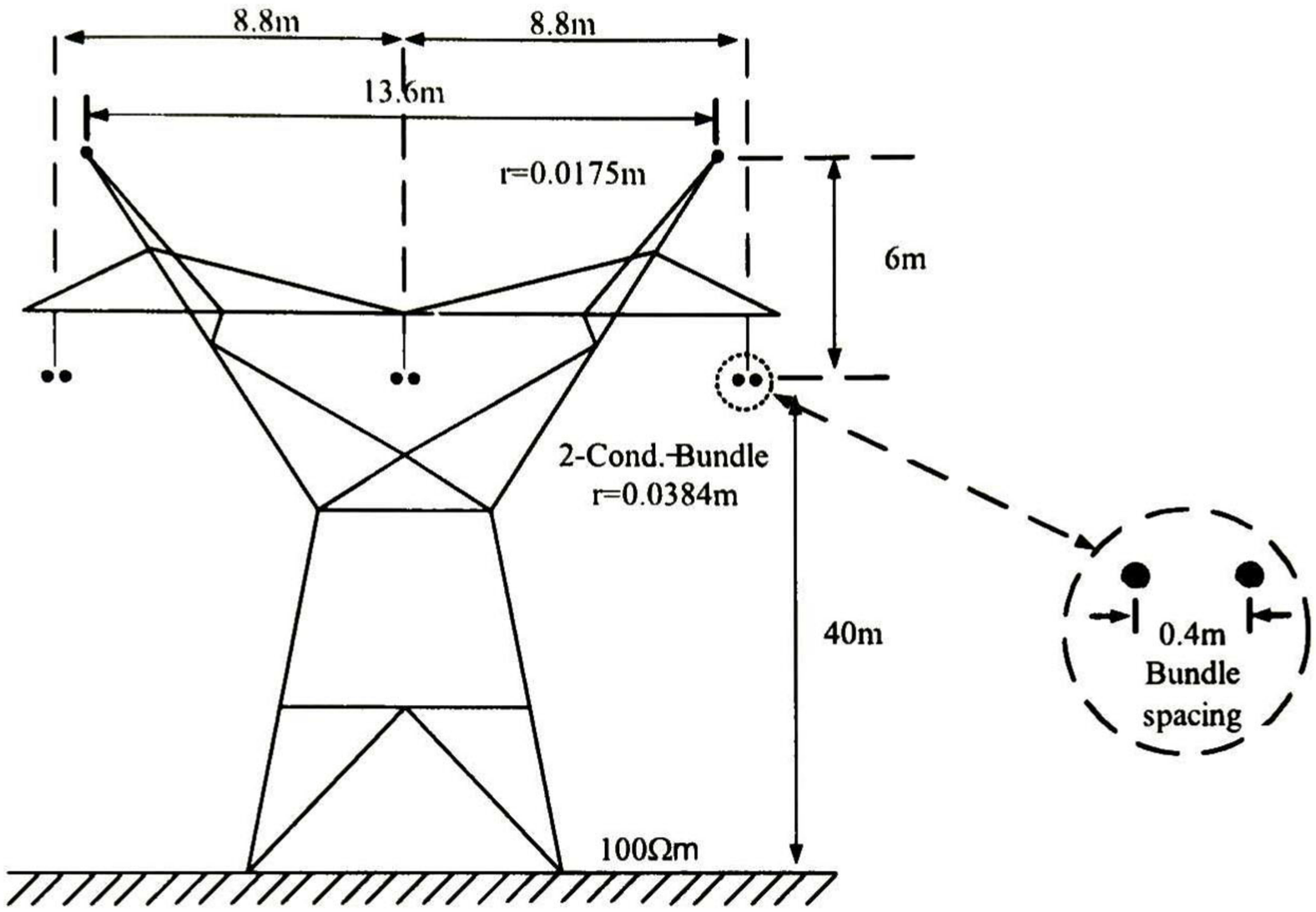


Figure 3.3: Transmission line configuration

Fig. 3.3 is presented. The closing of phases $a$, $b$ and $c$ is assumed to be at 180°, 120°, and 60°, respectively. At the receiving end a star-connected nonlinear load is assumed.

Fig. 3.4 shows the phase voltages $(v_a, v_b, v_c)$ and the harmonic content of $v_a$ at the receiving end of the line. The results from the DHD are compared with those obtained from the direct simulation of the system of nonlinear equations in the TD using a predictor-corrector type method and a time step of $\Delta t = 1\mu s$ for both solutions. Notice from Fig. 3.4 that both results (TD and DHD) are superimposed. Similarly, the corresponding currents $(i_a, i_b, i_c)$ and the harmonic content of $i_a$ are presented in Fig. 3.5.

For this example the per-phase nonlinear load, see (3.15), has been represented as a polynomial of order $n = 3$, and $h = 9$ has being considered.

It should be mentioned that, although the direct TD simulation takes much less time than the DHD, in the former the observation of the harmonic dynamics would need an additional post-processing procedure, such as the WFFT.

### 3.4.2 Frequency Analysis

A further analysis of the waveforms presented in Fig. 3.4b and 3.5b has shown that, in addition to the base *low* harmonics, mainly power frequency and third harmonic from the source, also *high* frequencies (not necessarily integer multiples of $h$) are present. For instance, Fig. 3.6 shows the resultant frequency content of the current waveform from Fig. 3.5(b) by using the discrete Fourier transform (obtained here through the FFT command from Matlab).

From Fig. 3.6, one can notice that the first nonharmonic frequency is about 748 Hz (between the 12th and 13th harmonic). This corresponds approximately to the frequency given by $1/1\tau$, being $\tau = 334\mu s$ the travel time for the 100-km line. The subsequent nonharmonic frequencies are spaced by approximately 1495 Hz, which corresponds to the first resonant peak of the line admittance (not shown here).

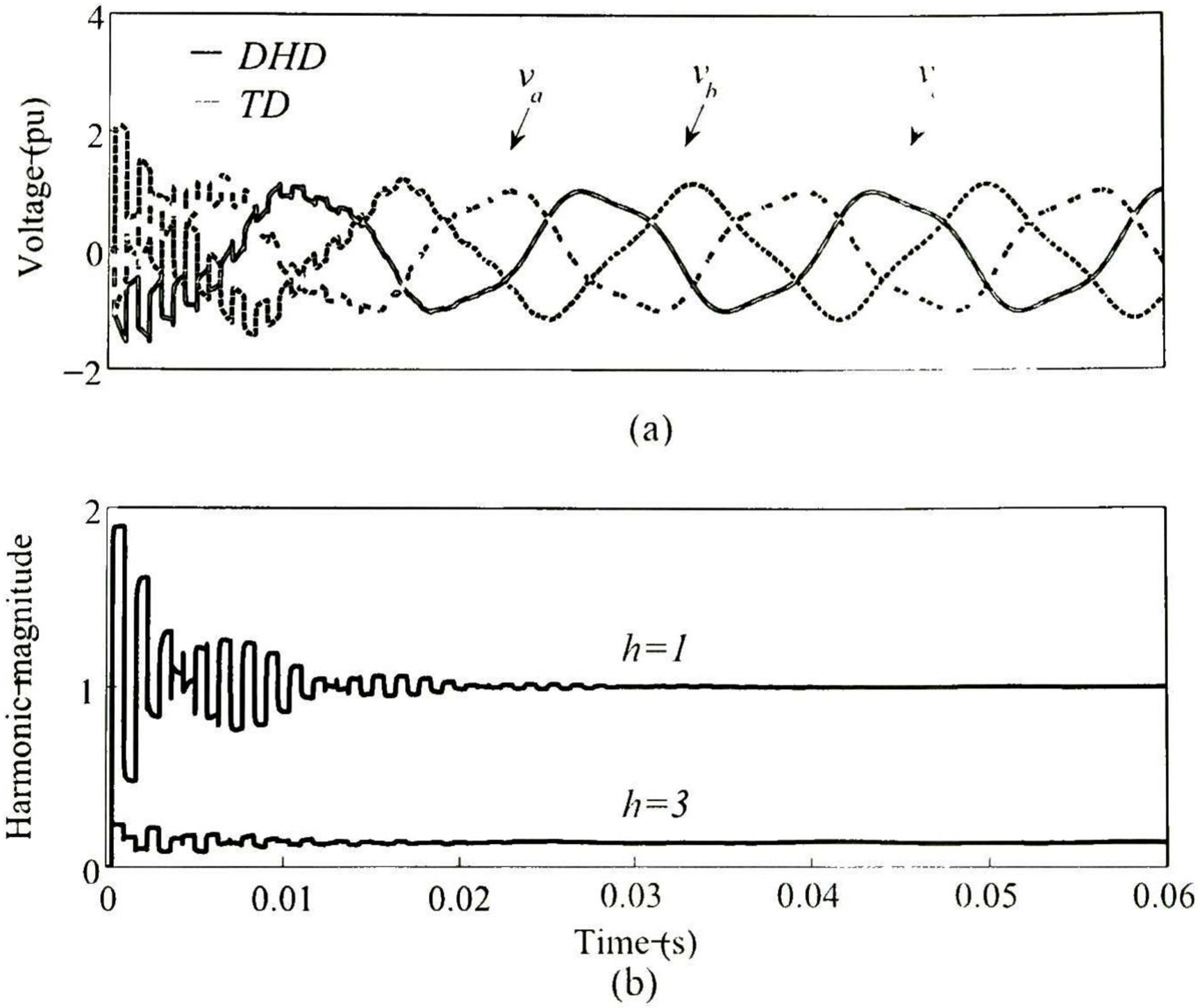


Figure 3.4: a) Voltage at bus $n$, and b) Its harmonic content phase $a$

The results outlined in the preceding paragraph demonstrate that the DHD has the capability of representing both the harmonic frequencies due to the source and the nonharmonic frequencies due to the natural frequencies of oscillation of the line. The latter cannot be represented explicitly in the DHD model; however, the harmonic coefficients take care of such frequencies by being nonconstant [11].

### 3.4.3 Power Quality Indices

Since the harmonic vectors are considered as time-varying in the DHD, the calculation of power quality indices can be made in a straightforward manner. As an illustrative example, Fig. 3.7 presents the apparent, real, reactive, and distortion powers at the load in phase $a$.

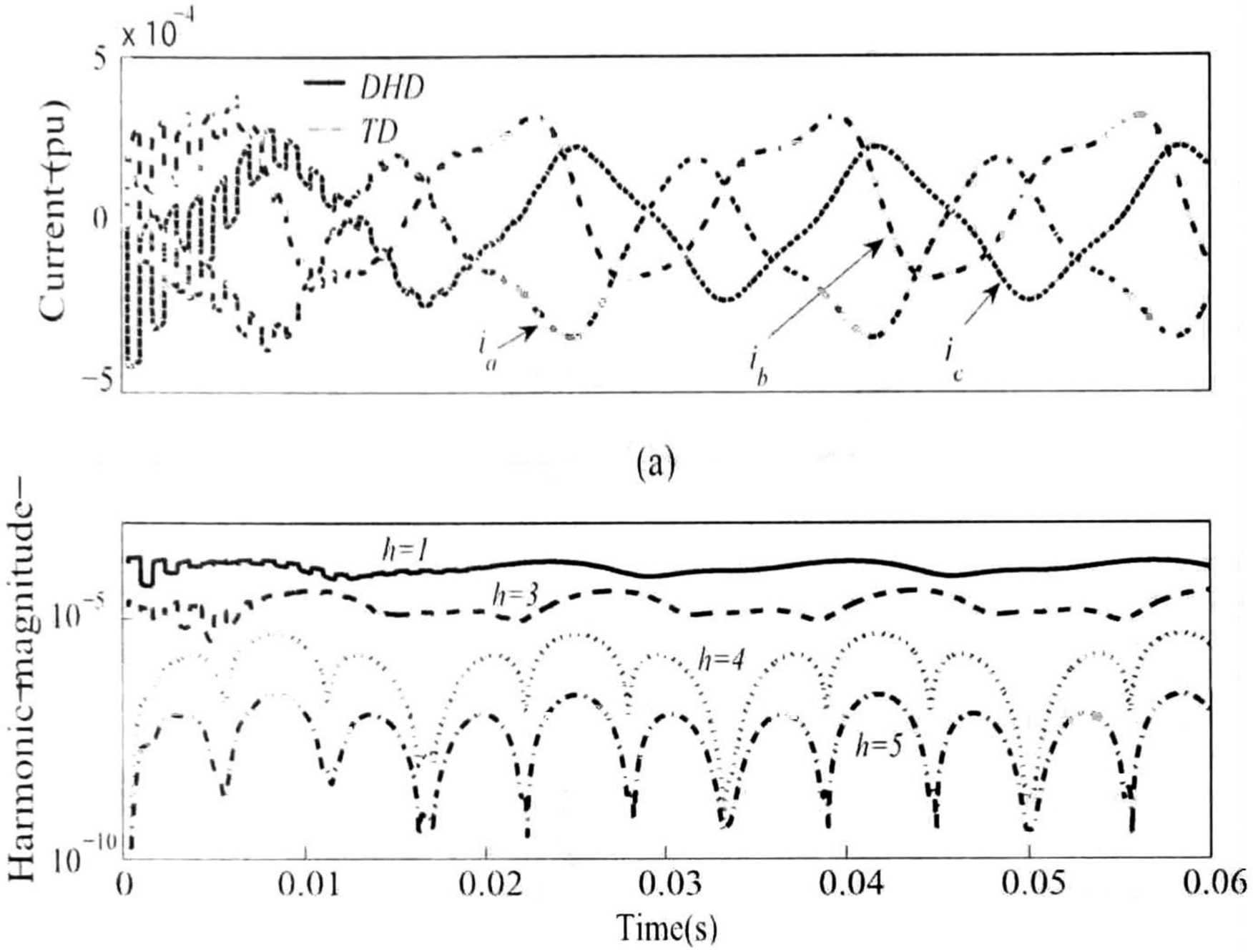


Figure 3.5: a) Current at bus $n$, and b) Its harmonic content phase $a$

yielded by the DHD and calculated by traditional formulae [7]:

$$S = \sqrt{\sum_{m=-\infty}^{\infty} \sum_{n=-\infty}^{\infty} |V_m|^2 |I_n|^2}, \tag{3.21a}$$

$$P = \sqrt{\sum_{m=-\infty}^{\infty} \sum_{n=-\infty}^{\infty} V_m I_{-m} V_n I_{-n}}, \tag{3.21b}$$

$$Q_H = \sqrt{\sum_{m=-\infty}^{\infty} |V_m|^2 |I_m|^2 - V_m I_{-m} V_m I_{-m}}, \tag{3.21c}$$

$$D_H = \sqrt{\sum_{m=-\infty}^{\infty} \sum_{n=-\infty, |n| \neq |m|}^{\infty} |V_m|^2 |I_n|^2 - V_m I_{-m} V_n I_{-n}}. \tag{3.21d}$$

From Fig. 3.7, one can see that the apparent power oscillates according to the line frequency mentioned above and reaches gradually the steady state. A further observation from Fig. 3.7 is that the envelope of the waveform presents an approximate second harmonic oscillation (120 Hz). Further potential applications of the proposed model to the power quality area, such as the analysis of disturbances, can be seen in [25].

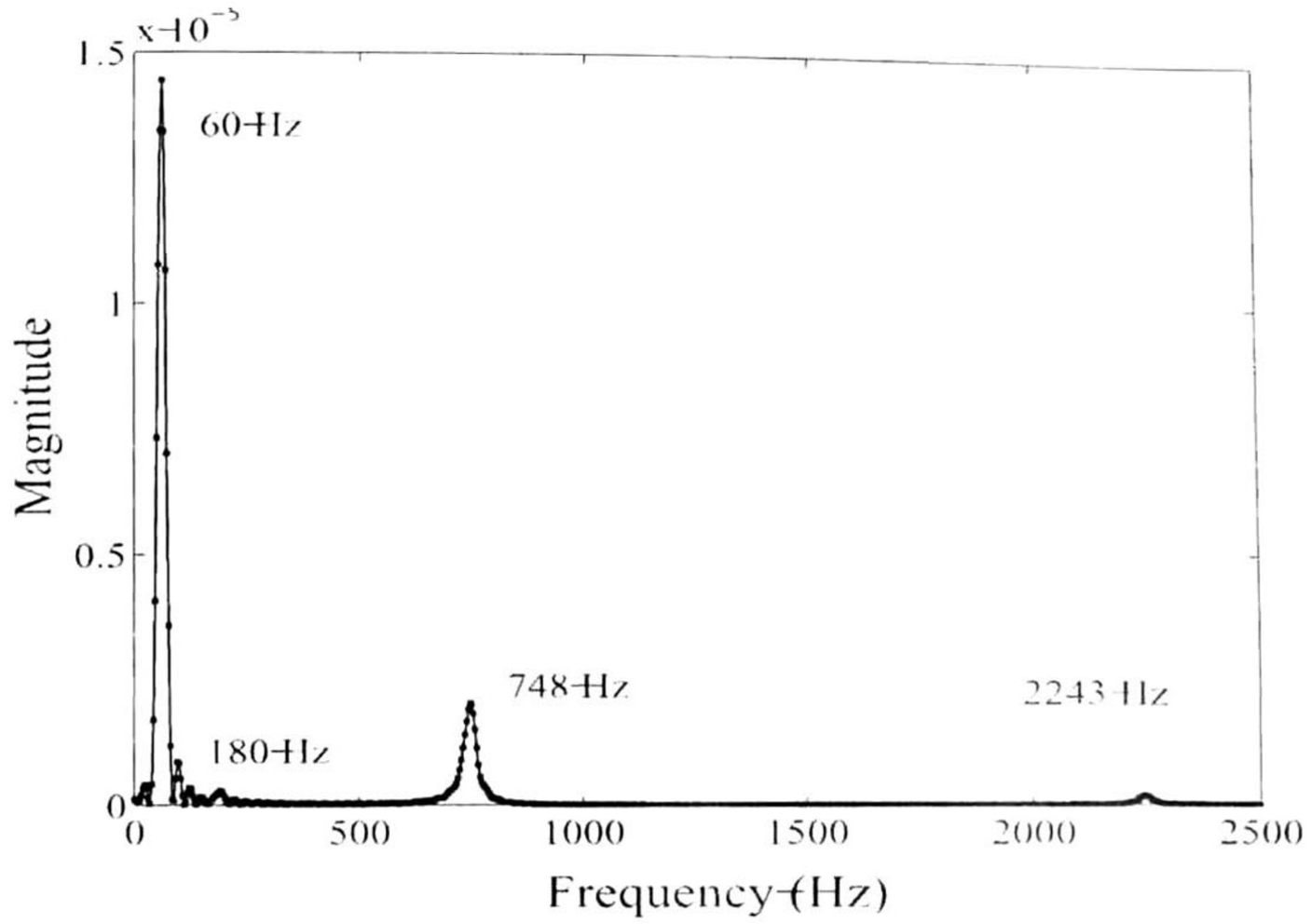


Figure 3.6: Frequency spectrum of current $i_n$ waveform phase $a$

## 3.5 Conclusions

In this Chapter, a DHD transmission line model capable of including the dynamics of the harmonics during transient state is proposed. The interfacing of nonlinear loads with a transmission line has been presented. Additionally, it has been shown that the time-varying harmonic coefficients are capable of representing the nonharmonic line frequencies involved during the transient. The validation of the proposed model has been made through the original nonlinear ODEs in the time domain.

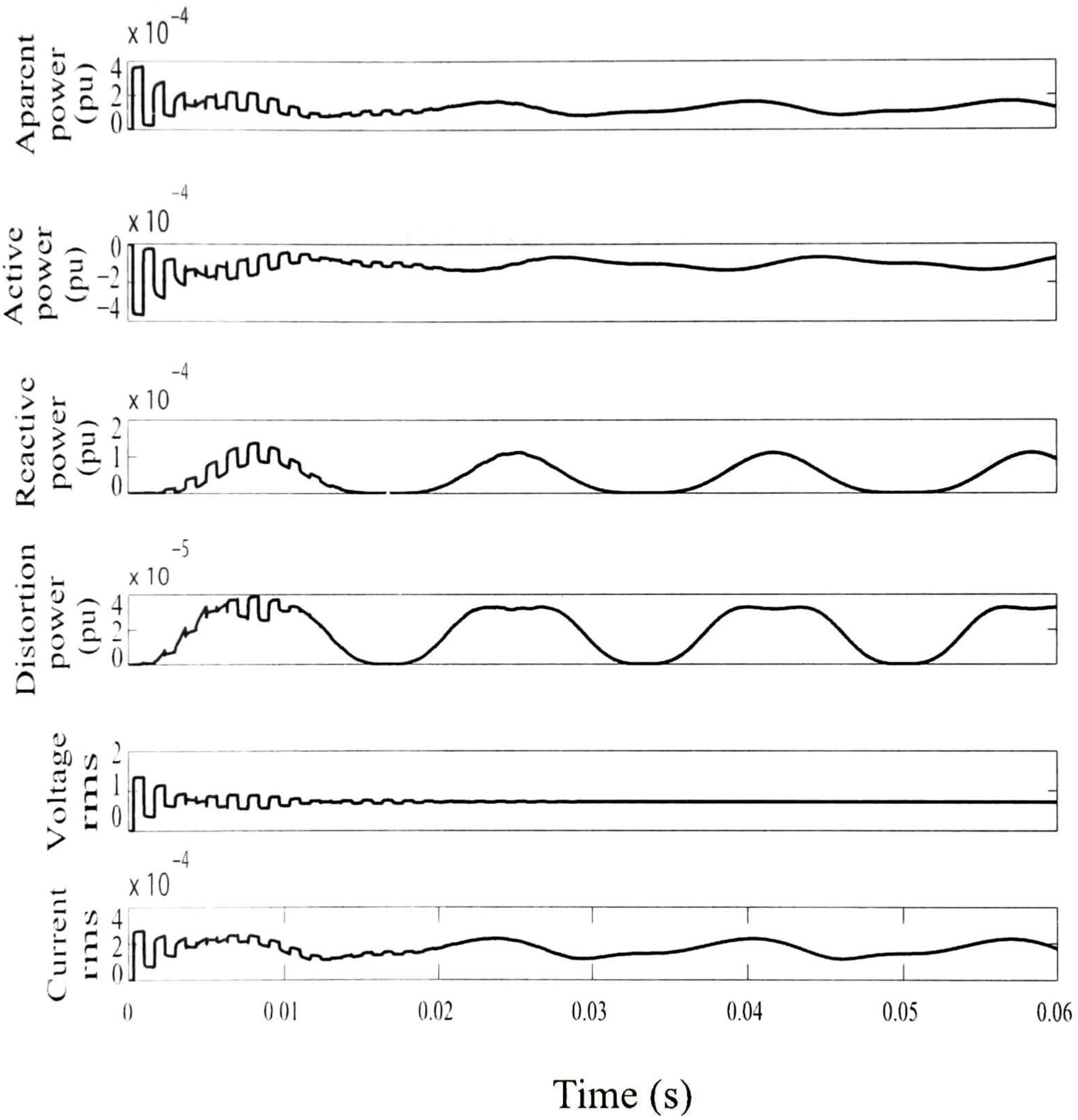


Figure 3.7: Power quality indices

Chapter 4

# Synchronous Machine-Transmission Line-Nonlinear Load System

THE interaction between synchronous generator, transmission line, and nonlinear loads has a significant bearing on the power quality of a system. It is well known that the operation of a synchronous machine under non-sinusoidal conditions can produce harmonics due to the intrinsic frequency conversion dynamics that exists between the stator and the rotor. The saturation of the rotor can enhance distortion in that frequency conversion process [26], [27]. In addition, the interconnection of a generator with an untransposed transmission line can produce resonances leading to over-voltages, failure of substation equipment, and even power system instability [28].

Several studies have been reported on the interconnection of a generator with a transmission line, a few of them dealing with harmonics [26]- [29]. However, most of the existing literature has focused on steady-state analysis. The need for harmonic analysis under transient conditions arises for filtering, control, and protection purposes due to the proliferation of a variety of nonlinear loads, especially fast switching power-electronic based loads.

## 4.1 Synchronous Machine Modeling

For this work, the notation from [30] has been adopted for the representation of a generator (the terms generator and synchronous machine are used interchangeably in this work) with two windings along the $d$-axis (F and D) and two along the $q$-axis (G and Q). The following definition is used:

$$\theta = \omega_o t + \theta_{rel}, \tag{4.1}$$

where $\omega_o$ is the electrical power frequency in rad/s, and the relative angle $\theta_{rel}$ is the deviation (from its uniformly rotating reference on phase $a$) of the rotor angle $\theta$ (defined as the angle between phase $a$ and the $d$-axis).

The synchronous machine can be represented in the TD as:

$$\begin{bmatrix} \mathbf{v}_s \\ \mathbf{v}_r \end{bmatrix} = \begin{bmatrix} \mathbf{R}_s & \\ & \mathbf{R}_r \end{bmatrix} \begin{bmatrix} \mathbf{i}_s \\ \mathbf{i}_r \end{bmatrix} + \frac{d}{dt} \begin{bmatrix} \boldsymbol{\Psi}_s \\ \boldsymbol{\Psi}_r \end{bmatrix}, \tag{4.2}$$

where the $s$ and $r$ subscripts describe stator and rotor quantities, respectively. The stator and rotor flux linkages are related to their corresponding currents by:

$$\begin{bmatrix} \Psi_s \\ \Psi_r \end{bmatrix} = \begin{bmatrix} \mathbf{L}_s & \mathbf{L}_{sr} \\ \mathbf{L}_{rs} & \mathbf{L}_r \end{bmatrix} \begin{bmatrix} \mathbf{i}_s \\ \mathbf{i}_r \end{bmatrix}. \tag{4.3}$$

Inserting (4.3) into (4.2) gives:

$$\begin{bmatrix} \mathbf{v}_s \\ \mathbf{v}_r \end{bmatrix} = \begin{bmatrix} \mathbf{L}_s & \mathbf{L}_{sr} \\ \mathbf{L}_{rs} & \mathbf{L}_r \end{bmatrix} \frac{d}{dt} \begin{bmatrix} \mathbf{i}_s \\ \mathbf{i}_r \end{bmatrix} + \left\{ \begin{bmatrix} \mathbf{R}_s & \\ & \mathbf{R}_r \end{bmatrix} + \frac{d}{dt} \begin{bmatrix} \mathbf{L}_s & \mathbf{L}_{sr} \\ \mathbf{L}_{rs} & \mathbf{L}_r \end{bmatrix} \right\} \begin{bmatrix} \mathbf{i}_s \\ \mathbf{i}_r \end{bmatrix} \tag{4.4}$$

In the DHD (4.4) becomes (without change of notation)

$$\begin{bmatrix} \mathbf{v}_s \\ \mathbf{v}_r \end{bmatrix} = \mathbf{L} \frac{d}{dt} \begin{bmatrix} \mathbf{i}_s \\ \mathbf{i}_r \end{bmatrix} + \left\{ \mathbf{R} + \mathbf{L}\mathbf{S}_{sr} + \frac{d}{d\theta}\mathbf{L} \right\} \begin{bmatrix} \mathbf{i}_s \\ \mathbf{i}_r \end{bmatrix}, \tag{4.5}$$

where (using Matlab notation)

$$\mathbf{L} = \begin{bmatrix} \mathbf{L}_s & \mathbf{L}_{sr} \\ \mathbf{L}_{rs} & \mathbf{L}_r \end{bmatrix}, \ \mathbf{R} = blkdiag\{\mathbf{R}_s, \mathbf{R}_r\},$$

$$\mathbf{S}_{sr} = blkdiag\{\mathbf{S}_s, \mathbf{S}_r\},$$

$$\mathbf{S}_s = blkdiag\{\mathbf{S}, \mathbf{S}, \mathbf{S}\}, \ \mathbf{S}_r = \{\mathbf{S}', \mathbf{S}', \mathbf{S}', \mathbf{S}'\},$$

$$\mathbf{S} = diag\{\ldots, -3j\omega_o, -j\omega_o, j\omega_o, 3j\omega_o, \ldots\},$$

$$\mathbf{S}' = diag\{\ldots, -4j\omega_o, -2j\omega_o, 0, 2j\omega_o, 4j\omega_o, \ldots\},$$

where it can be noticed that for stator (rotor) quantities only even (odd) harmonics are used.

The flux linkages are related to the currents by

$$\begin{bmatrix} \Psi_a \\ \Psi_b \\ \Psi_c \\ \Psi_F \\ \Psi_D \\ \Psi_G \\ \Psi_Q \end{bmatrix} = \begin{bmatrix} L_{aa} & L_{ab} & L_{ac} & L_{aF} & L_{aD} & L_{aG} & L_{aQ} \\ L_{ba} & L_{bb} & L_{bc} & L_{bF} & L_{bD} & L_{bG} & L_{bQ} \\ L_{ca} & L_{cb} & L_{cc} & L_{cF} & L_{cD} & L_{cG} & L_{cQ} \\ L_{Fa} & L_{Fb} & L_{Fc} & L_F & M_X & & \\ L_{Da} & L_{Db} & L_{Dc} & L_X & M_D & & \\ L_{Ga} & L_{Gb} & L_{Gc} & & & L_G & M_Y \\ L_{Qa} & L_{Qb} & L_{Qc} & & & L_Y & M_Q \end{bmatrix} \begin{bmatrix} \mathbf{i}_a \\ \mathbf{i}_b \\ \mathbf{i}_c \\ \mathbf{i}_F \\ \mathbf{i}_D \\ \mathbf{i}_G \\ \mathbf{i}_Q \end{bmatrix} \tag{4.6}$$

To illustrate the DHD structure of the inductance matrix (4.6), consider only four representative terms, using $\pm 3$ harmonics for the stator, and $\pm 2$ for the rotor, as described below [28].

### 4.1.1 Stator-Self Inductance

Consider the self-inductance for phase $a$

$$\begin{aligned} L_{aa} &= L_s + L_m \cos 2(\omega_o t + \theta_o) \\ &= Ls + \frac{Lm}{2} e^{-j2\theta_o} e^{-j2\omega_o t} + \frac{L_m}{2} e^{j2\theta_o} e^{j2\omega_o t} \\ &= L_{aa}^{o} + L_{aa}^{-2} e^{-j2\omega_o t} + L_{aa}^{+2} e^{j2\omega_o t} \end{aligned} \tag{4.7}$$

The harmonic content of $L_{aa}$ from (4.7) is included in a Topelitz-type matrix. This inductance matrix multiplies a stator current vector to produce a stator flux vector as follows:

$$\begin{bmatrix} L_{aa}^{o} & L_{aa}^{-2} & & \\ L_{aa}^{2} & L_{aa}^{o} & L_{aa}^{-2} & \\ & L_{aa}^{2} & L_{aa}^{o} & L_{aa}^{-2} \\ & & L_{aa}^{2} & L_{aa}^{o} \end{bmatrix} \begin{bmatrix} i_a^{-3} \\ i_a^{-1} \\ i_a^{+1} \\ i_a^{+3} \end{bmatrix} = \begin{bmatrix} \Psi_a^{-3} \\ \Psi_a^{-1} \\ \Psi_a^{+1} \\ \Psi_a^{+3} \end{bmatrix} \tag{4.8}$$

### 4.1.2 Stator-Rotor Inductance

We have the inductance between phase $a$ and the field winding as

$$\begin{aligned} L_{aF} &= M_F \cos(\omega_o t + \theta_o) \\ &= \frac{M_F}{2} e^{-j\theta_o} e^{-j\omega_o t} + \frac{M_F}{2} e^{j\theta_o} e^{j\omega_o t} \\ &= L_{aF}^{-1} e^{-j\omega_o t} + L_{aF}^{+1} e^{j\omega_o t} \end{aligned} \tag{4.9}$$

The resultant inductance matrix multiplies a rotor current vector to produce a stator flux vector as follows:

$$\begin{bmatrix} L_{aF}^{-1} & & & \\ L_{aF}^{+1} & L_{aF}^{-1} & & \\ & L_{aF}^{+1} & L_{aF}^{-1} & \\ & & L_{aF}^{+1} & \end{bmatrix} \begin{bmatrix} i_F^{-2} \\ i_F^{O} \\ i_F^{+2} \end{bmatrix} = \begin{bmatrix} \Psi_a^{-3} \\ \Psi_a^{-1} \\ \Psi_a^{+1} \\ \Psi_a^{+3} \end{bmatrix} \tag{4.10}$$

### 4.1.3 Rotor-Stator Inductance

In this case we have the inductance between the field winding and phase $a$, $L_{Fa} = L_{aF}$. The resultant inductance matrix multiplies a stator current vector to produce a rotor flux vector as follows:

$$\begin{bmatrix} L_{aF}^{+1} & L_{aF}^{-1} & & \\ & L_{aF}^{+1} & L_{aF}^{-1} & \\ & & L_{aF}^{+1} & L_{aF}^{-1} \end{bmatrix} \begin{bmatrix} i_a^{-3} \\ i_a^{-1} \\ i_a^{+1} \\ i_a^{+3} \end{bmatrix} = \begin{bmatrix} \Psi_F^{-2} \\ \Psi_F^{o} \\ \Psi_F^{+2} \end{bmatrix} \tag{4.11}$$

### 4.1.4 Rotor-Self Inductance

Consider the field inductance matrix, which multiplies a rotor current vector to produce a rotor flux vector as follows:

$$\begin{bmatrix} L_F & & \\ & L_F & \\ & & L_F \end{bmatrix} \begin{bmatrix} i_F^{-2} \\ i_F^{o} \\ i_F^{+2} \end{bmatrix} = \begin{bmatrix} \Psi_F^{-2} \\ \Psi_F^{o} \\ \Psi_F^{+2} \end{bmatrix} \tag{4.12}$$

All matrices in (4.8), (4.10)-(4.12) and the ones obtained from similar inductance terms, are used to form the total inductance matrix in (4.6).

The steady-state solution can be obtained by setting to zero the derivatives with respect to time in (4.5).

Alternatively, (4.5) can be expressed in a compact form as

$$\frac{d}{dt}\begin{bmatrix} \mathbf{i}_s \\ \mathbf{i}_r \end{bmatrix} = \mathbf{A}_g \begin{bmatrix} \mathbf{i}_s \\ \mathbf{i}_r \end{bmatrix} + \mathbf{L}^{-1} \begin{bmatrix} \mathbf{v}_s \\ \mathbf{v}_r \end{bmatrix} \tag{4.13}$$

where:

$$\mathbf{A}_g = -\mathbf{L}^{-1}\left\{\mathbf{R} + \mathbf{L}\mathbf{S}_{sr} + \frac{d}{d\theta}\mathbf{L}\right\}$$

Additionally, the mechanical dynamics of the machine is described (for a single-mass rotor) by:

$$\dot{\omega}_{rel} = \frac{\omega_o}{2H}[T_e - T_m + k_d\omega_{rel}], \tag{4.14a}$$

$$\dot{\theta} = \omega_{rel} - \omega_o, \tag{4.14b}$$

where $k_d$ represents a damping constant, $T_m$ is the mechanical torque, and the electrical torque is given by:

$$T_e = \frac{1}{2}\mathbf{i}^T \frac{d\mathbf{L}}{d\theta}\mathbf{i}. \tag{4.15}$$

In (4.15) the currents vector (**i**) contains stator and rotor currents. Also, from (4.15) one can notice that the complete set of harmonics contribute to the scalar electrical torque.

## 4.2 Interfacing Line and Synchronous Machine

The transmission line model in the DHD (see Chapter III) is now interfaced to the synchronous machine equations. In addition, linear/nonlinear loads connected at the receiving end of the line are included to form a small network.

From the output expression (3.13) the relation between sending end voltage and current is given by (note that $\mathbf{i}_m = -\mathbf{i}_s$ and $\mathbf{v}_s = \mathbf{v}_m$)

$$\mathbf{v}_s = \mathbf{D}_2^{-1}(2\mathbf{i}'_s - \mathbf{C}_2\mathbf{x}_3 - \mathbf{i}_s). \tag{4.16}$$

Substituting (4.5) into (3.13a) and taking into account (4.13) the transmission line and the generator models are linked as

$$\dot{\mathbf{x}}_3 = (\mathbf{A}_2 - \mathbf{S} - \mathbf{B}_2\mathbf{D}_2^{-1}\mathbf{C}_2)\mathbf{x}_3 + 2\mathbf{B}_2\mathbf{D}_2^{-1}\mathbf{i}'_s \quad \mathbf{B}_2\mathbf{D}_2^{-1}\mathbf{i}_s, \tag{4.17}$$

$$\frac{d}{dt}\begin{bmatrix} \mathbf{i}_s \\ \mathbf{i}_r \end{bmatrix} = \mathbf{G}_m \begin{bmatrix} \mathbf{i}_s \\ \mathbf{i}_r \end{bmatrix} - \mathbf{L}_{g1}^{-1}\mathbf{D}_2^{-1}\mathbf{C}_2\mathbf{x}_3 + 2\mathbf{L}_{g1}^{-1}\mathbf{D}_2^{-1}\mathbf{i}_s' + \mathbf{L}_{g2}^{-1}\mathbf{v}_r, \tag{4.18}$$

where

$$\mathbf{G}_m = -\mathbf{L}^{-1}\left\{ \begin{bmatrix} \mathbf{R}_s + \mathbf{D}_2^{-1} & \\ & \mathbf{R}_r \end{bmatrix} + \mathbf{L}\mathbf{S}_{sr} + \frac{d}{d\theta}\mathbf{L} \right\}.$$

Combining (4.17) and (4.18) into a state-space representation, we obtain

$$\begin{bmatrix} \mathbf{G}_m & -\mathbf{L}_{g1}^{-1}\mathbf{D}_2^{-1}\mathbf{C}_2 \\ \begin{bmatrix} -\mathbf{B}_2\mathbf{D}_2^{-1} & 0 \end{bmatrix} & \mathbf{A}_2 - \mathbf{S}_s - \mathbf{B}_2\mathbf{D}_2^{-1}\mathbf{C}_2 \end{bmatrix} \begin{bmatrix} \mathbf{i}_s \\ \mathbf{i}_r \\ \mathbf{x}_3 \end{bmatrix}$$
$$+ \begin{bmatrix} 2\mathbf{L}_{g1}^{-1}\mathbf{D}_2^{-1} & \mathbf{L}_{g2}^{-1} \\ 2\mathbf{B}_2\mathbf{D}_2^{-1} & 0 \end{bmatrix} \begin{bmatrix} \mathbf{i}_s' \\ \mathbf{v}_r \end{bmatrix} = \frac{d}{dt}\begin{bmatrix} \mathbf{i}_s \\ \mathbf{i}_r \\ \mathbf{x}_3 \end{bmatrix} \tag{4.19}$$

## 4.3 Algorithm for Transient Harmonic Analysis

The complete set of ODEs representing the generator-line-load system given by (3.16), (3.18), (4.19), and (4.14) considering a nonlinear load at the end of the line, can be expressed in compact form as

$$\begin{bmatrix} \dot{\mathbf{x}}_e \\ \dot{\mathbf{x}}_m \end{bmatrix} = \begin{bmatrix} \mathbf{A}_e & \\ & \mathbf{A}_m \end{bmatrix} \begin{bmatrix} \mathbf{x}_e \\ \mathbf{x}_m \end{bmatrix} + \begin{bmatrix} \mathbf{B}_e \\ \mathbf{B}_m \end{bmatrix} \mathbf{u}, \tag{4.20}$$

where $\mathbf{x}_e$ and $\mathbf{x}_m$ represent the harmonic vectors of electrical and mechanical state variables, respectively. Since the generator contains slow and fast dynamics at the same time, a hybrid algorithm is used for the numerical integration of (4.20) such that the stiffness of the complete system is overcome. The algorithm consists of the following four steps:

**Step 1**. Assume that the simulation begins with the system in steady-state. Initialize all the system variables.

**Step 2**. Using the Trapezoidal Rule for (4.20) the electrical state variables and the electrical torque are calculated at steps $k+1$ and $k+1/2$ by

$$\mathbf{m}_1\mathbf{x}_e^{k+1} = \mathbf{m}_2\mathbf{x}_e^k + \frac{\mathbf{B}_e^k}{2}(\mathbf{u}_k + \mathbf{u}_{k+1}), \tag{4.21a}$$

$$\mathbf{n}_1\mathbf{x}_e^{k+1/2} = \mathbf{n}_2\mathbf{x}_e^k + \frac{\mathbf{B}_e^k}{2}(\mathbf{u}_k + \mathbf{u}_{k+1/2}), \tag{4.21b}$$

where

$$\mathbf{m}_{1,2} = \left( \frac{1}{\Delta t}\mathbf{I} \mp \frac{1}{2}\mathbf{A}_e^k \right), \quad \mathbf{n}_{1,2} = \left( \frac{2}{\Delta t}\mathbf{I} \mp \frac{1}{2}\mathbf{A}_e^k \right),$$

and

$$\mathbf{x}_e^k = [\mathbf{x}_1, \mathbf{x}_2, \mathbf{x}_3, \mathbf{x}_4, \mathbf{i}_r, \mathbf{i}_s]^T$$

The electrical torque is obtained by

$$T_e^{k+1/2} = \frac{1}{2}\mathbf{i}_{s,k+1/2}^T \frac{d}{d\theta}\mathbf{L}^{k+1/2}\mathbf{i}_{s,k+1/2}. \tag{4.22}$$

**Step 3**. First, a predicted value of $\omega_{rel}$ is given by

$$p_1\hat{\omega}_{rel}^{k+3/2} = p_2\omega_{rel}^{k+1/2} + \frac{\omega_o}{2H}(T_e^{k+1/2} - T_m), \tag{4.23}$$

where $p_{1,2} = \frac{1}{\Delta t} \mp \frac{\omega_o k_d}{4H}$.

Then, a corrected value for $\theta_{rel}$ is obtaining using

$$\theta_{rel}^{k+3/2} = \theta_{rel}^{k+1/2} + \frac{\Delta t}{2}(\hat{\omega}_{rel}^{k+3/2} + \omega_{rel}^{k+1/2}) - \omega_o\Delta t. \tag{4.24}$$

Finally, with $\hat{\omega}_{rel}^{k+3/2}$ and $\theta_{rel}^{k+3/2}$ calculate inductance matrix $\mathbf{L}_\theta^{k+3/2}$ with

$$\frac{d}{d\theta}\mathbf{L}_\theta^{k+1} = (\frac{d}{d\theta}\mathbf{L}_\theta^{k+1/2} + \frac{d}{d\theta}\mathbf{L}_\theta^{k+3/2})/2, \tag{4.25}$$

**Step 4**. The average values for the electrical states and torque are computed as

$$\mathbf{x}_{ea} = (\mathbf{x}_e^{k+1/2} + \mathbf{x}_e^{k+1})/2, \tag{4.26a}$$

$$T_{ea} = (1/2)\mathbf{x}_{ea}^T\frac{d}{d\theta}\mathbf{L}^{k+1}\mathbf{x}_{ea}, \tag{4.26b}$$

$$p_1\omega_{rel}^{k+3/2} = p_1\omega_{rel}^{k+1/2} + \frac{\omega_o}{2H}(T_{ea} - T_m). \tag{4.26c}$$

## 4.4 Case Study

To ascertain the accuracy of the proposed algorithm, a case study is presented. The results provided here were compared against those obtained by PSCAD/EMTDC. In this software package the synchronous machine is based on a *dq* model (the proposed model is entirely in *abc* frame) and the transmission line is based on a frequency dependent line model.

Fig. 4.1(a) shows the test case where a 555MVA, 24 kV synchronous machine is connected to a $Y - Y$ transformer with $L = 0.08$pu and to a 100km open-ended transmission line. The geometry of the untransposed line is shown in Fig. 3.3. The synchronous machine parameters were obtained from [31]. Simulation results for steady-state as well as transient conditions are analyzed in the following subsections.

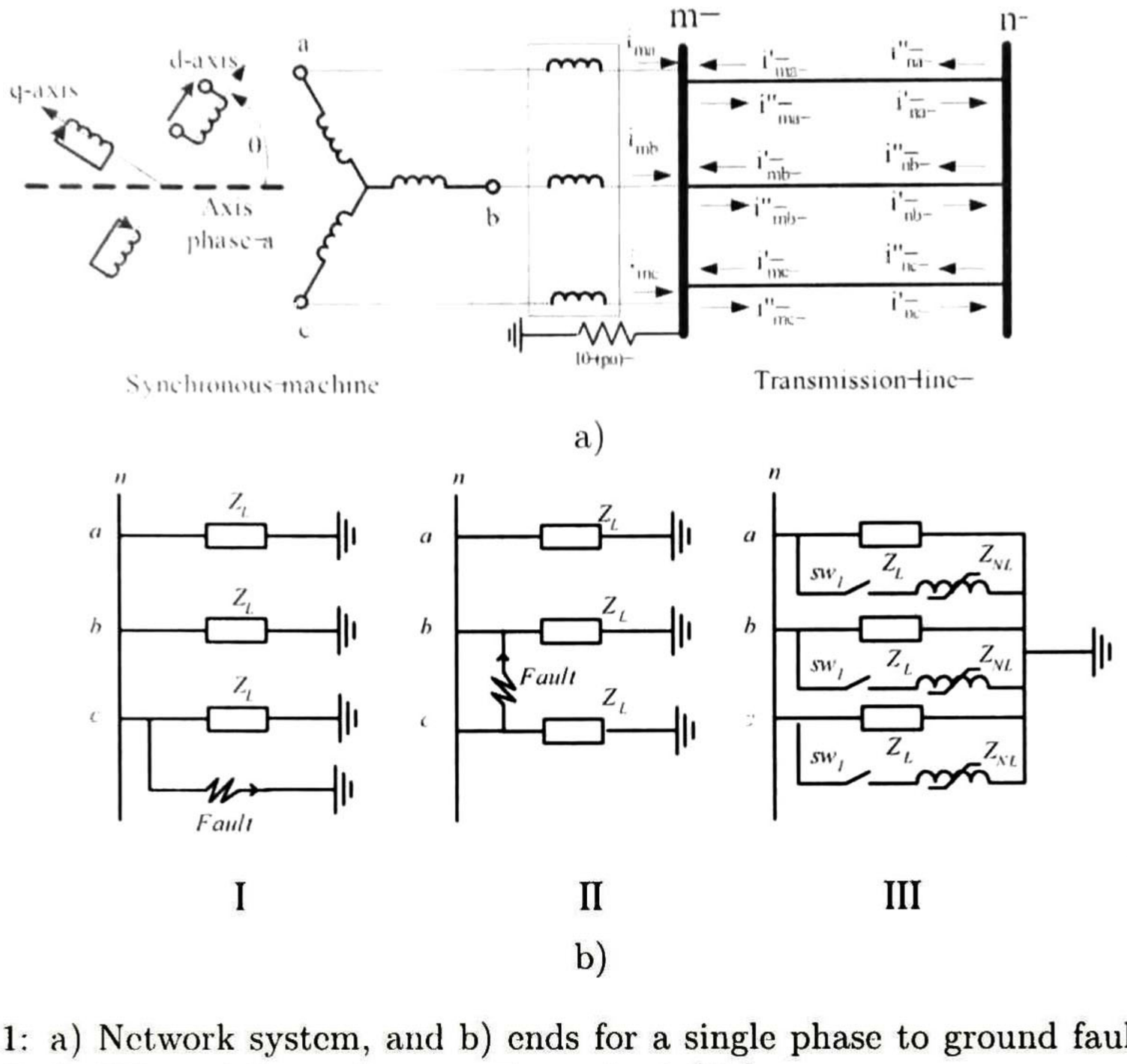


Figure 4.1: a) Network system, and b) ends for a single phase to ground fault (I), phase-to-phase fault (II), and three-phase nonlinear load (III).

### 4.4.1 Single-Phase Fault

The simulation starts in steady-state with the far end of the line having a load with $R = 10$pu and $L = 0.1$pu. After 0.0332s (second cycle) phase $c$ is connected to ground through a $10^{-3}$ pu resistance to simulate a phase to ground fault. Then at 0.05262s the fault is cleared and the same RL load is reconnected (fourth cycle, current crossing at zero) until a new steady-state is reached (see Fig. 4.1(b)-I). The instantaneous voltage waveforms at the line terminal, phase $c$ ($v_{nc}$), from both the DHD and the PSCAD/EMTDC, are presented in Fig. 4.2a. The corresponding harmonic content obtained through the DHD is also shown (lower vertical limit set to $10^{-9}$) in Fig. 4.2b. For the DHD simulation up to the $9^{th}$ harmonic was considered since the magnitudes of the remaining harmonics were negligible.

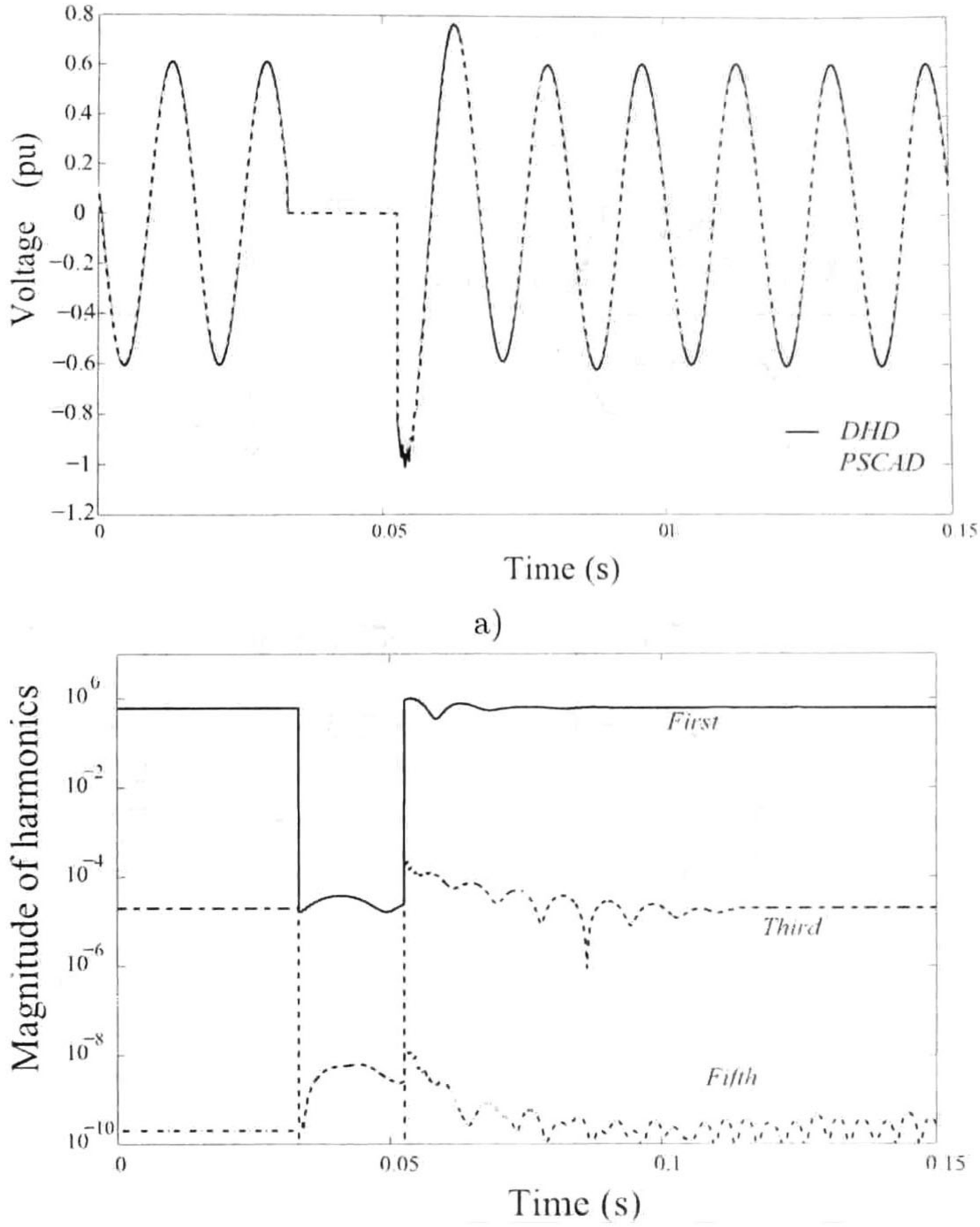


Figure 4.2: a) Voltage $v_{nc}$, and b) harmonic content of $v_{nc}$ during the single-phase fault.

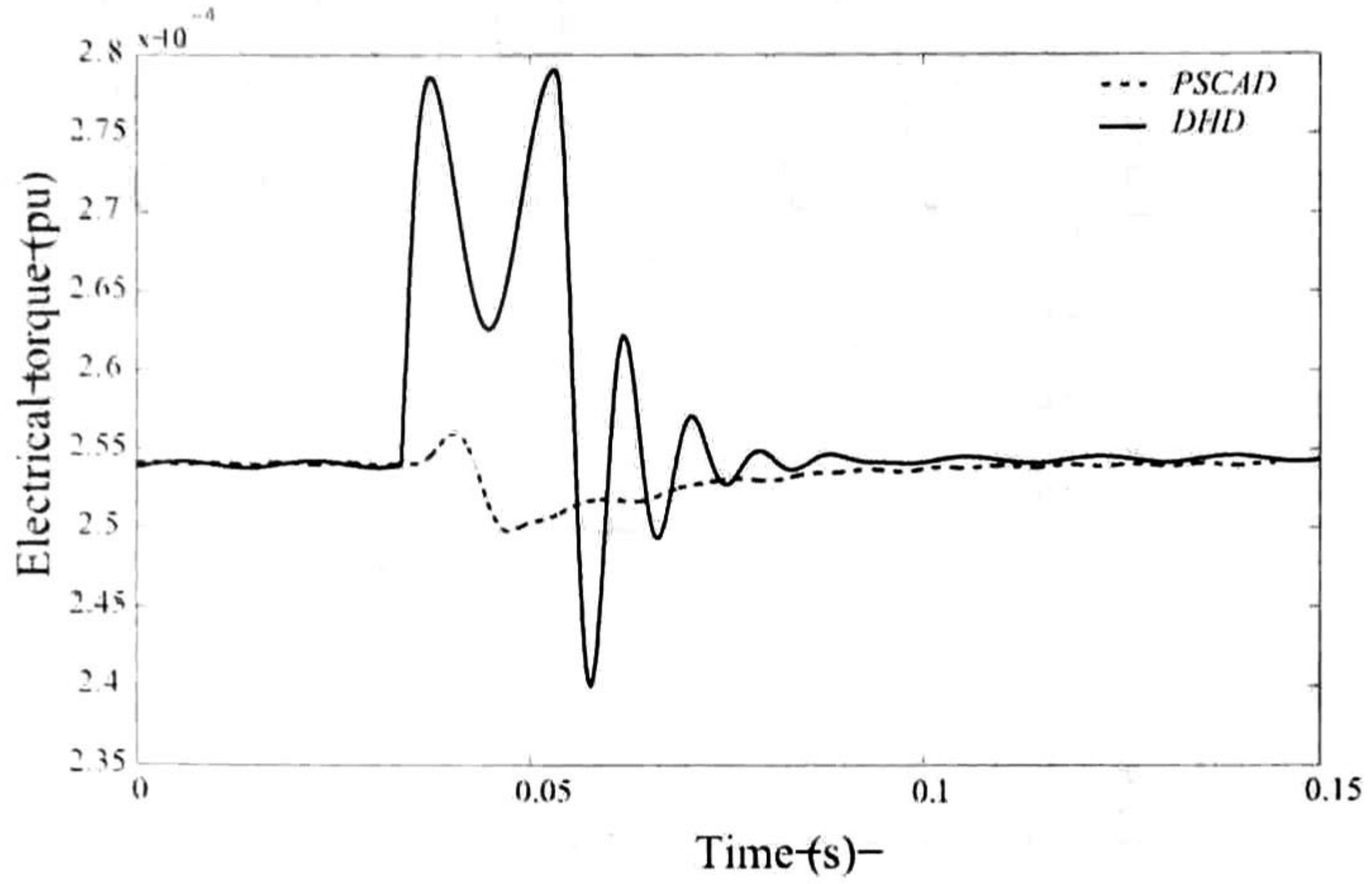


Figure 4.3: Machine electrical torque and speed during the single-phase fault.

From Fig. 4.2 one can notice the following:

a) During steady state all harmonics behave as constants, as expected.

b) Harmonics react instantaneously to system disturbances. Their dynamics are followed in a natural way by the DHD whilst post-processing techniques such as WFFT would have a slow harmonic time response [11], as proved in Section 2.4.

c) The proportionality of harmonic magnitudes for a given signal (voltage or current) changes from steady-state to the transient state.

d) Harmonic oscillations during a transient behave according to the line resonant frequency, traveling time, and excitation-related frequencies, as proved in Section 3.4.2.

e) After removing a fault, steady state is reached faster by low harmonics than by high harmonics.

f) Simply examining the time-domain results it is difficult to discern the steady-state condition. The DHD provide a visually active indicator of the transient and steady-state conditions in a signal.

For this specific example, the fault produced almost no distortion in the electrical torque, as shown in Fig. 4.3. Additionally, the machine speed remained constant and equal to 377 rad/s.

### 4.4.2 Phase-to-Phase Fault

A phase-to-phase fault is simulated between phases $b$ and $c$ as illustrated in Fig. 4.1(b)-II. The simulation starts in steady-state and after the second cycle a fault is inserted through a $10^{-3}$ pu resistance. Finally, after another two cycles the fault is cleared. Fig. 4.4(a) shows the current at bus **n**, phase $b$ ($i_{nb}$) and Fig. 4.5(a) shows the stator current at phase $b$ ($i_{sb}$) with their corresponding harmonic content shown in Figs. 4.4(b) and Fig. 4.5(b), respectively. From Figs. 4.4 and 4.5 we can notice that the system tries to reach a different steady-state sequentially, and all of the observations from the single-phase fault case are also applicable to the phase-to-phase fault.

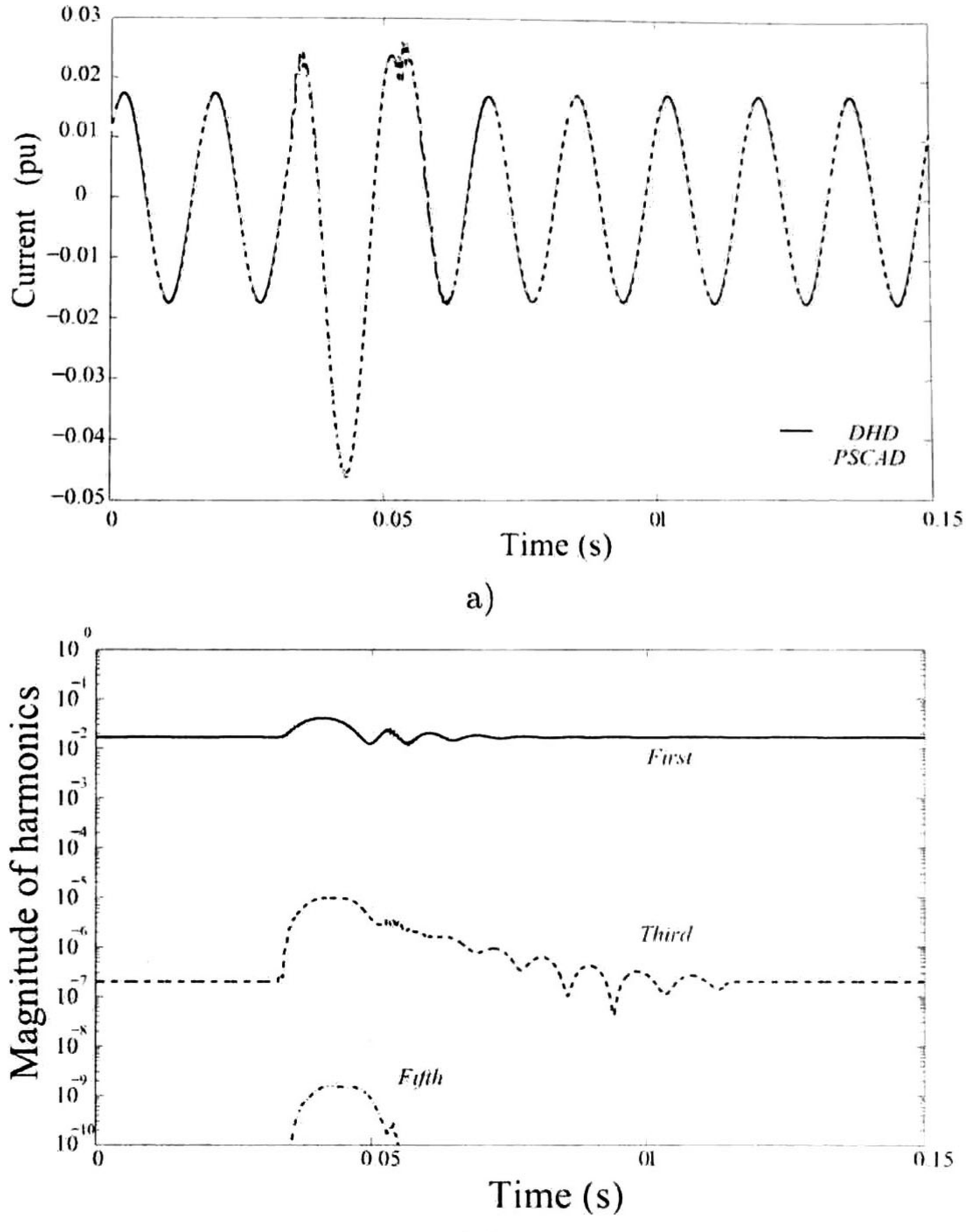


Figure 4.4: a) Current $i_{nb}$, and b) harmonic content of $i_{nb}$, during the line-to-line fault.

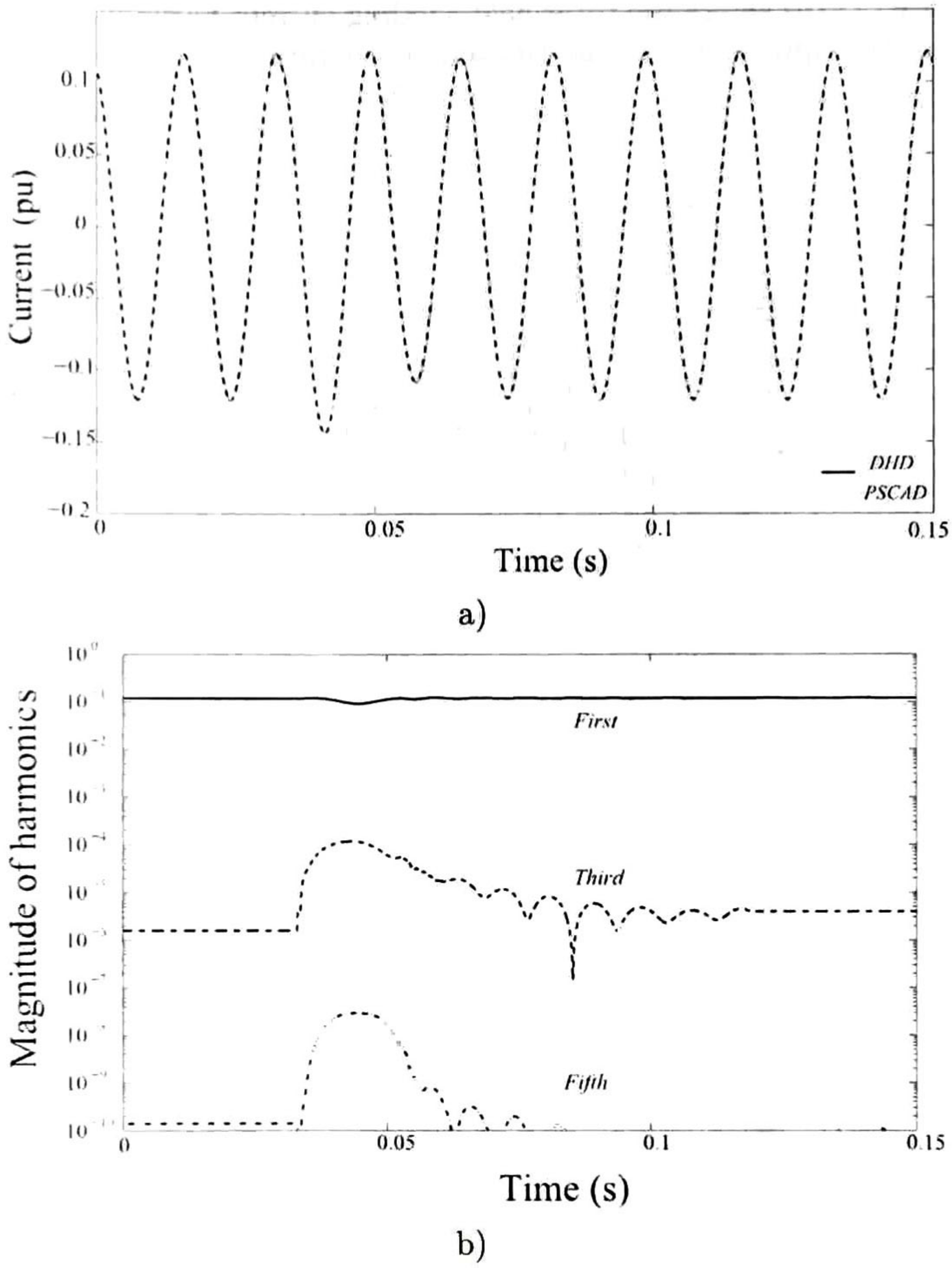


Figure 4.5: (a) Current $i_{mb}$ and b) harmonic content of $i_{mb}$, during the phase-to-phase fault.

### 4.4.3 Three-Phase Nonlinear Load

The proposed DHD methodology is now applied to an example with a nonlinear reactor as a load. For this example the simulation starts in steady-state, and after $0.0332s$ a nonlinear load ($\alpha = 0.5$, $\beta = 5 \times 10^6$) in parallel with a 10 pu resistance is connected in each phase at bus **n**. The simulation ends at $0.15s$. In Fig. 4.6, the voltages at bus **n** are shown. As expected, one can notice from the figures that the harmonic distortion is larger when the nonlinear load is introduced into the network compared to the preceding cases using linear loads. In this example it is found that nine harmonics were sufficient. In other cases the number can be more or less depending on the type of nonlinear elements included in the network. A steady-state solution using the HD can be used to figure out the approximate number of harmonic coefficients required in a dynamic study.

Additionally, Fig. 4.7 shows the rotor current ($i_r$) and its various components. $i_F$ is the field winding current which produces flux in the direct axis (connected to the DC source of the excitation system); $i_D$ is the quadrature axis winding current which represents

slowly changing fluxes produced by deep-flowing eddy currents; $i_G$ is the direct axis winding current which represents damping bar effects; $i_Q$ is the quadrature axis winding representing damping bar effects.

Fig. 4.7(b) shows the rotor field winding current harmonic magnitudes, where only even harmonics appear due to the DC source excitation.

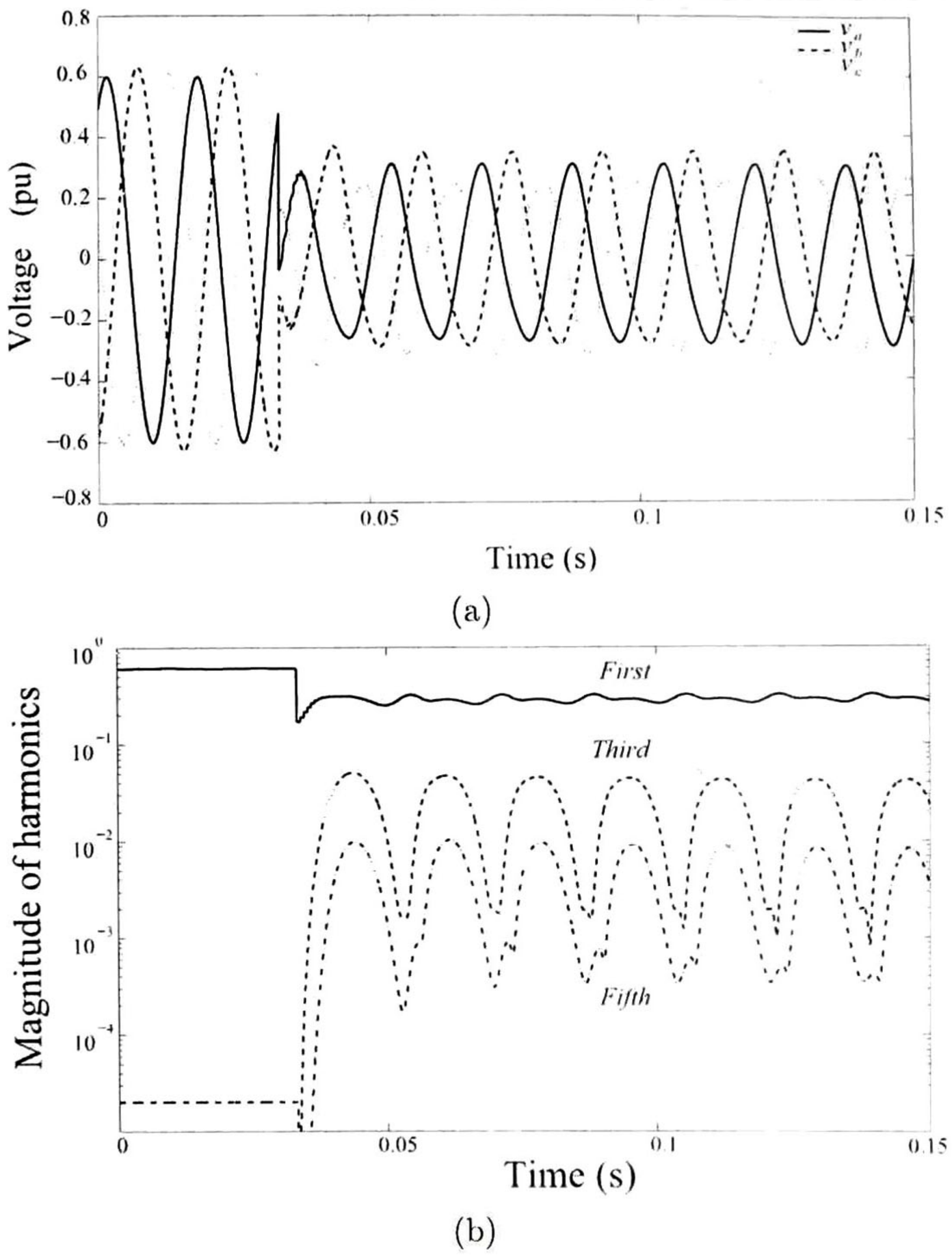


Figure 4.6: (a) Voltage $v_n$, and (b) harmonic content of $v_{na}$, for a three-phase nonlinear-load.

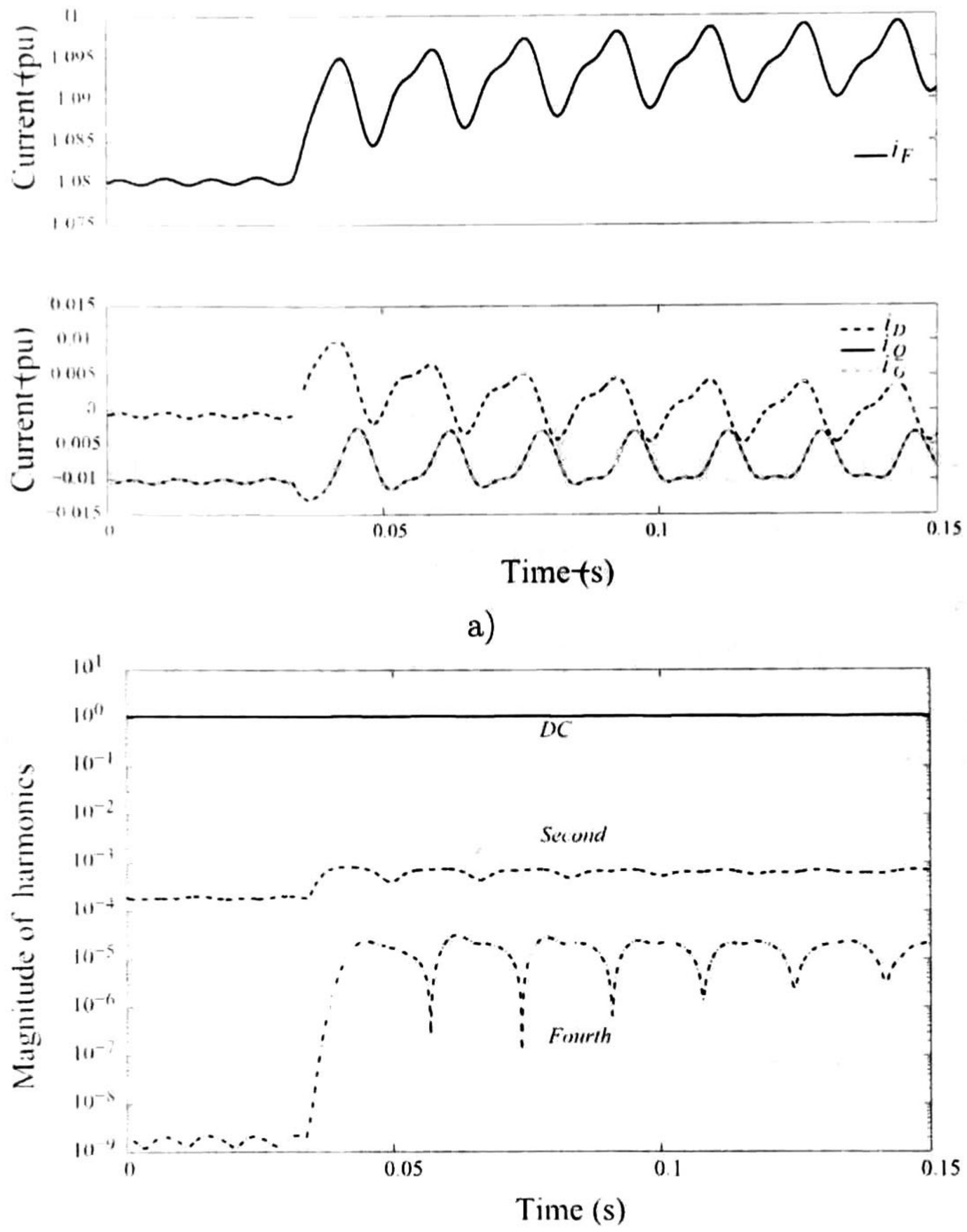


Figure 4.7: a) Rotor current $i_r$, and b) harmonic content of $i_F$, for a three-phase nonlinear-load.

### 4.4.4 Power Quality Indices

Power quality assessment under transient conditions has a significant impact at the design and development of active filters. However, the traditional method of using windowed FFT does not yield accurate harmonic information under transient conditions as show in Section 2.4. The DHD allows to obtain the power quality indices directly which can be calculated by traditional formulae (see section 3.4.3).

Fig. 4.8 shows the evolution of the most popular power quality indices (power factor and distortion factors can also be derived) for the generator-line-nonlinear load example outlined above. As expected, the quantities are constant in periodic steady-state and register significant changes during transient conditions due to the dynamic harmonic behavior.

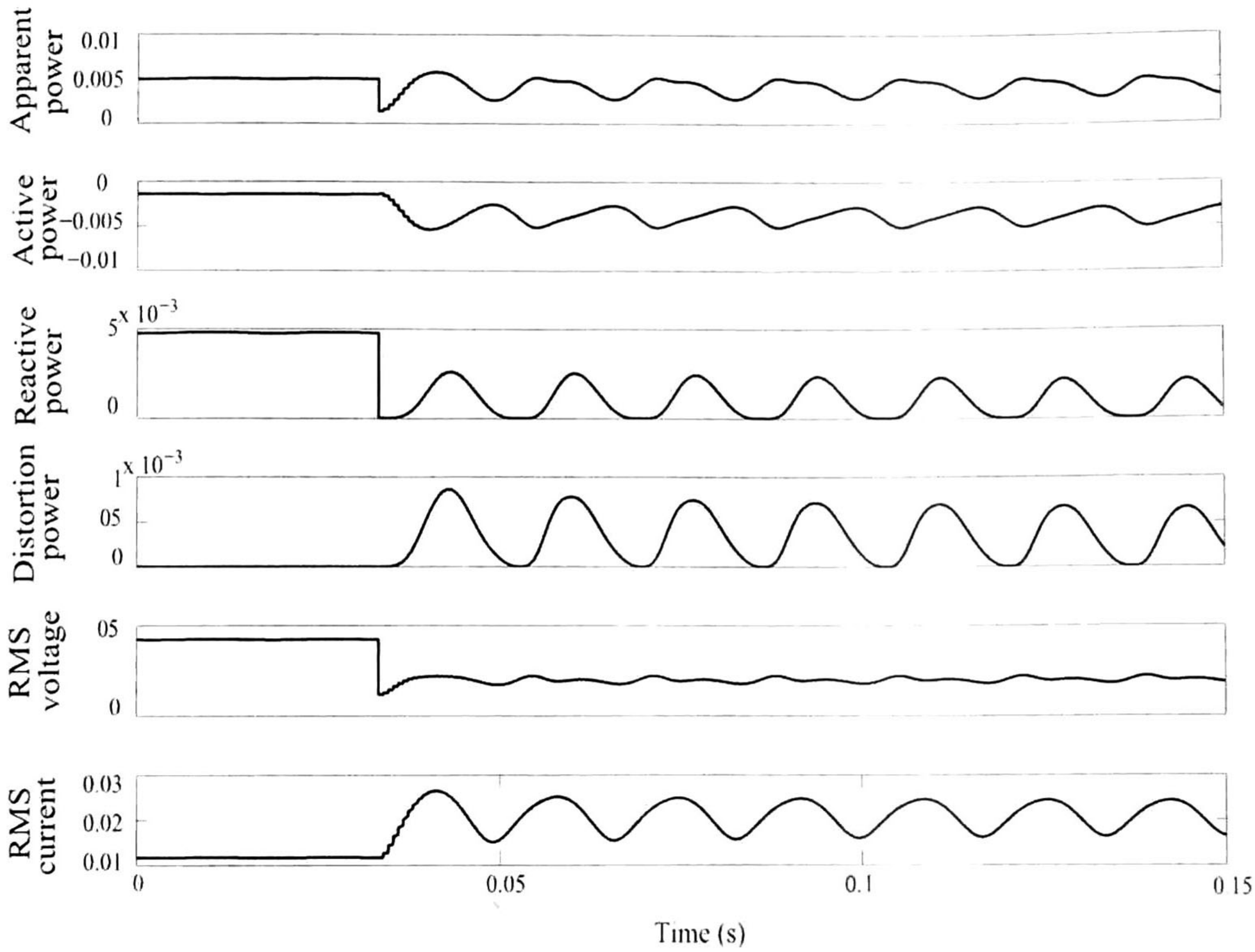


Figure 4.8: Power quality parameters for bus **n** with a three phase nonlinear-load.

## 4.5 Conclusions

In this Chapter the DHD interfacing of the synchronous generator and an untransposed transmission line for analyzing harmonics behavior under transient conditions has been presented. The accuracy of the proposed methodology was verified for a single machine-line-load system; however, the method is applicable to larger systems provided enough computational resources are available. This is because in the DHD, the size of the ODE system becomes large as the instantaneous variables are transformed into harmonic vectors. It has been observed that the inclusion of nonlinear loads enhance the harmonic content of voltage/curent waveforms. The applications of the algorithm includes the study of harmonics in transient state for control, protection and power quality purposes, and also the study of ferroresonance.

Chapter 5

# Eigenanalysis-Based Harmonic Resonance Assessment of a Network Including Switching Devices

THE harmonic interaction between a network and electronic devices can have a significant effect in equipment functioning and performance of the corresponding control schemes [36]. This becomes especially important when some of the harmonics are magnified due to resonance conditions. The fact that switching devices produce a wide range of harmonics, not all of them filtered out, and the fact that the network impedance changes continuously may produce a possible resonance interaction that magnifies the voltage/current at some points of the network.

Usually, frequency scans are performed to identify spikes in the driving-point impedances of the network under analysis [37], [38], [41]. The harmonic impedance response has been also proposed for identifying resonance conditions by varying the length of the transmission system while keeping the rest of the network parameters unchanged [28].

There are a few works using analytical formulations to identify harmonic resonances, for instance the one in [39] is based on Floquet theory [40] and was applied to a simple lossless circuit. Although this is an elegant way of finding resonance points, such theory becomes difficult (if not impossible) to apply for larger networks.

A previous research work [24] has been proposed for analyzing the harmonic interaction of a system including a generator and an open ended (or slightly loaded) transmission line by using the HD technique. This work proposes the extension of the theory from [24] to include switching devices. The methodology is based on the eigenanalysis of the transfer harmonic domain admittance (or impedance) matrix (HDAM) [9], [42] that relates the linear part of the network with the one involving switching devices. The admittance corresponding to the electronic device is expressed as function of its conduction angles. A sweeping of those angles provides the values where a possible resonance condition exists. Since the proposed method handles conduction angles as variables, the calculation of voltage resonance is straightforward without the need of iterative schemes or network simulations.

The extended method is compared here with a time domain based method, *i.e.*, PSCAD/EMTDC

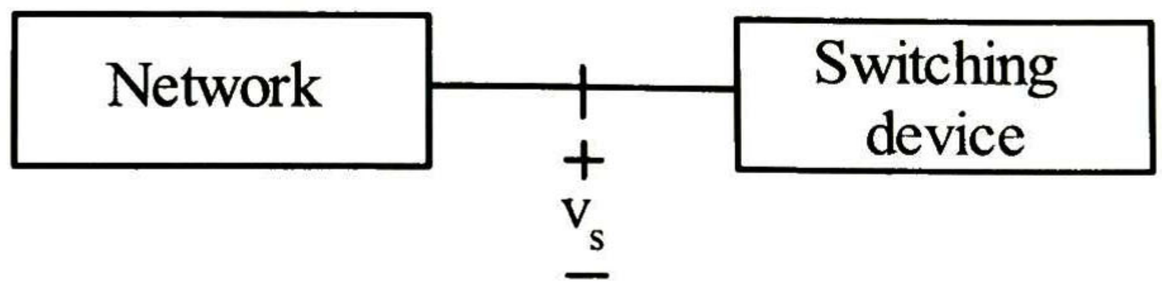


Figure 5.1: Representation of the total network.

simulation. Although only illustrative examples are presented here, the applicability of the method can be for instance in the analysis of resonances in HVDC systems and in large industrial installations using power quality conditioners. The issue of including controls is relegated for future research work.

## 5.1 Eigenanalysis Process

Consider the complete network divided in two subsystems, as shown in Fig. 5.1. The partition is done at the bus where a resonance study is required, in this work it is the bus connecting the switching device (see Fig. 5.1).

The eigenanalysis process described in the following is applied to calculate the resonance conditions at that bus.

- First, the total network is formulated in the HD through its nodal representation:

$$\begin{bmatrix} i_N \\ i_s \end{bmatrix} = \begin{bmatrix} \mathbf{Y}_{11} & \mathbf{Y}_{12} \\ \mathbf{Y}_{21} & \mathbf{Y}_{22} \end{bmatrix} \begin{bmatrix} v_N \\ v_s \end{bmatrix} \tag{5.1}$$

In (5.1), $i_N$ contains current sources and fictitious currents (set equal to zero) inside the linear network; $i_s$ corresponds to the injected current to the switching device. Similarly, $v_N$ corresponds to the network internal node voltages and $v_s$ to the bus where the switching element is connected. Elimination of $v_N$ in system (5.1) gives:

$$\mathbf{v}_s = H i_N, \tag{5.2}$$

where the HDAM is given by $H = -\left[Y_{22} - Y_{21}Y_{11}^{-1}Y_{12}\right]^{-1} Y_{21}Y_{11}$. It is mentioned at this point that the HDAM is a function of constant admittance matrices and admittances corresponding to the electronic device. The latter are function of the conduction angle.

- Second, the modal decomposition of $H$ is given by:

$$v_s = T\Lambda T^{-1} i_N = T\Lambda i_{Nm}, \tag{5.3}$$

where $i_{Nm}$ is the "modal" representation of $i_N$ and $\Lambda$ corresponds to a diagonal matrix with the eigenvalues of $H$. An alternate representation of (5.3) is:

$$\mathbf{v}_s = \sum_k t_k \lambda_i i_{Nmk}, \tag{5.4}$$

where $t_k$ is the $k$-th column (normalized to unity by Matlab) of the eigenvector matrix $T$. From (5.4) one can notice the possibility of an amplification of the output voltage $v_s$

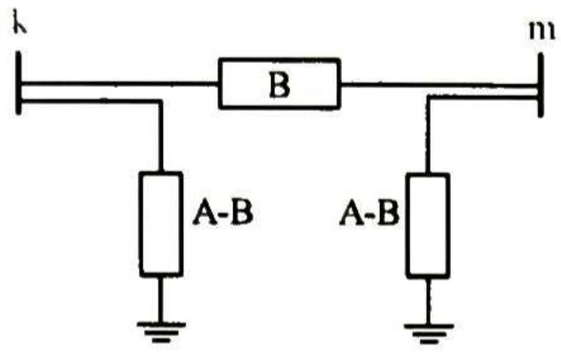


Figure 5.2: Two-port transmission line/cable representation.

for each eigenvector $t_k$ by the corresponding product of $\lambda_k$ and $i_{Nm}$; the elements of the corresponding eigenvector $t_k$ containing the information on which harmonics are amplified by the $k$-th product $\lambda_k i_{Nmk}$.

## 5.2 Network Elements

### 5.2.1 Transmission Line and Underground Cable

The transmission line and underground cable are modeled as frequency dependent elements using the HD [7]. In this work the following two-port network representation is used:

$$\begin{bmatrix} i_k \\ i_m \end{bmatrix} = \begin{bmatrix} A & B \\ B & A \end{bmatrix} \begin{bmatrix} v_k \\ v_m \end{bmatrix}, \tag{5.5}$$

where

$$A = Y_c \coth(\Gamma l),$$

$$B = -Y_c \operatorname{csc\,h}(\Gamma l),$$

where $\Gamma = \sqrt{YZ}$, and $Y_c = \sqrt{YZ^{-1}}$ are the propagation function, and the characteristic admittance, respectively. The $(A, B)$ parameters are calculated by using the complex depth for overhead lines [24], and Carson series for underground cables [24]. The corresponding nodal representation is shown in Fig. 5.2.

### 5.2.2 The SVC

The representation of the static VAR compensator (SVC) admittance (composed by a parallel arrangement of a thyristor-controlled reactor (TCR) and a capacitance) in the HD is [7] given as:

$$Y_{svc} = \frac{1}{L}\mathbf{S}^{-1}\mathbf{S}_w + C\mathbf{S}, \tag{5.6}$$

where $\mathbf{S}_w$ is the switching function given by [7]:

$$S_{wo} = (\sigma_1 + \sigma_2)/(2\pi), \tag{5.7a}$$

$$\mathbf{S}_{wh} = \frac{1}{h\pi}\left(\sin\frac{h\sigma_2}{2}\cos h\pi + \sin\frac{h\sigma_1}{2}\right)e^{jh\theta_x} \tag{5.7b}$$

where $\sigma_1$ and $\sigma_2$ represent the conduction angles for the positive and the negative SVC voltage terminal waveform, respectively.

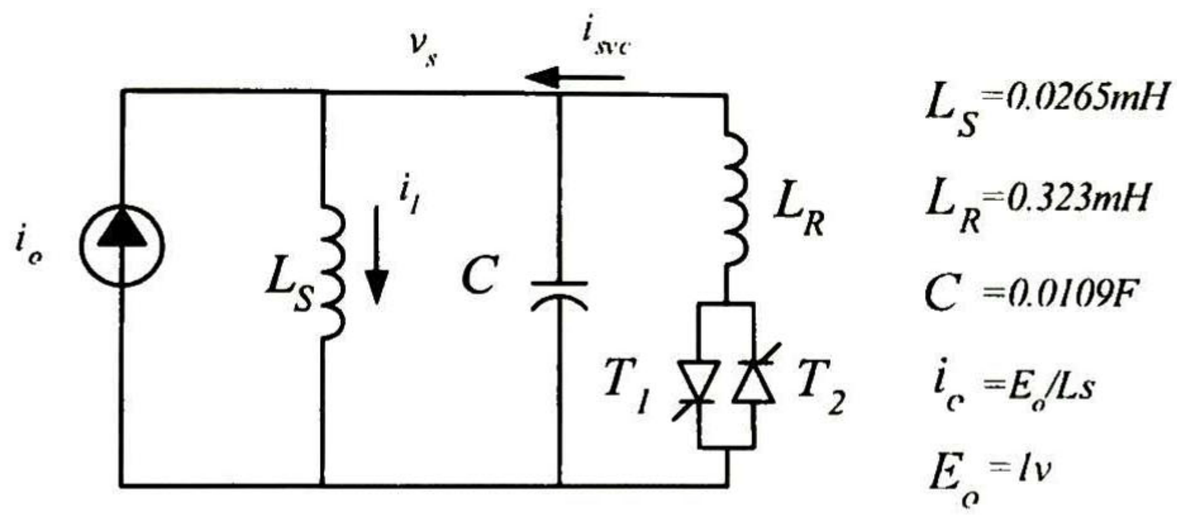


Figure 5.3: Simplified SVC circuit.

A three-phase SVC consists of three single-phase SVCs delta or star connected. The representation of the admittance for a three-phase SVC in star connection is given by:

$$Y_{svc-Y} = \begin{bmatrix} Y_{svc-A} & 0 & 0 \\ 0 & Y_{svc-B} & 0 \\ 0 & 0 & Y_{svc-C} \end{bmatrix} \tag{5.8}$$

The delta connection has been used to confine the 3rd, 9th, and 15th harmonic currents within the delta connection. The expression of the admittance for the SVC delta connection is given by (5.9)

$$Y_{svc-\Delta} = \frac{1}{3}\begin{bmatrix} Y_{svc-A/B} + Y_{svc-C/A} & -Y_{svc-A/B} & -Y_{svc-C/A} \\ -Y_{svc-A/B} & Y_{svc-B/C} + Y_{svc-A/B} & -Y_{svc-B/C} \\ -Y_{svc-C/A} & -Y_{svc-B/C} & Y_{svc-C/A} + Y_{svc-B/C} \end{bmatrix} \tag{5.9}$$

## 5.3 Illustrative Example

One of the first works on analyzing resonance conditions including electronic devices is presented in [39], where a comprehensive analysis of the circuit shown in Fig. 5.3 is described, finding two resonance points at $\sigma = 48^o$ and $\sigma = 64.3^o$ In that work, the first point was corroborated by a numerical method whilst the second one was not found [39]. The eigenanalysis-based method proposed here is used to confirm the existence of those points.

The relations for the linear network and for the electronic device are:

$$v_s = L_o\mathbf{S}[i_o - i_1], \tag{5.10a}$$

$$v_s = -\left[\frac{1}{L}\mathbf{S}^{-1}\mathbf{S}_w + C\mathbf{S}\right]^{-1} i_{svc}, \tag{5.10b}$$

respectively.

According to the quantities (5.4), the upper plot in Fig. 5.4 shows the magnitude of the eigenvalues $\lambda_k$, the middle plot the magnitude of the products $\lambda_k e_{Nmk}$ and the lower plot the norm of $v_s$ obtained by sweeping the conduction angle (considering that $\sigma_1 = \sigma_2$) of the TCR from $0^o$ to $180^o$

The harmonic components of $v_s$ are shown in Fig. 5.5, for three different conduction angles ($48^o, 64^o$, and $90^o$). Notice that the first two angles, predicted in [39], correspond

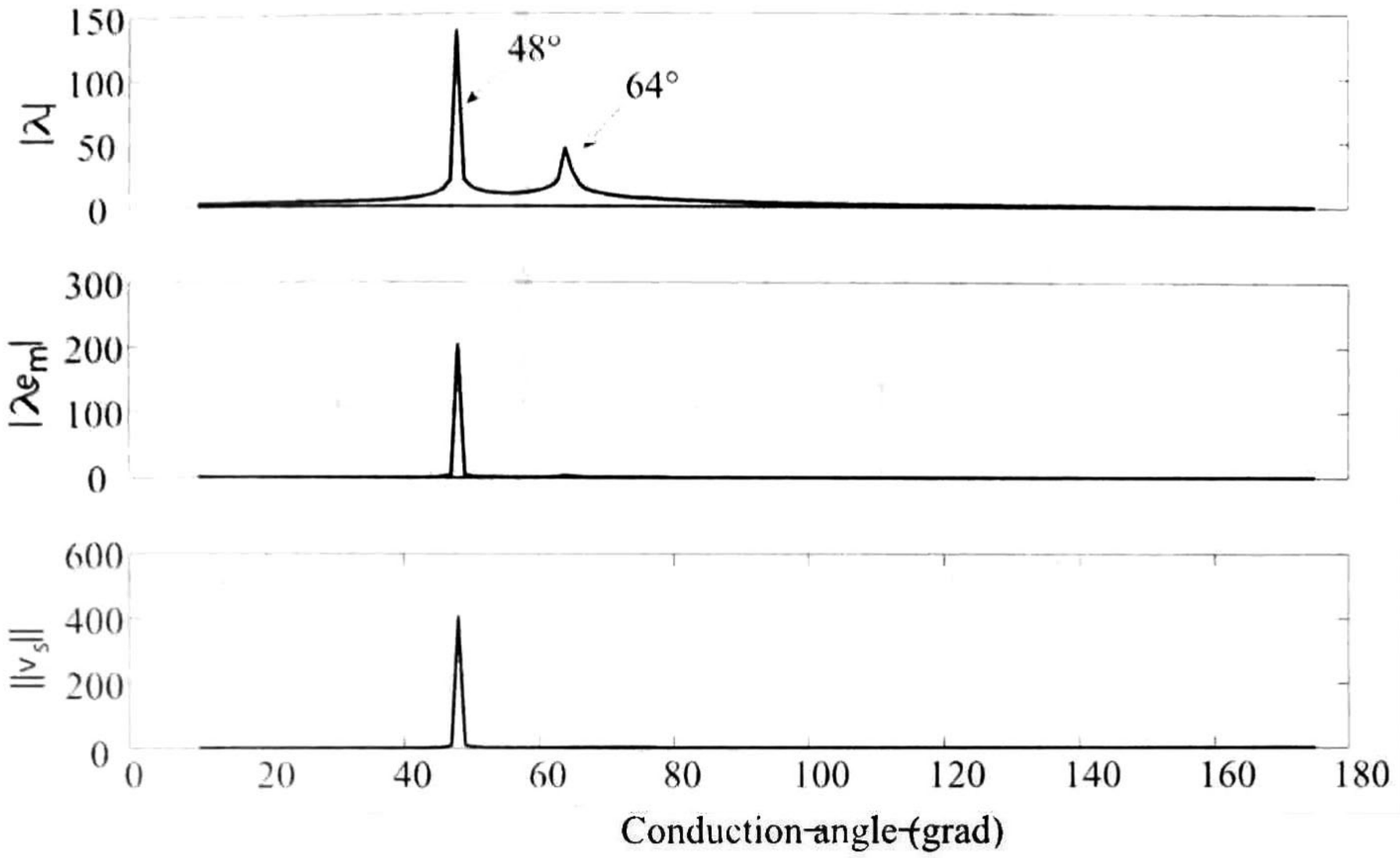


Figure 5.4: Magnitude of eigenvalues $\lambda$, product $\lambda i_m$, and norm of the voltage.

to resonance conditions with the one equal to $64^o$ noticeable only in the upper plot of Fig. 5.4. Also, from Fig. 5.5 one can notice that the conduction angle $48^o$ shows that the resonance has its major contribution from the 5th harmonic. Additionally, Fig. 5.5 shows that fundamental frequency does not present substantial changes for the three angles (the third one has been chosen arbitrarily).

## 5.4 Transmission Network Example

A more elaborated example involving the transmission network shown in Fig. 5.5, is presented in this Section. The transmission network consists on a 10km long three-phase UC and two identical 100km lines. The geometries of the underground cable is shown in Fig. 5.6 and for the transmission lines in Fig. 3.3. An SVC is connected at bus 4 in star and in delta connections. The parameters of the SVC are: $L_{tcr} = 0.323$mH and $C = 0.0109$F. The rest of the parameters are: a three-phase source $E_a = \sin(\omega_o t)$, $E_b = \sin(\omega_o t + 120)$, $E_c = \sin(\omega_o t + 240)$, $\omega_o = 377$ rad/s, $Y_o = 1 \times 10^9$, $Y_1$ is a parallel load with $R = 10\Omega$, and $L = 0.323$H, and $Y_2 = Y_3 = 10\mho$.

Table 5.1: Resistivity and permeability of the UC

| | Resistivity $\varphi\Omega m$ | Permeability $\mu Hm$ |
|---|---|---|
| Conductor | $3.365 \times 10^{-8}$ | 2.85 |
| Insulator 1 | 2.85 | 1 |
| Sheath | $1.71 \times 10^{-8}$ | 1 |
| insulator 2 | 2.51 | 1 |

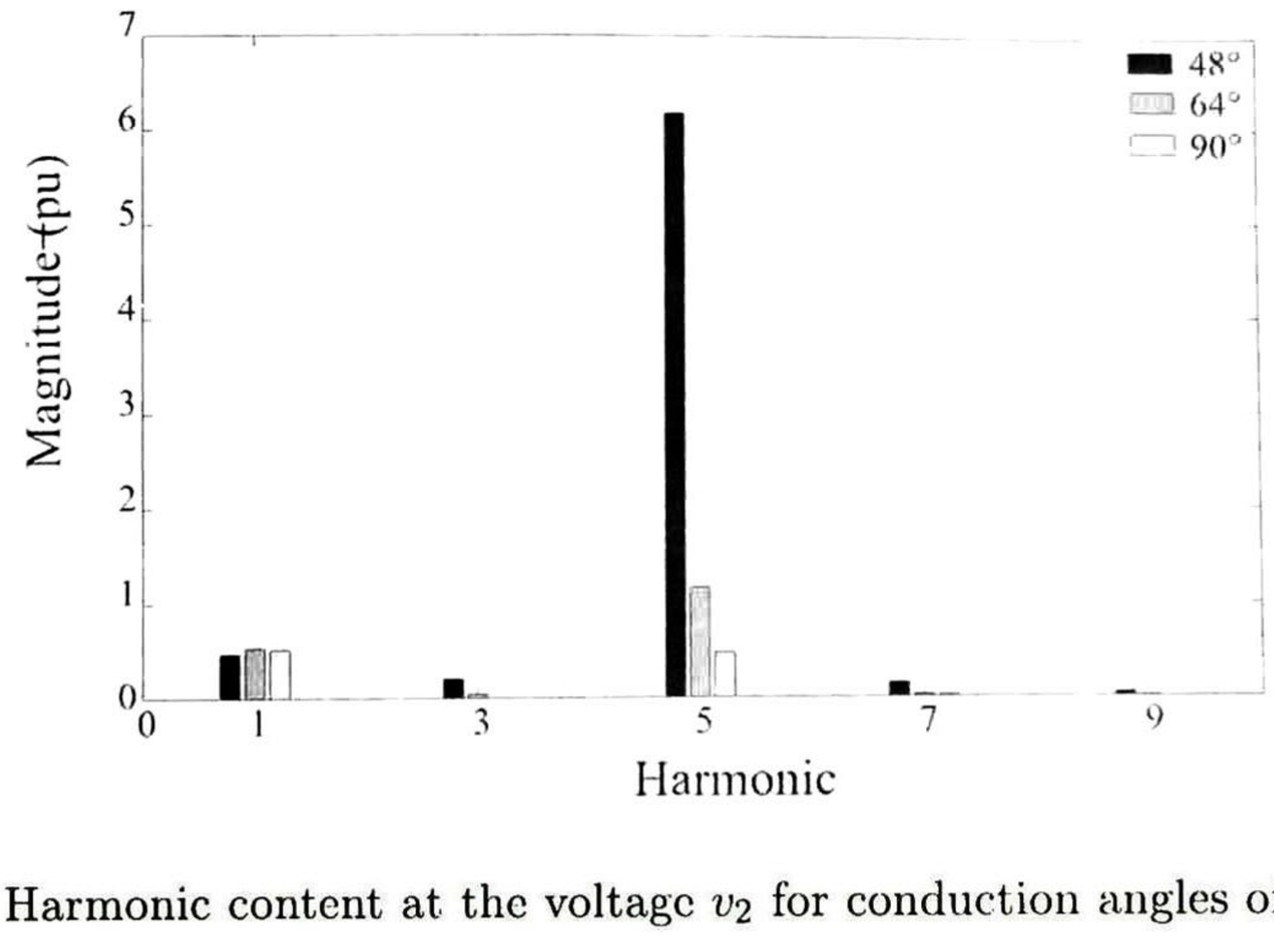


Figure 5.5: Harmonic content at the voltage $v_2$ for conduction angles of $48^o$, $64^o$, $90^o$

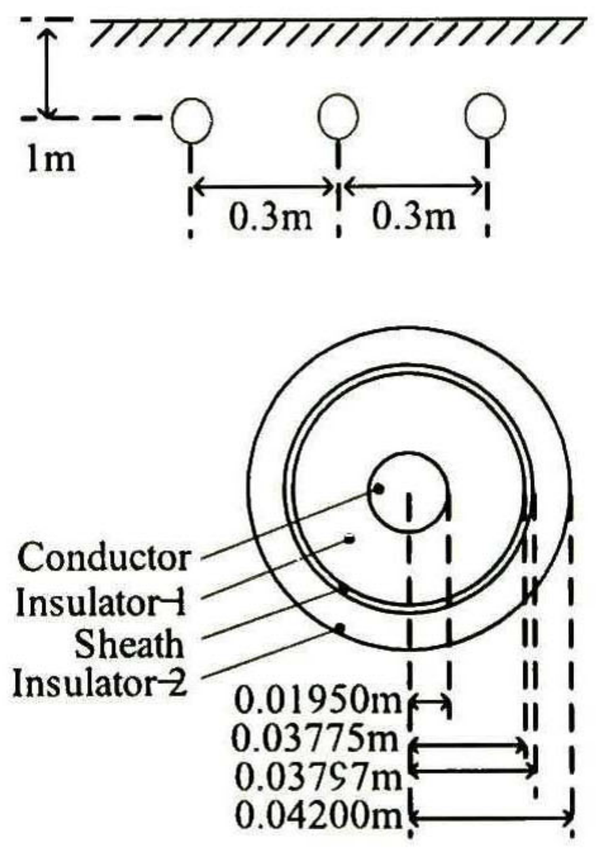


Figure 5.6: Untransposed underground cable configuration.

### 5.4.1 SVC Star Configuration at Bus 4

The characteristic quantities given by (5.4) are presented in Fig. 5.8, where two resonance points are clearly visible, i.e. at $44^o$ and $127^o$.

The harmonic components of $v_s$ are shown in Fig. 5.9 for three different conduction angles, in this case chosen as the two corresponding to resonance condition angles and an arbitrary angle where the voltage is close to unity. The analysis was done considering up to the 51st harmonic, showing in Fig. 5.9 only the first 10 harmonics. From Fig. 8 one can notice that, for this network, the major contribution to the resonance is by the fundamental frequency.

Fig. 5.10 shows the voltage at bus 4 with an angle equal to $127^o$ (a resonance condition). Note that due to the untransposed transmission lines, the resultant voltages are different in magnitude.

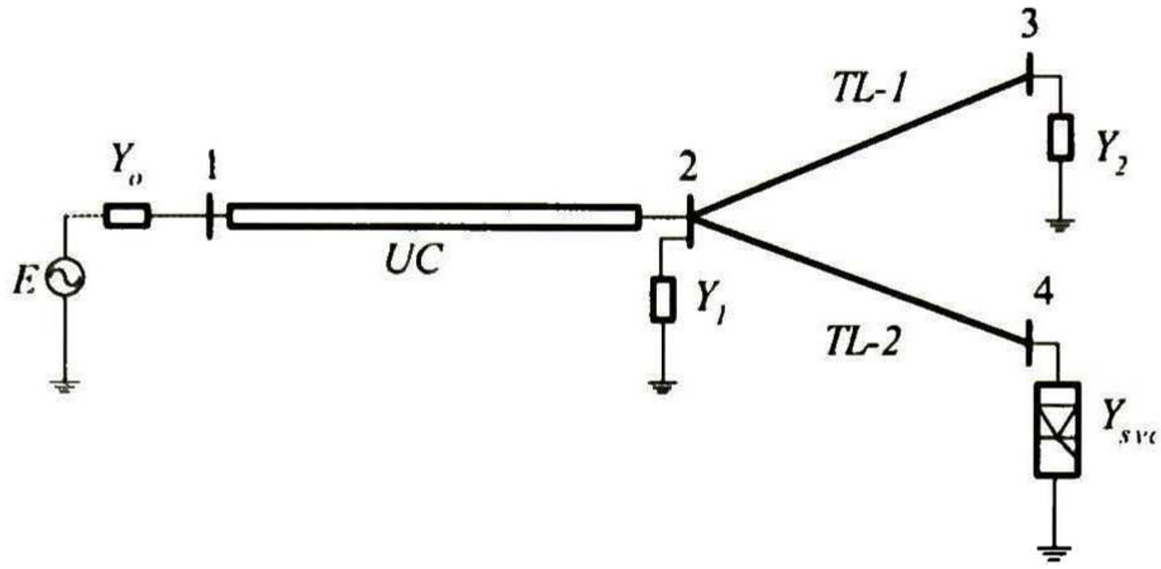


Figure 5.7: Three-phase transmission line network with SVC.

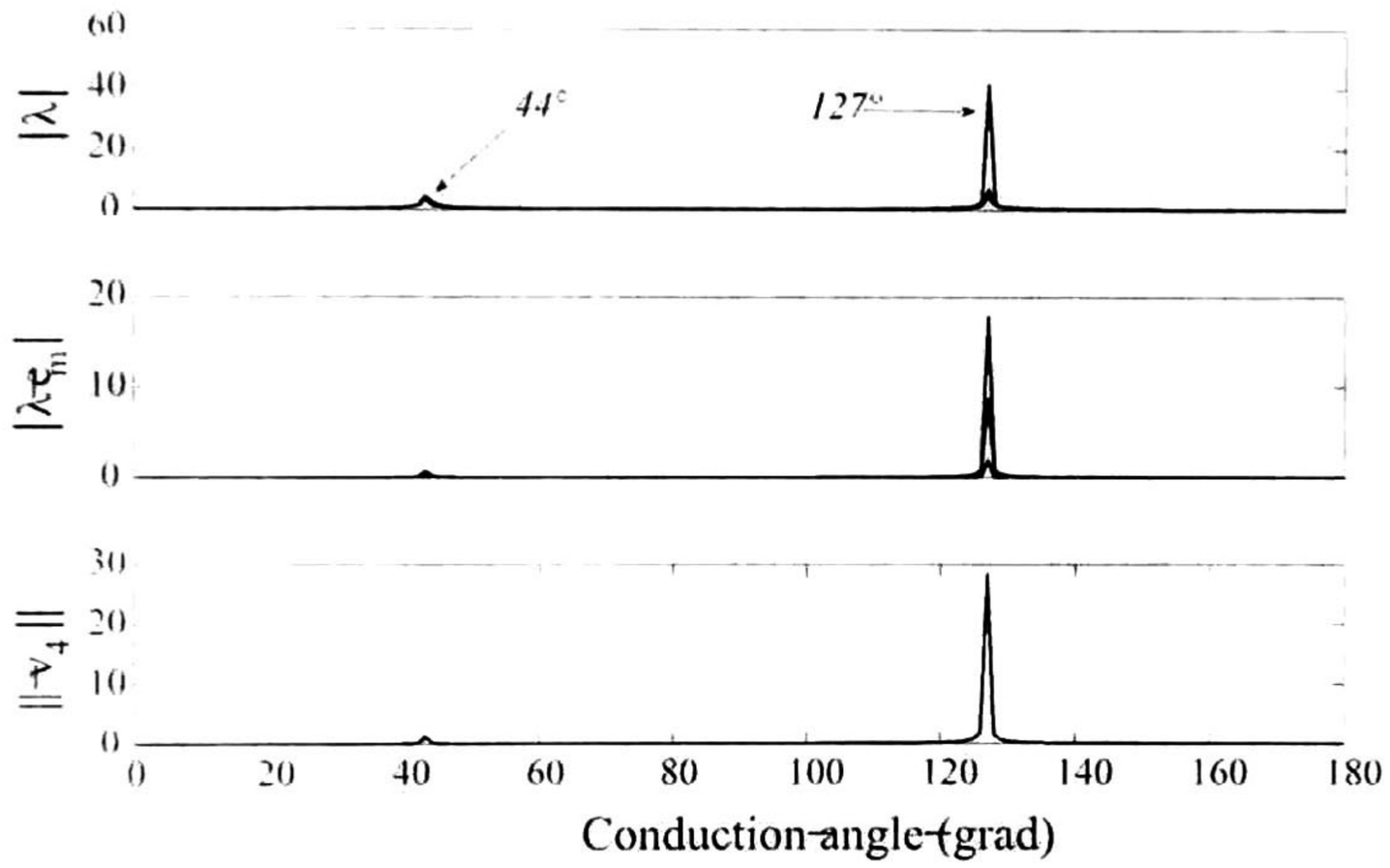


Figure 5.8: Magnitude of eigenvalues $\lambda$, product $\lambda e_m$, and norm of the voltage.

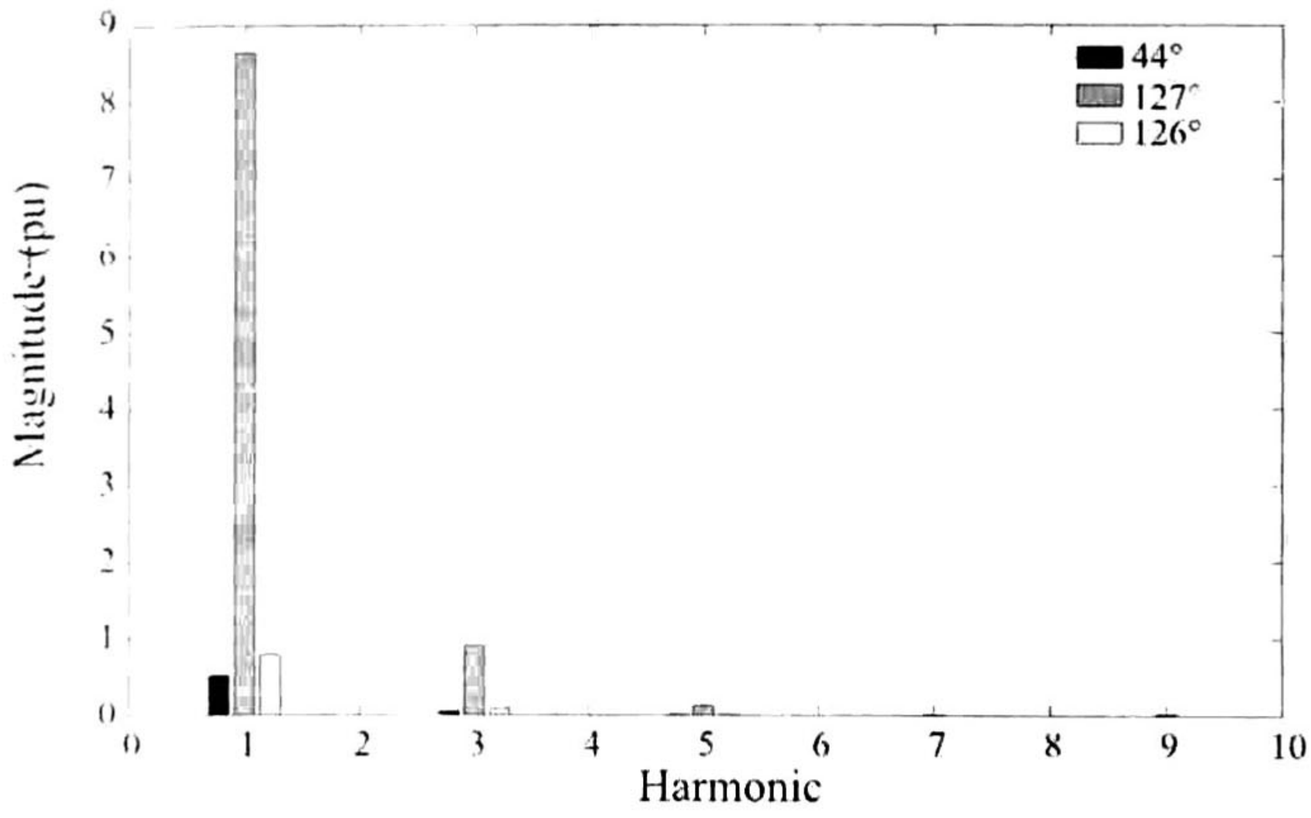


Figure 5.9: Harmonic content at the voltage $v_4$ for a SVC star connection; conduction angles of $44^o$, $127^o$, $126^o$ .

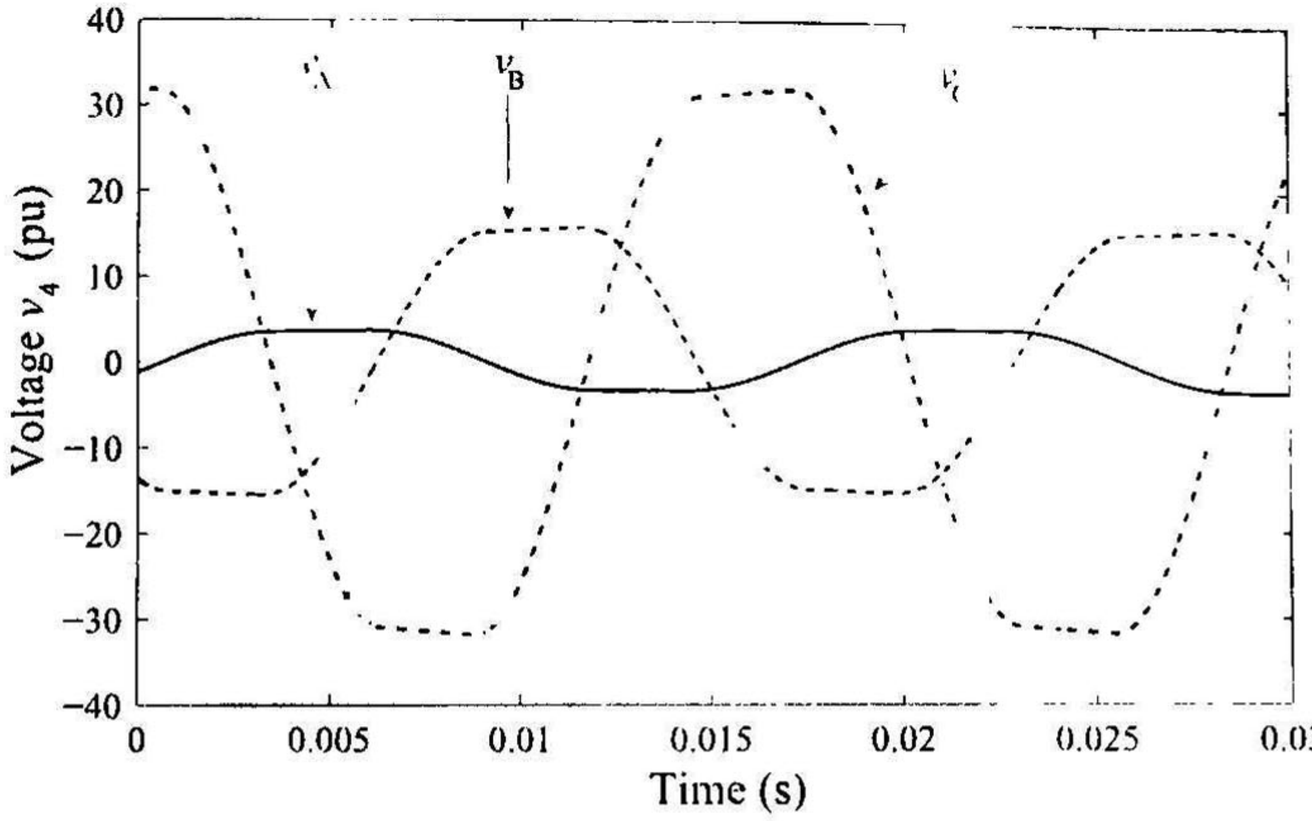


Figure 5.10: Voltage $v_4$ in resonance conditions, conduction angle of $127^o$.

The results provided in Fig 5.10 were compared against those obtained by PSCAD/EMTDC. In this software package the ground plane for the underground cable is solved by the Wedephol's approximation method of Pollaczek's integral and the SVC was built based on three SVCs as described by (5.8). Fig. 5.11 shows the voltage during obtained by PSCAD/EMTDC where it can be noticed that it takes about a second to reach the steady-state. A close up of Fig. 5.11 is presented in Fig. 5.12, where a clear agreement between the proposed method and PSCAD/EMTDC is observed.

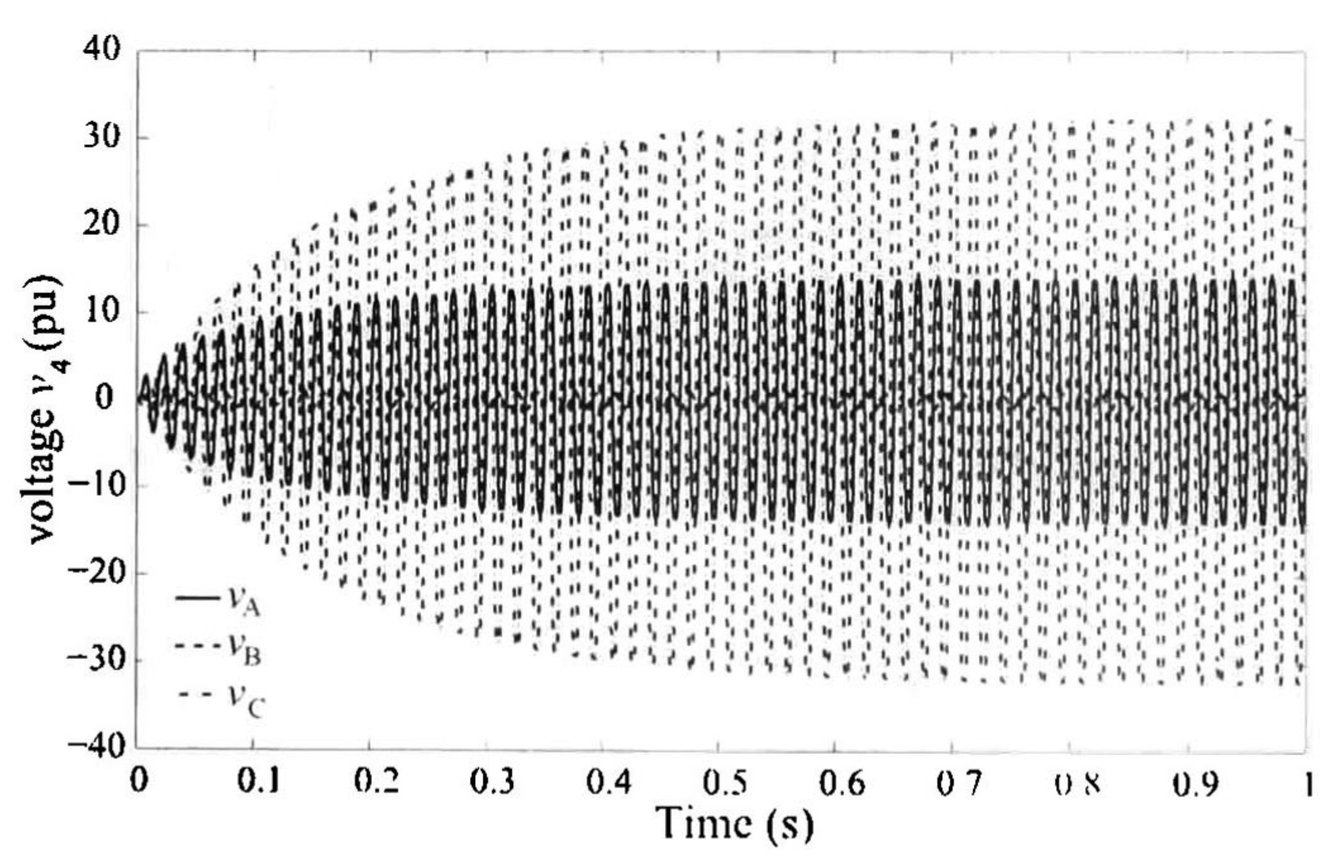


Figure 5.11: Voltage $v_4$ in resonance conditions obtained from PSCAD/EMTDC.

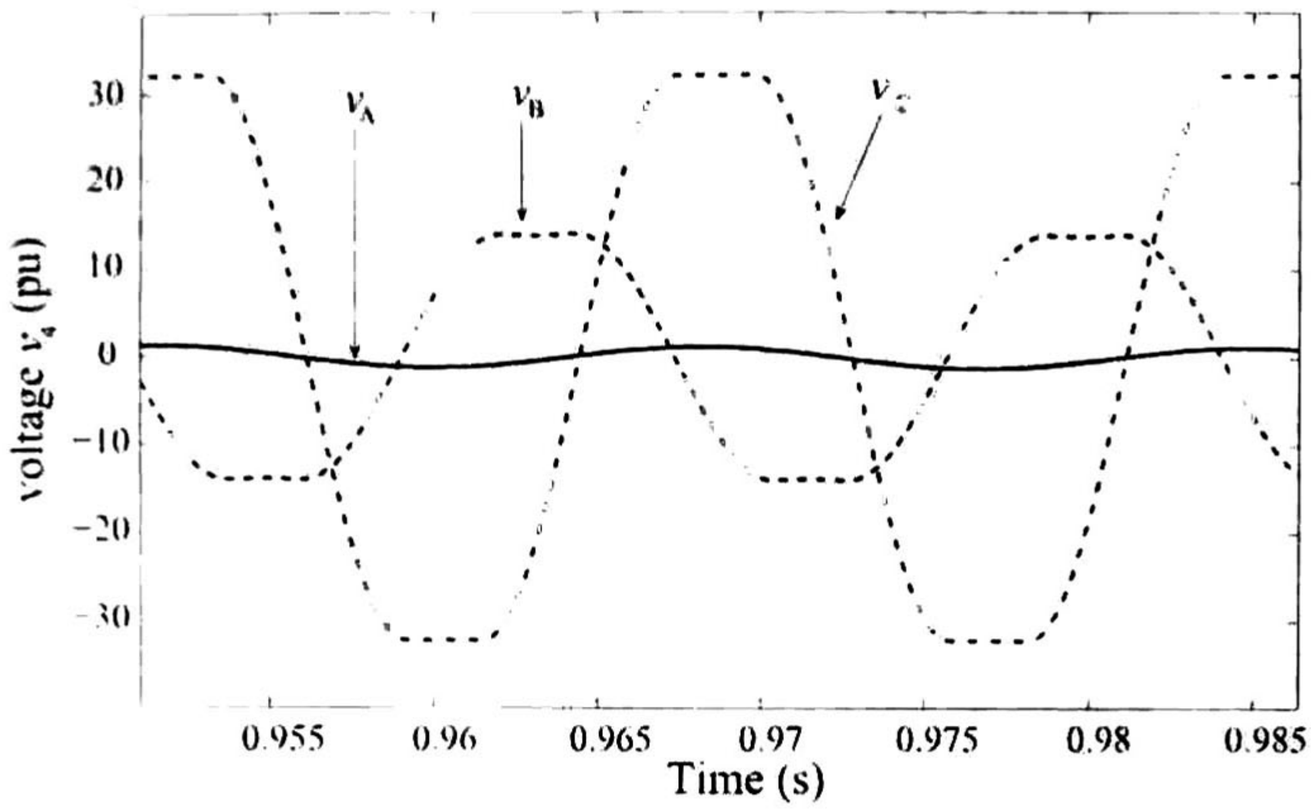


Figure 5.12: Voltage $v_4$ zoom obtained by PSCAD/EMTDC.

### 5.4.2 SVC Delta Configuration at Bus 4

The network from Fig. 5.7 is now simulated with a delta-connected SVC. The results of the eigenvalue analysis are presented in Fig.5.13 where three resonance points can be observed.

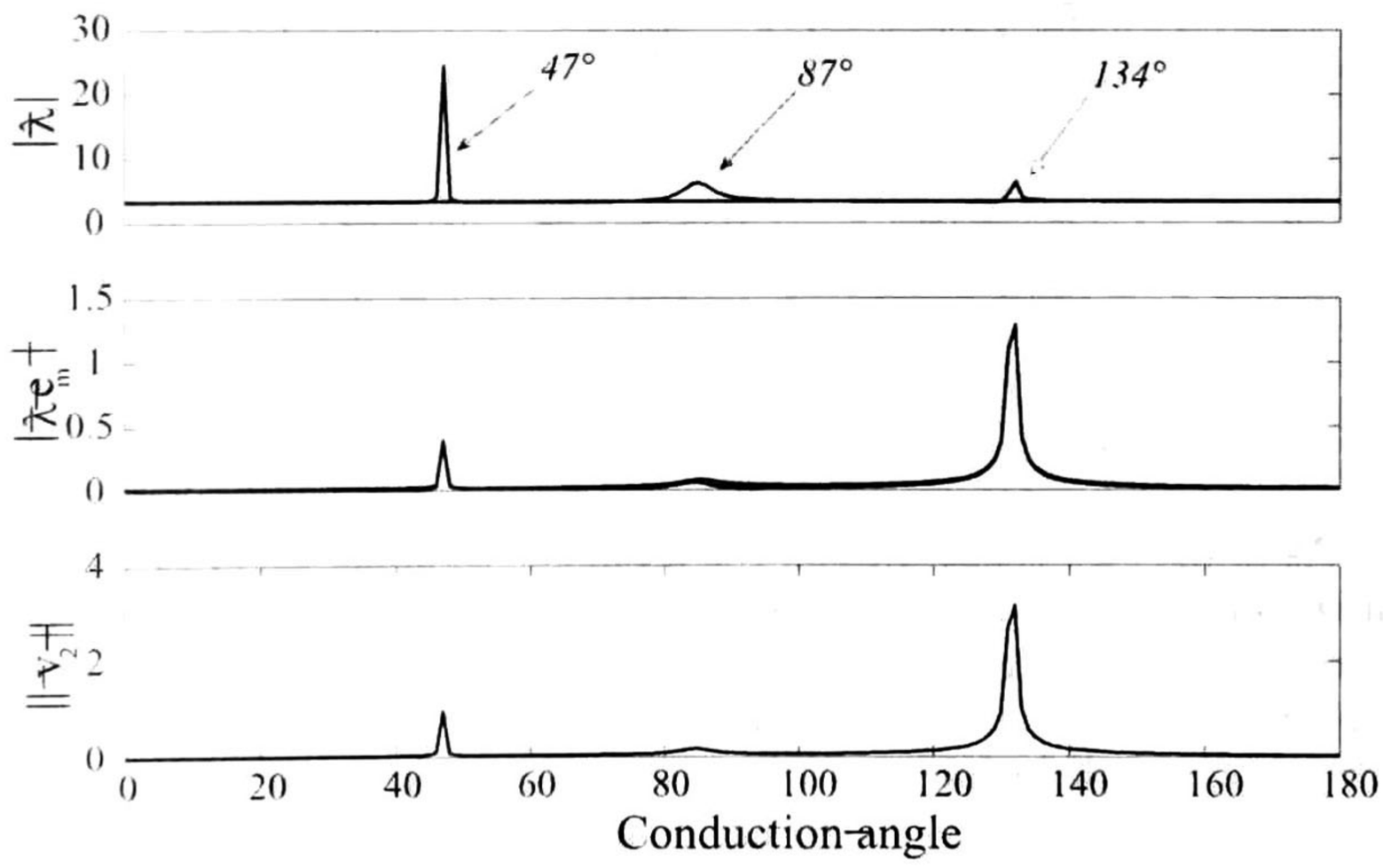


Figure 5.13: Magnitude of eigenvalues $\lambda$, product $\lambda e_m$, and norm of the voltage $v_4$.

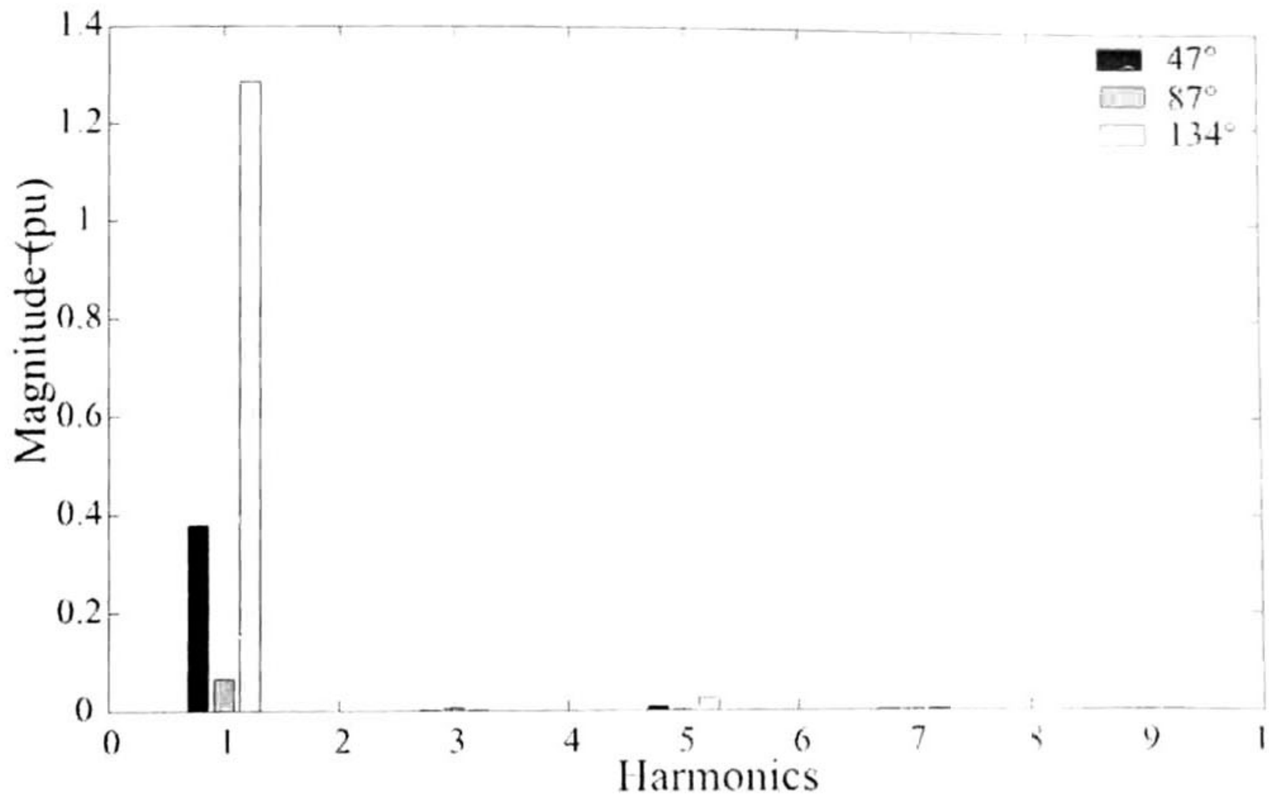


Figure 5.14: Harmonic content at the voltage $v_4$ for a SVC star connection; conduction angles of $47^o$, $87^o$, $134^o$ .

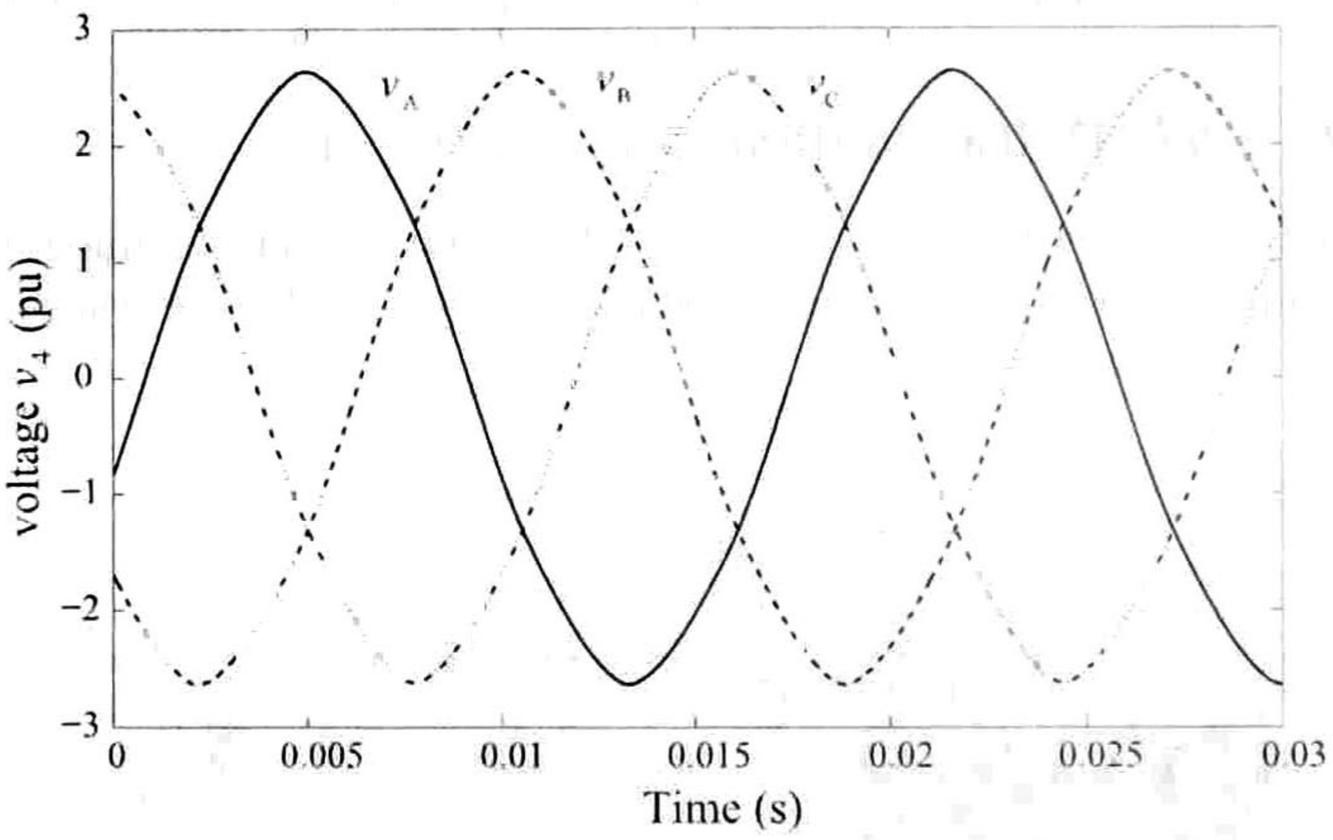


Figure 5.15: Voltage $v_4$ in resonance conditions angles of $134^o$

As in the star configuration, the harmonic components of $v_2$ are shown in Fig. 5.14 for three different conduction angles, in this case chosen as the two eigenvalues corresponding to resonance condition angles and an arbitrary angle where the voltage is close to unity. The analysis was done considering up to the $51^{th}$ harmonic, showing in Fig. 5.14 only the first 10 harmonics which are the most representatives for this example. Also, it can be seen a poor contribution of the harmonics $3^{th}$, $9^{th}$ and $15^{th}$ to the total signal. From Fig. 5.15, unlike Fig.5.6, the voltage magnitude is seen to be close to balance conditions due to the delta connection, and the resonance at $134^o$ has produced a voltage 2.5times of the the source.

## 5.5 Conclusions

A harmonic domain methodology, based on eigenanalysis, has been used to assess resonance conditions on a network that includes electronic devices. It has been observed that, in these networks, resonances can arise due to the harmonic interaction with the electronic device, depending on the angle operation of the latter. This can produce failures in the network and tripping of protective devices.

It has been observed that the resonance condition does not depend only on the biggest eigenvalue, but on its product with the source component $i_{Nmk}$.

Chapter 6

# Real-Time Implementation

SIMULATION has always been the pillar at all stages of the development and operation of power systems-planning, design, prototyping, and testing [50]. Digital computers and analog simulators, based on scale-down models, were the elements commonly used to emulate and predict the behavior of actual power systems. Nowadays, digital simulators have replaced those elements. Currently, several offline digital simulation software tools are available, with several degrees of modeling and simulation capabilities. Among these tools are PSCAD/EMTDC, MATLAB/SIMULINK, EMTP-RV, PSS/E, and SPICE. However, one of their main drawbacks is that they often lack the capability of interfacing with actual hardware, such as digital controllers or protective relays. A real-time digital simulator with adequate computational bandwidth can overcome this obstacle. The main requirement of a real time digital simulator is to ensure that the calculation for a time-step is completed within the chosen step-size.

There are several real-time simulators reported in the literature which are based on different specialized processors such as DSP, RISC, and VLSI technology [43]- [48]. In this chapter a real-time simulation of the transmission line in the DHD and linear loads was carried out on a state-of-art PC-Cluster based real-time simulator [32]. The simulator is in the Real-Time eXperimental Laboratory (RTX-Lab) in the Power Engineering Group at the University of Alberta.

## 6.1 RTX-Lab Simulator Details

### 6.1.1 Hardware

Fig. 6.1 shows the hardware architecture of the RTX-Lab. The simulator has been built on a high-speed computer cluster (known as the target) which works as the main computational engine, and also on a host cluster which is used for model development and monitoring the results. Additionally, field programmable gate arrays (FPGA)-based I/Os provide external communication from physical equipment, and a gigabit ethernet network is used for communication between the computers [51], [52].

### A) Target Cluster

The target cluster is the heart of the RTX-Lab. It contains high-speed computers that work as the computational engine for the real-time simulator. During the simulation one of the clusters works as the master and the others work as slaves. The master manages the communications between the hosts and the target cluster. Slaves are used for computational purposes. The user is able to choose the master and slaves from the available cluster nodes, see Fig. 6.1.

For this specific equipment, the target cluster consists of eight cluster nodes connected in parallel through two different communication links. The target cluster is highly flexible, and the computational power can be scaled up by adding more nodes. Each node has two 3.0 GHz dual Intel Xeon processor that can be run interactively or independently. The two processor communicate with each other through the shared memory.

### B) Host Cluster

The host cluster is the group of computers used for the model development, compilation, and loading the compiled programs to the cluster nodes. Through the hosts, the user can obtain full access to and utilization of the target cluster. The host cluster is one of the external hardware for obtaining simulation results and feeding control values to the target cluster in real time. The number of hosts that can be connected to the target is unlimited; the RTX-lab simulator currently uses eight hosts networking with the target cluster. Each host has a 3.0-GHz Intel Pentium IV procesor with hyper-threading (HT).

### C) FPGA-Based I/Os and Signal Conditioning

Physical hardware of various types (analog, digital, PMW, timers, encoders, etc.) can be interfaced with the target cluster through the FPGA-based multichannel I/O modules.

### D) Communication

The four types of communications involved in the RTX-Lab simulators are as follows: 1) the internal CPU communication, 2) data transfer between the cluster nodes, 3) interfacing the external hardware to the simulator, and 4) executable loading and results acquisition between the hosts and the cluster nodes. All these communication needs have been addressed by one o several corresponding communication technologies: 1) shared memory; 2) infinity band link; 3) signalwire link; and 4) gigabit ethernet link, see Fig. 6.1.

## 6.1.2 Software

Fig. 6.2 shows the software architecture of the RTX-Lab [51], [52].

### A) Target Operating Systems

The target cluster runs on RedHawk Linux, a state-of-the-art real-time version of the open-source Linux. In the target the following functions are performed:

- real-time execution of the model;
- real-time communication between target nodes and I/Os;

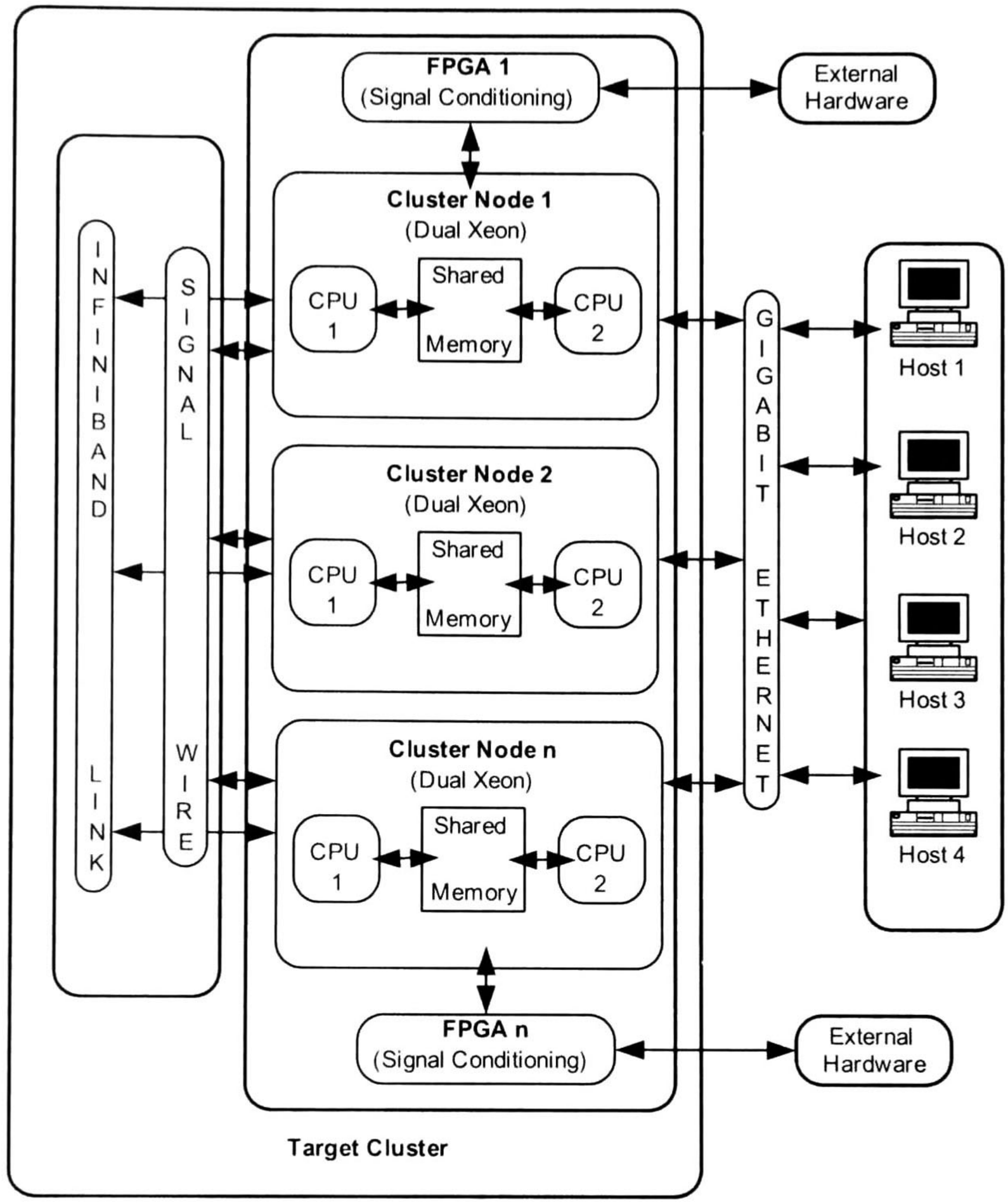


Figure 6.1: Hardware architecture of the RTX-Lab simulator [51].

- data acquisition and system initialization;
- implementation of parameter changes while the simulation is running;
- recording and sending data to the host or to any external monitoring devices;
- enabling I/O connection and signal conditioning.

**B) Host Operating Systems**

The host could be running either in Windows or Linux OS. The RTX-Lab host uses Windows XP as the resident operation system. The host is mainly used to:

- prepare, edit, and customize the power system and the control models;
- manipulate model parameters and acquire simulation results;

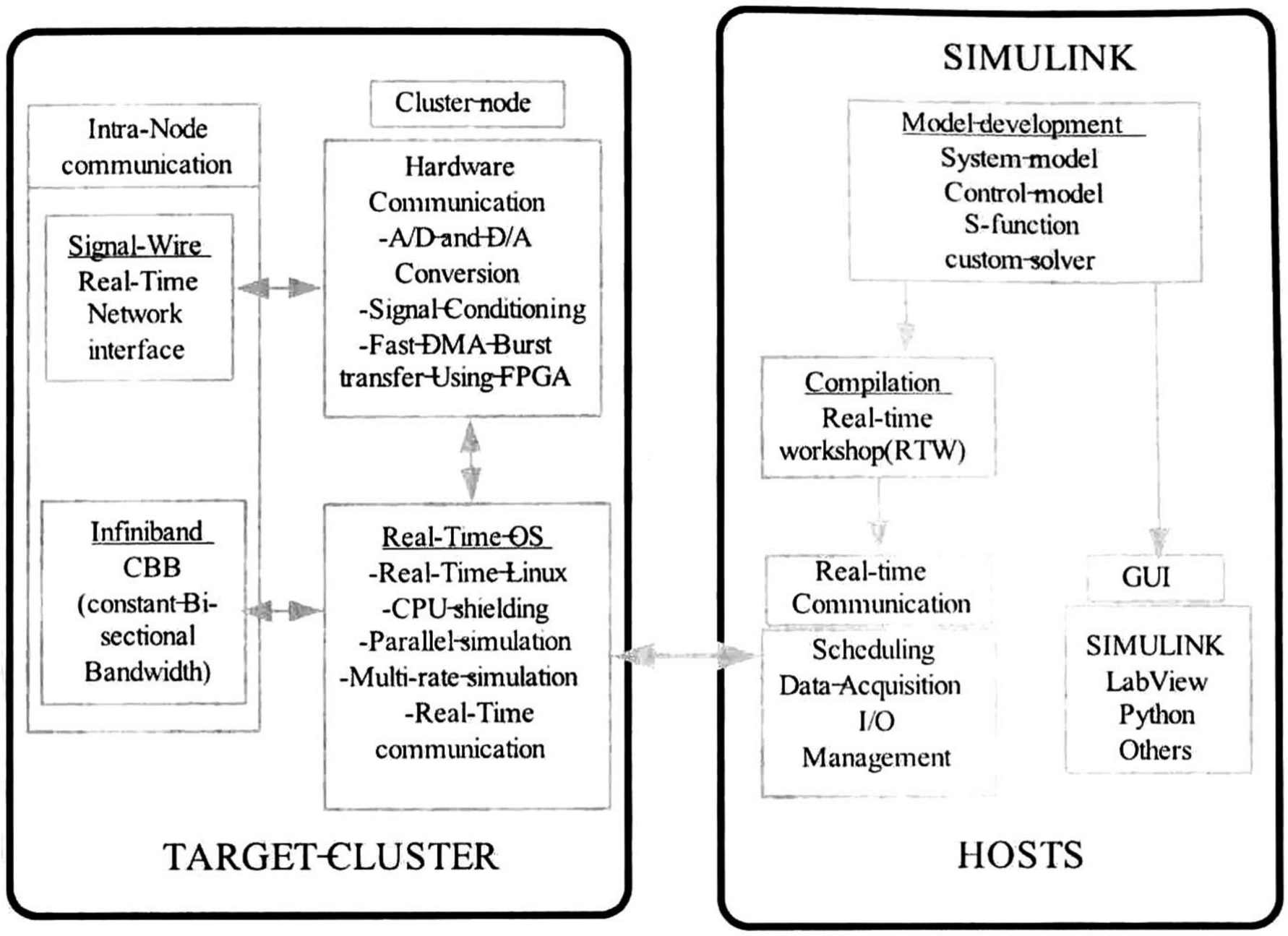


Figure 6.2: Software architecture of the RTX-Lab simulator [51].

- perform the offline verification simulation of the model in the Matlab/SIMULINK environment;
- divide large and complex systems into subsystems;
- compile the model and generate the executable code ready for real-time simulation;
- control the simulators task sequence.

### C) Model Development Software

The Matlab/SIMULINK environment is employed for the development of power and control system models. Most physical systems and their control can be modeled with the built-in Matlab/SIMULINK tool-boxes; however, user-defined models and solver algorithms written in Matlab or other high level languages, such as C/C++ or Fortran, can also be included through the Matlab/SIMULINK S-function interface. Large systems can be divided into several subsystems and distributed over parallel operating cluster nodes.

### D) User Interface-Command and Control

The Matlab/SIMULINK environment provides the user with interfacing tools to monitoring and controlling the inputs/outputs of real-time simulations and control.

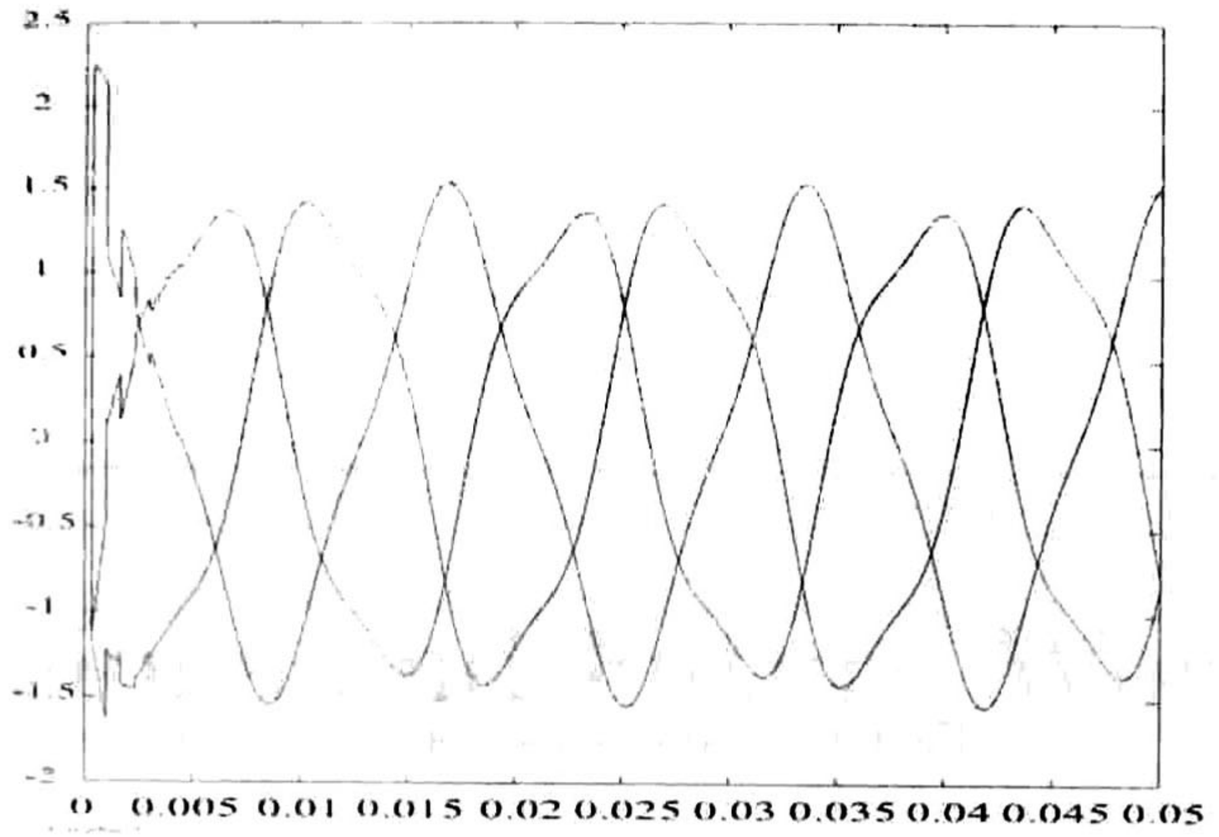


Figure 6.3: Voltage $v_n$ (pu).

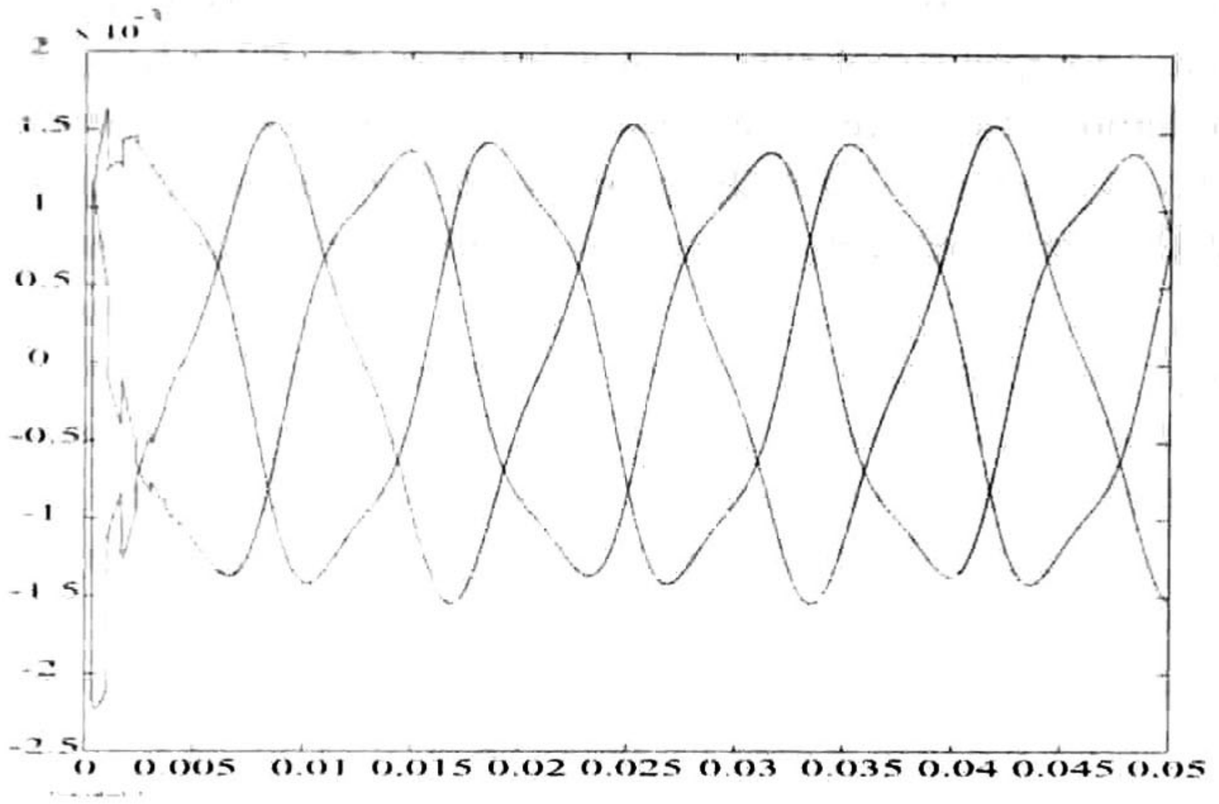


Figure 6.4: Current $i_n$ (pu).

## 6.2 Real-Time Implementation of the Transmission Line and Linear Loads

The model for the transmission line described in Chapter III was coded entirely in C language and embedded as a dynamically linked program (S-function) in SIMULINK. SIMULINK uses a state-space approach to solve the system.

The network under analysis consists on a source $v_o = \cos(\omega_o t) + \frac{1}{8}\cos(3\omega_o t)$ (see Fig. 3.2), and a 100km transmission line with a linear load admittance $Y_L = 0.001$pu (see Fig. 3.3 on Chapter III for geometrical parameters).

Figs.6.3 and 6.4 show the voltage and the current at bus n for an open ended transmission line (see Fig. 3.1), respectively. Also on Fig.6.5 it is shown the harmonic content of the voltage at bus **n**. The minimum step of time was $50\mu s$, the observation time was $0.5s$.

From Fig.6.5 one can notice that the harmonic behavior during a transient obeys the line resonant frequency, traveling time, and excitation related frequencies. When a steady-state is reached the waveform shows a constant magnitude of the harmonics.

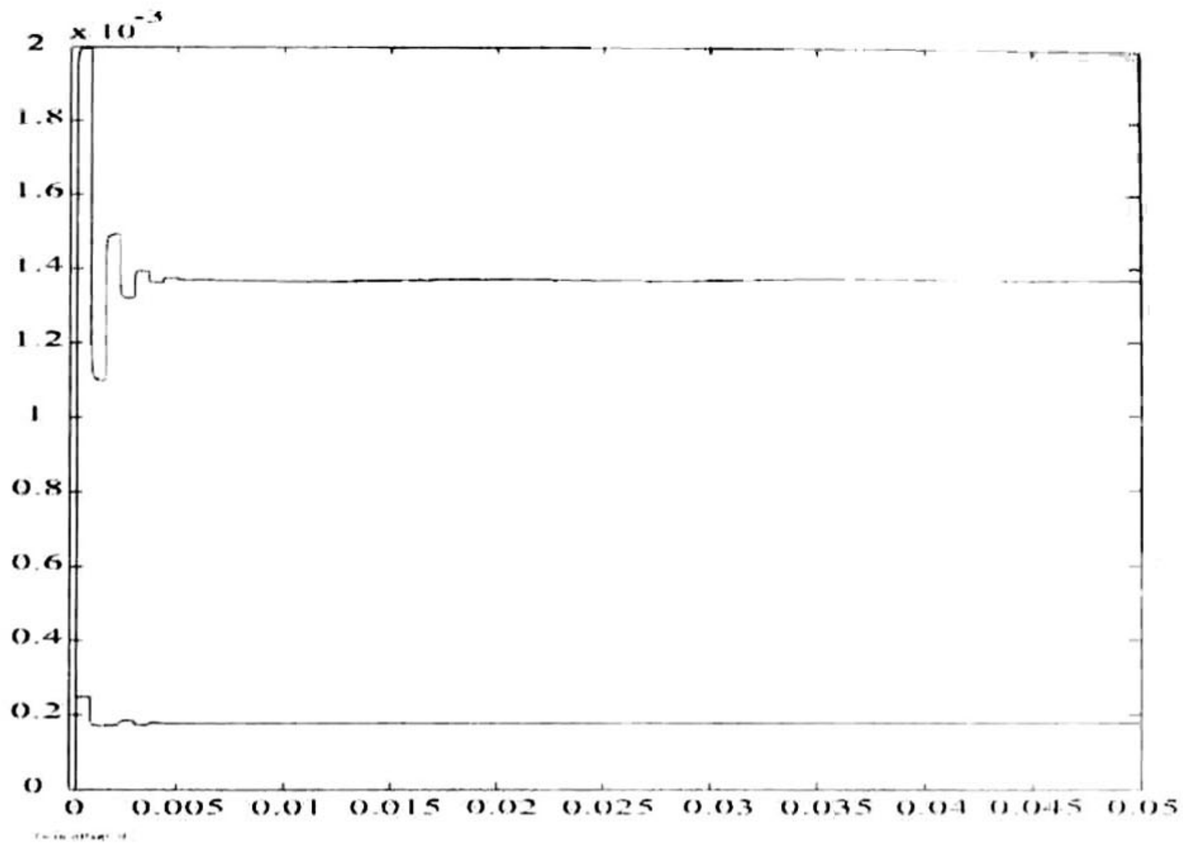


Figure 6.5: Harmonic magnitude of the voltage $v_n$.

## 6.3 Conclusions

Real-time implementation of the transmission line DHD model develop in Section III was carried out in the state-of-the-art simulator in the RTX-Lab and results in SIMULINK are given to demonstrate the performance of the model. The execution time of the simulation is on a $50\mu s$ time-step. Thus the problem of large simulation times originated by the nature of the DHD has been overcome using the real-time simulator.

Chapter 7

# Conclusions and Future Work

## 7.1 Conclusions

The dynamic harmonic domain technique was described and applied to power system networks that include: linear and nonlinear elements, transmission lines and synchronous generators, yielding results that were validated through TD techniques.

In addition, the interfacing of the synchronous generator-transmission line-linear/nonlinear loads had been presented.

The DHD permits to follow step-by-step the harmonics behavior along the transients with accuracy dictated by a predefined number of harmonics and without the need of a post-processing procedure. Additionally, it has been shown that the time-varying harmonic coefficients are capable of representing the nonharmonic line frequencies involved during the transient. The instantaneous voltage/current waveform can be constructed from its corresponding harmonic coefficients which are arranged as a DHD vectors. It has been observed that the inclusion of nonlinear loads enhance the harmonic content of voltage waveforms.

Power quality assessment under transient conditions has a significant impact at the design and development of active filters. However, the traditional method of using windowed FFT does not yield accurate harmonic information under transient conditions, as proven in Section 2.1. The DHD allows to obtain the power quality indices directly which can be calculated by traditional formulae (see section 3.4.3). The applications of the algorithm includes the study of harmonics in transient state for control, protection and power quality purposes, and also in the study of ferroresonance.

A major disadvantage of the DHD is the increased size of the ODE system that becomes large as the instantaneous variables are transformed into harmonic vectors.

The problem of large simulation times originated by the nature of the DHD has been overcome by using a fast real-time simulator. To demonstrate the performance of the DHD models the real-time implementation of the transmission line DHD model was carried out in the state-of-art simulator in the RTX-Lab.

In addition, the methodology of eigenanalisys used to assess resonance conditions between a generator and a transmission line has been extended to include electronic devices. This methodology presents an easy way to find harmonic resonance conditions through the harmonic domain admittance matrix obtained at the point joining the electronic device with the rest of the network.

## 7.2 Contributions of this Thesis

- Novel DHD transmission line and synchronous machine models have been proposed.
- A DHD technique for interfacing of synchronous machine-transmission line-linear/nonlinear loads has been presented.
- An extension of a pre-existing method for harmonic resonances to include electronic devices has been proposed.

## 7.3 Future Work

The DHD technique coupled with the fast computational facilities make it very attractive for research. In fact, future research as continuation of the work reported in this thesis can be listed as shown below.

- Switching devices DHD models including controls.

In this thesis the modeling of switching devices was only for steady-state analysis and without controls.

- Dynamic harmonic domain electromagnetic transient program.

By assembling the DHD models presented in this thesis, a DHD electromagnetic transient program can be created with the aid of the real-time simulator in the RTX-Lab.

- Hybrid DHD-TD method for electromagnetic transients.

Due to the characteristics of the DHD, models of elements in the DHD can be interfaced with networks modeled in TD taking the advantages of both methodologies.

- Extension of the eigenanalysis-based harmonic resonance assessment.

Following the basis explained in this work, it can be extended to add different switching devices.

# Bibliography


[1] E. L. Owen, "A history of harmonics in power systems", *IEEE Industry Application Magazine*. vol. 4, no. 1, Janyuary-February 1998, pp. 6-12.

[2] A. E. Eigeles, "Harmonics in the early years of electrical enginеering: a brief review od events, people and documents", *Proceedings of ICHQP* vol. 1, October 2000, pp. 1-7.

[3] W. M. Grady, and G. Santoso, "Understanding power system harmonics", *IEEE Power Engineering Review,* vol. 21, no. 11, November 2001, pp. 8-11.

[4] J. S. Subjak, and J. S. MacQuilkin, "Harmonics-causes, effects, measurments and analysis-update", *IEEE Trans. on Industry Applications,* vol. 26, no. 6, December 1990, pp. 1034-1042.

[5] R. N. Bracewell, *The Hartley Transform,* Oxford University, Press, 1986.

[6] M. Madrigal, and E. Acha, "A Hartley three phase synchronous machine model for three phase harmonic analysis and EMTP initialization", *Proceedings of ICHQP-96,* Las Vegas, USA, October 1996, pp. 412-418.

[7] E. Acha, and M. Madrigal, *Power Systems Harmonics-Computer Modeling and Analysis*. New York: John Wiley & Sons, Ltd, 2001.

[8] J. J. Rico, M. Madrigal, and E. Acha, "Dynamic harmonic evolution using the extenden harmonic domain", *IEEE Trans. on Power Delivery,* vol. 18, April 2003, pp. 587-594.

[9] T. Noda, A. Semlyen, and R. Iravani, "Entirely harmonic domain calculation of multiphase nonsinusoidal steady-state", *IEEE Trans. on Power Delivery,* vol. 19, no. 3, July 2004, pp. 1368-1377.

[10] H. DAngelo *Linear Time-Varying Systems: Analysis and Synthesis,* Boston, MA: Allyn & Bacon, 2003.

[11] J. J. Chavez,and A. Ramirez, "Dynamic harmonic domain modeling of transients in three-phase transmission lines", *IEEE Trans. on Power Delivery,* vol. 23, no. 4, October 2008, pp. 2294-2301.

[12] G. T. Heydt, P. S. Fjeld, C. C. Liu, D. Pierce, L. Tu, and G. Hensley, "Applications of the windowed FFT to electric power quality assessment", *IEEE Trans. on Power Delivery,* vol. 14, no. 4, October. 1999, pp. 1411-1416.

[13] M. Karimi-Ghartemani, and R. Iravani, "Measurement of harmonics/Interharmonics for time varying frequencies", *IEEE Trans. on Power Delivery,* vol. 20, no. 1, January. 2005, pp. 23-31.

[14] S. Qian, and D. Chen, "Joint time-frequency analysis", *IEEE Signal Processing Magazine,* vol. 16, no. 2, March. 1999, pp. 52-57.

[15] A. Semlyen, and A. Dabuleanu, "Fast and accurate switching transient calculations on transmission lines with ground return using recursive convolutions", *IEEE Trans. on Power Apparatus and Systems,* vol. PAS-94, no. 2, March-April. 1975, pp. 561-571.

[16] J. R. Marti, "Accurate modelling of frequency-dependent transmission lines in electromagnetic transient simulation", *IEEE Trans. on Power Apparatus and Systems,* vol. PAS-101, no. 1, January. 1982, pp. 147-157.

[17] T. Noda, N. Nagaoka, and A. Ametani, "Phase domain modeling of frequency-dependent transmission lines by meas n of an ARMA model", *IEEE Trans. on Power Delivery,* vol. 11, no. 1, January. 1996, pp. 401-411.

[18] F. J. Marcano and J. R. Marti, "Idempotent line model: Case studies", *Int. Conf. Power Systems Transients,* Seattle, WA., June 1997.

[19] H.V. Nguyen, H.W. Dommel, and J. R. Marti, "Direct phase-domain modelling of frequency-dependent overhead transmission lines", *IEEE Trans. on Power Delivery,* vol. 12, no. 3, July 1997, pp. 1335-1342.

[20] F. Castellanos, and J. R. Marti, "Full frequency-dependent phase-domain transmission line model", *IEEE Trans. on Power Systems,* vol. 12, no. 3, August. 1997, pp. 1331-1339.

[21] B. Gustavsen, and A. Semlyen, "Combined phase and modal domain calculation of transmission line transients based on vector vitting", *IEEE Trans. on Power Delivery,* vol. 13, no. 2, April 1998, pp. 596-604.

[22] A. Morched, B. Gustavsen, and M. Tartibi, "A universal model for accurate calculation of electromagnetic transiensts on overhead lines and undergroud cables", *IEEE Trans. on Power Delivery,* vol. 14, no. 3, July. 1999, pp. 1032-1037.

[23] N. Watson, and J. Arrillaga, *Power Systems Electromagnetic transients simulation,* London, UK.: IEE, 2003.

[24] H. W. Dommel, *EMTP Theory Book,* Vancouver, Canada, 1996.

[25] M. H. J. Bollen, I. Y. H. Gu, *Signal processing of power quality disturbances,* IEEE Press, USA, John Wiley & Sons, 2006.

[26] A. Semlyen, J.F. Eggleston, and J. Arrillaga, "Admittance matrix model of a synchronous machine for harmonic analysis", *IEEE Trans. on Power System,* vol. PAS-2, no. 4, November 1987, pp. 833-840.

[27] W. W. Xu, H. W. Dommel, and J. R.Marti, "A synchronous machine model for three-phase harmonic analysis and EMTP initialization", *IEEE Trans. on Power Systems,* vol. 6, no. 4, Novemeber 1991, pp. 1530-1538.

[28] A. Ramirez, A. Semlyen, and R. Iravani, "Harmonic domain characterization of the resonant interaction between generator and transmission line", *IEEE Trans. on Power Delivery*, vol. 20, no. 2, April 2005, pp. 1753-1762.

[29] A. Semlyen E. Acha, J. Arrillaga, "Newton-type algorithms for the harmonic phasor analysis of nonlinear power circuits in periodical steady state with special reference to magnetic nonlinearities", *IEEE Trans. on Power Delivery*, vol. 3, no. 3, July 1988, pp. 1090-1098.

[30] P. M. Anderson, B. L. Agrawal, and J. E. Van Ness, *Resonance in Power Systems*, New York, IEE Press, 1990.

[31] P. Kundur, *Power Systems Stability and Control*, New York, MacGrawn Hill, 1994.

[32] J. G. Proakis, D. G. Manolakis, *Digital signal processing : principles, algorithms, and applications*. N.J., Prentice Hall, 1996.

[33] D. Xia, and G. T. Heydt, "Harmonic power flow studies Part I-Formulation and solution" *IEEE Trans. on Power Apparatus and Systems*, vol. PAS-101, no. 6, June 1982, pp. 1257-1265.

[34] D. Xia, and G. T. Heydt, "Harmonic power flow studies Part II-Implemantation and practical aplication", *IEEE Trans. on Power Apparatus and Systems*, vol. PAS 101, no. 6, June 1982, pp. 1266-1270.

[35] T. J. Densem. P. S. Bodger, J. Arrillaga, "Three phase transmission system modelling for harmonic penetration studies", *IEEE Trans. on Power Apparatus and Systems*, vol. PAS 103, no. 2, February 1984, pp. 310-317.

[36] R. Koch, and N. Gumede, "The impact of harmonic resonace conditions on the connection rules for larger industrial installations", *IPES 2005, Conference and Exposition in Africa*, South Africa, July 2005, pp. 320-325.

[37] N. Kaul, and R. M. Mathur, "Solution to the problem of low order harmonic resonance from HVDC converters", *IEEE Trans. on Power Systems*, vol. 5, no. 4, November 1990, pp. 1160-1167.

[38] D. Muller, "Case studies of harmonic problems, analysis, and solutions on transmission systmes" *9th Electrical Power Quality and utilisation*, Barcelona, October 2007.

[39] L. J. Bohmann, and R. H. Lasseter, "Harmonic interaction in thyristor controlled reactor circuits" *IEEE Trans. on Power Delivery*, vol. 4, no. 3, July 1989, pp. 1919-1926.

[40] C. Chicone. *Ordinary differential equations with applications*, New York: Springer-Verlag, Ltd, 1999.

[41] X. Jiang, and A. M. Gole, "A frequency scanning method for the identification of harmonics instabilities in HVDC systems", *IEEE Trans. on Power Delivery*, vol. 10, no. 4, October 1995, pp. 1875-1881.

[42] A. Semlyen, and M. Shtash, "Principles of modular harmonic power flow methodology", *IEEE Procedings Generation Transmission and Distribution*, vol. 147, no. 1, January 2000, pp. 1-6.

[43] X. Wang and R. M. Mathur, "Real-time digital simulator of the electromagnetic transients of transmission lines with frequency dependence", *IEEE Trans. on Power Systems,* vol. 4, no. 4, October 1989, pp. 2249-2255.

[44] P. G. McLaren, R. Kuffel, R. Wierckx, J. Giesbrecht, and L. Arendt, "A real time digital simulator for testing relays", *IEEE Trans. on Power Delivery,* vol. 7, no. 1, January 1992, pp. 207-213.

[45] M. Foley, Y. Chen, and A. Bose, "A real time power system simulation laboratory enviroment", *IEEE Trans. on Power Systems,* vol. 5, no. 4, November 1990, pp. 1400-1406.

[46] J. R. Marti, and L. R. Linares, "Real-time EMTP-based transients simulation", *IEEE Trans. on Power Systems,* vol. 9, no. 3, August 1994, pp. 1309-1317.

[47] H. Taoka, I. Iyoda, H. Noguchi, N. Sato, and T. Nakazawa, "Real-time digital simulator for power system analysis on a hypercube computer", *IEEE Trans. on Power Systems,* vol. 7, no. 1, February 1992, pp. 1-10.

[48] J. A. Hollman, and J. R. Marti, "Real time network simulation with PC-cluster", *IEEE Trans. on Power Systems,* vol. 18, no. 2, May 2003, pp. 563-569.

[49] *RT-LAB 8.x Users Manual,* Opal-RT Technology Inc., Montreal, QC, Canada, 2006, pp. 1-80

[50] D. Jakominich, R. Krebs, D. Retzmann, and A. Kumar, "Real time digital power system simulator design considerations and relay performance evaluation", *IEEE Trans. on Power Delivery,* vol. 14, no. 3, July 1999, pp. 773-781.

[51] L.F. Pak, M. O. Faruque, X. Nie, and V. Dinavahi, "A versatile cluster-based real-time digital simulator for power enginnering research", *IEEE Trans. on Power Syst.,* vol. 21, no. 2, May 2006, pp. 455-465.

[52] B. Asghari, M. O. Faruque, and V. Dinavahi, "Detailed real-time transient model of the "scn" transformer", *IEEE Trans. on Power Delivery,* vol. 23, no. 3, July 2008, pp. 1513-1521.

[53] H. E. J. Houston, and A. E. Kenelly, "The harmonics of electrical current", *Electr. World,* June 1894, pp. 735-737.

[54] IEEE Std 100, "The Authoritative Dictionary of IEEE Standards Terms Seventh Edition", 2000.

Appendix A

# List of Publications


[1 ] J. Jesus Chavez and Abner Ramirez, "Dynamic harmonic domain modeling of transients in three-phase transmission lines", *IEEE Trans. on Power Delivery*, vol. 23, no. 4, pp. 2294-2301, October 2008.

[2 ] Jose de Jesus Chavez, Abner Ramirez, and Venkata Dinavahi, "Dynamic Harmonic Domain Modeling of Synchronous Machine and Transmission Line Interface", submitted to *IEEE Trans. on Power Delivery*, paper TPWRD-00454-2008.R1.

[3 ] J. Chavez, A. Ramirez, V. Dinavahi, R. Iravani, J. A. Martinez, J. Jatskevich, and G. W. Chang "Interfacing Techniques for Time-Domain and Frequency-Domain Simulation Methods" Submitted to *IEEE Trans. on Power Delivery*, paper TPWRD-00459-2009.

[4 ] J.J. Chavez, A. Ramirez, and J.L. Naredo, "Dynamic harmonic domain transmission line modeling for transients", Proceedings of the International Conference on Power Systems, Lyon, France, June 2007.

# CENTRO DE INVESTIGACIÓN Y DE ESTUDIOS AVANZADOS DEL I.P.N.
# UNIDAD GUADALAJARA

El Jurado designado por la Unidad Guadalajara del Centro de Investigación y de Estudios Avanzados del Instituto Politécnico Nacional aprobó la tesis

Modelos Avanzados de Dispositivos de Sistemas de Potencia en el Dominio Armónico Dinámico

del (la) C.

José de Jesús CHÁVEZ MURO

el día 20 de Agosto de 2009.

Dr. Pablo Moreno Villalobos
Investigador CINVESTAV 3C
CINVESTAV Unidad Guadalajara

Dr. Juan Manuel Ramírez Arredondo
Investigador CINVESTAV 3C
CINVESTAV Unidad Guadalajara

Dr. Amner Israel Ramírez Vázquez
Investigador CINVESTAV 3B
CINVESTAV Unidad Guadalajara

Dr. José Manuel Cañedo Castañeda
Investigador CINVESTAV 3A
CINVESTAV Unidad Guadalajara

Dr. VENKATA DINAVAHI R.
PROFESSOR
UNIVERSITY OF ALBERTA